Effects of Processing Parameters on Friction Stir Welded Lap Joints of AA7075-T6 and AA6022-T4

by

Michael Booth

A thesis

Presented to the University Of Waterloo

in fulfilment of the

thesis requirement for the degree of

Master of Applied Science

in

Mechanical Engineering

Waterloo, Ontario, Canada, 2016

Author's Declaration

I hereby declare that I am the sole author of this thesis. This is a true copy of the thesis, including any required final revisions, as accepted by my examiners.

I understand that my thesis may be made electronically available to the public.

Abstract

Friction stir welding (FSW) is a solid-state welding process that has a number of advantages over traditional fusion welding techniques when attempting to join aluminum or dissimilar material workpieces. It is expected to play a large role in the automotive industry, where aluminum alloys are becoming more prevalent in mass-production vehicles.

The research in this thesis evaluates overlap FSW joints between thin sheets of AA7075-T6 and AA6022-T4 when the welding parameters of tool geometry and welding speed are varied. The resulting joints are characterized by optical microscopy, overlap shear tests, microhardness tests, and temperature measurements. The effect of a post-weld heat treatment is also examined. The main objective of the research are to determine a tool geometry that can produce good quality welds over a wide range of operating conditions, for use in an industrial setting.

Friction stir welds of good quality are made successfully at speeds of up to 500mm/min, and it is found that weld microhardness and joint strength are greater at faster welding speeds; whereas temperatures in the weld area are lower at faster welding speeds. Five different tool geometries are tested, and the tool design that delivers the best performance is a one that uses a concave shoulder shape, and a pin with a tapered profile, threads, and 3 flats. A post-weld heat treatment at 180^{o}C for 30 minutes is found to increase joint strength by approximately 10%.

Future studies involving transmission electron microscopy, corrosion testing, and fatigue testing are recommended in order to supplement the results presented in this thesis.

Acknowledgements

First and foremost, I would like to acknowledge the assistance of Adrian Gerlich, my supervising professor. His continued patience and guidance throughout my Master's program are what made this research possible.

Second, I would like to acknowledge the assistance of the other researchers on this project, namely: Zhikang Shen and Yuquan Ding of the University of Waterloo; as well as Olga Gopkalo, Xu Liu, and Brad Diak of Queen's University. Their collaboration during this project was a great help.

Third, I would like to acknowledge the contributions of Ford Motor Company towards sponsoring the research in this thesis. Specifically: Joy Forsmark and Elizabeth Hetrick, whose suggestions and feedback were always valuable.

Last, I would like to thank the many other members of the Center for Advanced Materials Joining Group at the University of Waterloo, who provided me with a productive and co-operative research environment for the duration of my Master's program.

Table of Contents

List of Figures

List of Tables

1.0 Introduction

Aluminum is a common structural material that has many useful material properties – such as a natural resistance to corrosion, excellent electrical and thermal conductivity, and good formability; however it is probably most well-known for its low density and high strength-to-weight ratio [1]. This trait has made it invaluable to many transportation industries striving for higher fuel efficiency through weight reductions. Historically, aluminum and its alloys have been used in applications that demand high performance components but are generally less concerned with elevated costs and long manufacturing times – for example: military and commercial aerospace, high speed trains, and high performance automobiles. This limitation is not only due to aluminum being higher cost than steel, but also a result of the complications that arise when attempting to join the metal by traditional means.

Conventional fusion welding techniques were developed to join iron and steel components, and involve melting the base metal of the workpieces and then adding a molten filler metal that, upon solidification, forms a solid joint [1] [2]. When these methods are applied to aluminum workpieces, the melting and re-solidification is highly detrimental to the material and is known to result in hot cracking, hydrogen cracking, and liquation cracking; not to mention the loss of strength due to dissolution of strengthening precipitates formed during the heat treatment process [2] [3]. Over many years, engineers and materials scientists have developed alloy compositions and welding techniques that make it possible to achieve acceptable aluminum welds. These processes, however, are quite restrictive – they require highly skilled welders, and only certain alloy compositions can be easily welded with confidence. The strongest aluminum alloys which are produced by artificial heat treatment still remain virtually un-weldable by arc welding due a loss of strength and defect formation upon re-solidification [2]. Other joining methods, such as adhesives or rivets, introduce other issues including: additional weight, insufficient joint strength, and the formation of stress concentrations, to name a few.

Friction stir welding (FSW) is a relatively new process that was developed at The Welding Institute in 1991 [4]. Since its conception it has received much attention in both industry and academia due to being a simple and low cost process of material joining, as well as being more environmentally friendly than fusion welding due to lower energy requirements and the lack of necessary consumables [5]. There have been a considerable number of studies on the process since it was invented [6], and it has been shown to allow joining of aluminum, magnesium, steel, copper, titanium and other alloys in thicknesses up to 25 mm in a single pass [5] [7]. In FSW, a rotating, non-consumable tool consisting of a cylindrical shoulder and protruding pin with a smaller diameter is plunged into the workpiece. The rotating tool creates frictional heating and plastic deformation while providing a forging force that serves to consolidate the metal and create an effective joint. It is particularly suited to joining difficult to weld aluminum alloys given the solid-state nature of the process (meaning that the metal does not melt material), avoiding many of the solidification issues that arise during traditional fusion welding [5]. A further advantage of the FSW process is its ability to join dissimilar alloys or different metals altogether [5]. Many of the challenges in joining dissimilar materials are also products of metal re-solidification after welding, and are therefore largely overcome or avoided by the use of a solid-state welding process such as FSW [2].

The recent push for increased fuel economy in civilian automobiles has driven the commercial automotive industry to investigate the more widespread use of aluminum in their vehicles. In most cases, the easily weldable aluminum alloys do not provide sufficient strength to meet crash safety standards, while the use of the stronger alloys is too expensive at a large scale. Interest in joining different series of aluminum alloys is of particular interest to transportation industries, where it is often required that certain components be made of stronger, heavier materials than others. The weight savings that can be gained by constructing some components out of lighter materials is significant enough for there to be continued interest in dissimilar metal joining techniques. The emergence of FSW

as a means of joining a wide variety of high-strength, precipitation hardened aluminum alloys has allowed companies in many sectors to begin to consider these metals as a viable construction material.

1.1 Thesis Description

The research discussed in this work has been sponsored by Ford Motor Company, in order to investigate the effect of different welding parameters on FSW lap joints in thin aluminum sheets. It is specifically a study of FSW overlap joints between thin sheets of AA7075-T6 and AA6022-T4.

1.2 Thesis Objectives

The objectives of the research are as follows:

1. Identify processing parameters to produce FSW joints between thin sheets (thickness of 2mm or smaller) of AA7075-T6 and AA6022-T4 alloys in terms of tool geometry and travel speed.
2. Investigate and compare the mechanical properties between the FSW joints made under different process parameters
3. Determine a FSW tool geometry that can provide good quality welds across a wide range of travel speeds for use in an industrial manufacturing setting

1.3 Thesis Layout

The body of the thesis is divided into four sections. Section 2.0 will introduce background information pertaining to age-hardenable aluminum alloys, and discuss the difficulties that arise with traditional aluminum joining techniques. Section 3.0 will provide a detailed description of the FSW process parameters, and review some existing literature that is relevant to the research. Section 4.0 will outline the experimental approach and the equipment used for testing. Section 5.0 will present the results and discussion, and is divided into two parts. First: a preliminary study on lap FSW between two

sheets of AA7075-T6 using three tool geometries and three travel speeds; and second: the main study on lap joining between AA7075-T6 and AA6022-T4 alloy sheets using five tool geometries and five travel speeds. The final sections, 6.0 and 7.0, will summarize the findings and make suggestions for future work in this area.

2.0 Background Information I – Challenges in Aluminum Fusion Welding

Fusion welding processes are the most well-known and widely used welding techniques, and involve melting the base metal to form a joint between components. Some of the earliest examples include oxyacetylene welding (OAW) and shielded metal arc welding (SMAW); and contemporary techniques inclide gas-metal arc welding (GMAW), gas-tungsten arc welding (GTAW) and laser beam welding (LBW) [2] [5]. Through years of continued use and development, fusion welding processes have proven themselves to be versatile and effective for joining a wide variety of metals. Aluminum, however, has always posed a unique set of challenges which stem from two main factors: the dissolution of strengthening precipitates; and the formation of defects upon re-solidification. This section will discuss these issues in detail.

2.1 Precipitation Behaviour of Aluminum Alloys

Aluminum alloys achieve their desirable mechanical properties through age hardening (also known as precipitation hardening or ageing) – a process in which specific heat treatments are applied to the material. These thermal cycles cause alloying elements within the metal to form compounds and precipitate out of the supersaturated solid solution (SSSS) to create small particles that increase the hardness and strength of the material [1]. This will occur when the SSSS is raised to an intermediate temperature below the melting temperature and held there for an amount of time (hence the term “age”-hardening). The temperature and time required for precipitation hardening vary widely depending on the alloy system in question – some alloys are age-hardenable at room temperature (referred to as “natural ageing”), while some require the application of relatively high temperatures to form strengthening particles (this is referred to as artificial ageing) [1]. It is necessary to have an

understanding of the age-hardening process in aluminum alloys in order to understand how these strengthening particles – and the resulting material properties – will react when subjected to a welding process.

Precipitation hardening occurs because the system is seeking to lower its Gibb's free energy and become more thermodynamically stable [8]. Figure 1 illustrates that a different arrangement of atoms in the same alloy system can provide a lower Gibb's free energy; in this case: both arrangements A and B are stable (ΔG=0) but arrangement A is has a lower free energy than arrangement B, so A is referred to as the stable state and B is considered a metastable state.

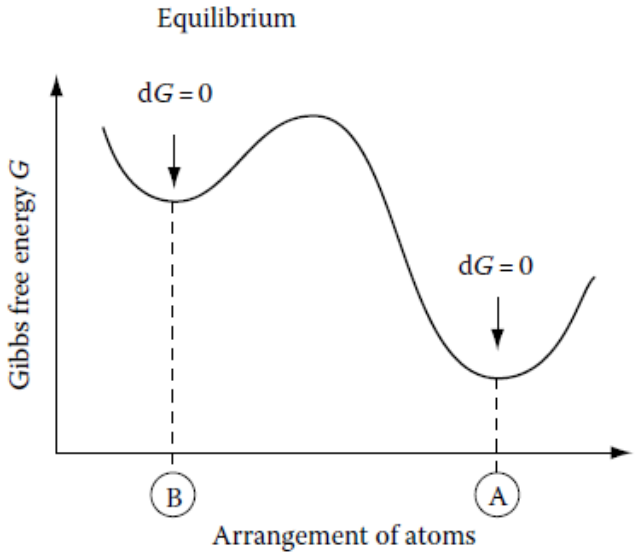

Figure 1: Schematic depiction of Gibb's free energy arrangement with different arrangement of atoms in the same system [8]

For the system to move between states, an energy barrier must be overcome, represented in Figure 1 by the small increase in Gibb's free energy before the large decrease down to stable arrangement A. The heat applied during precipitation hardening acts as the activation energy that allows the system to precipitate the more stable state. In most real systems of age-hardenable alloys, there are many metastable states, and so there is a precipitation sequence that is followed [1] [8]. With each step

in the precipitation evolution sequence, a different metastable phase is formed and the total free energy of the system is slightly lowered. The very last phase transformation in the sequence is the formation of a stable phase that brings the system to the lowest possible Gibb's free energy [8].

Strengthening of the material is a result of the small precipitate compounds that form throughout the alloy during phase transformations, increasing strength by impeding the movement of dislocations [1]. The 2xxx (Al-Cu), 6xxx (Al-Mg-Si) and 7xxx (Al-Zn-Mg) series aluminum alloys are common alloy classifications that are strengthened by age-hardening. Precipitate phases provide different amounts of strengthening to the alloy system depending on their shape, size and composition. In general, precipitates provide the greatest amount of strengthening when they are: small (ie: < 100 nm) and closely spaced; harder than the surrounding matrix; and round in shape rather than plate-like. In almost all cases, it is one of the intermediate metastable phases that provide maximum strengthening to the alloy [8]. Therefore, if a precipitation hardenable alloy is heated for too long or if the applied temperatures are too high, the system will move past the desirable metastable phase and form softer metastable phases or even reach a stable phase – this phenomenon known as overageing [8]. With continued heating, smaller precipitates will dissolve and their solute atoms will be redistributed to form larger particles in order to lower the total energy of the system. This phenomenon is known as precipitate coarsening, and will decrease the strength of the alloy. The rate of coarsening increases with increasing temperature, and again is due to a decrease in free energy – a small number of large particles yield a lower free energy than a large number of small particles [8].

Precipitation is used to strengthen many other metals, including magnesium alloys and some stainless steels [1], however the research in this thesis will focus on the aluminum systems. It is common to schematically modify phase diagrams to represent metastable phases formed during the precipitation

process. An example is shown in Figure 2, where the metastable θ'', θ', and GP zones can exist only at lower temperatures.

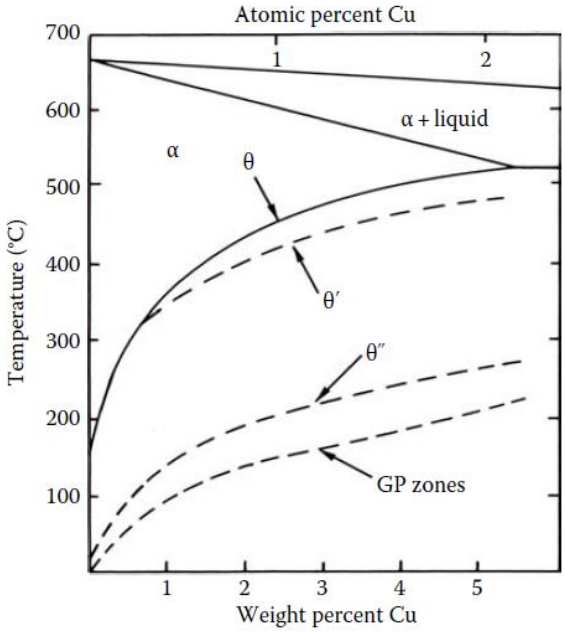

Figure 2: 2xxx (Al-Cu) alloy system phase diagram showing metastable particle solvus lines [8]

In the case of aluminum alloys, the typical precipitation evolution begins with the formation of coherent clusters of solute atoms, which have the same structure as the matrix but slightly different lattice parameters. The next stage is the formation of Guinier-Preston Zones (GP Zones), which are areas of solute with a different structure than the surrounding matrix, but are still coherent [2] [8]. With continued heating and time, the formation of metastable particles will occur. These particles are typically denoted by a Greek letter and a prime or double-prime (θ' and θ'' in 2xxx, β' and β'' in 6xxx, η' in 7xxx). These precipitates are either coherent or semi-coherent with the surrounding matrix, and typically provide the maximum amount of strengthening in age-hardenable aluminum alloys due to their size, shape, and hardness. With further heat input and time, metastable precipitates will coarsen and dissolve, and stable precipitates will begin to form. These are denoted by the same Greek letter without a prime (θ, β, η). These particles are larger and often incoherent with the surrounding matrix, resulting

in less strengthening. An aluminum alloy is considered under-aged if it has only been heat treated to the point of the formation of GP zones; peak-aged if it has formed fine metastable particles; and over-aged if the metastable particles have dissolved or coarsened and formed stable precipitates [1]. Figure 3 shows the evolution of precipitates in a common 2xxx series aluminum alloy:

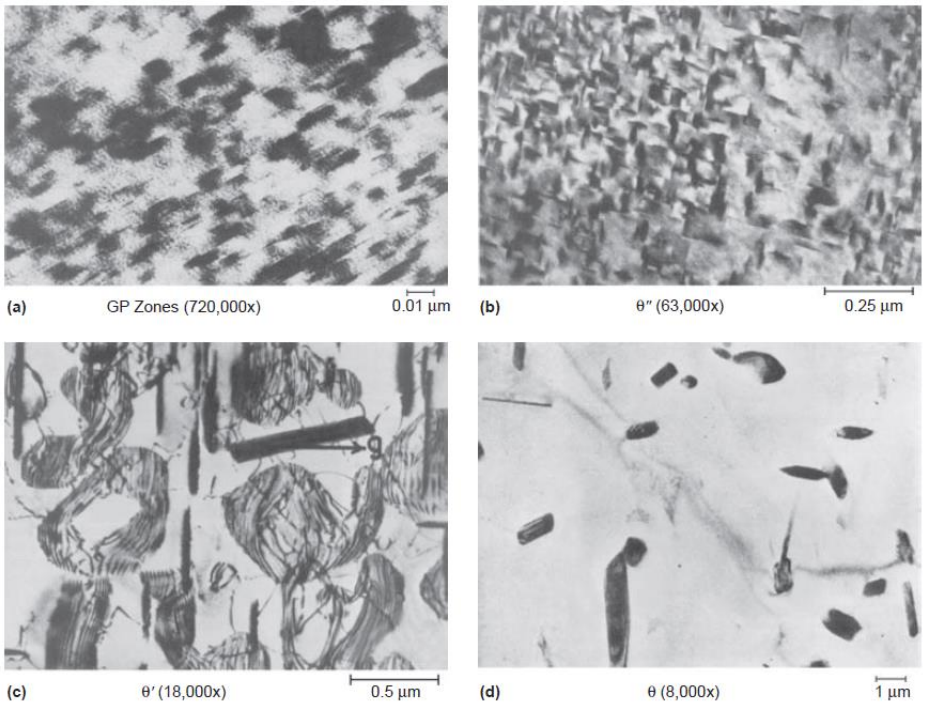

Figure 3: Precipitation evolution sequence of an Al-Cu system [9]

The 6xxx series of aluminum alloys are primarily an Al-Mg-Si system, of which the precipitation behavior is well understood. The literature shows that the precipitates follow the following evolution sequence [10]:

SSSS -> Clusters -> Coherent GP -> needle-like coherent β'' -> rod-like β' -> lath-type Q' -> β

The main strengthening precipitates are the Mg_2Si intermetallics that form as the β'' phase, though β' and Q' precipitates are known to provide some strengthening as well [10].

The 7xxx series aluminum alloys are primarily an Al-Zn-Mg system, of which the precipitation behavior is well understood. The literature presents the following precipitation evolution sequence [11]:

SSSS -> Clusters -> coherent GP I -> coherent spherical GP II ->semicoherent platelike η' (Zn_2Mg) -> η

The GP zones are produced at low temperatures, typically between 20-125°C. GP I Zones are areas rich in Mg and Zn (stable up to ~115°C), and GP II Zones are nucleated by vacancy-rich clusters of solute (stable up to ~150°C). Ageing at 125°C for 20 hours can transform GP II Zones into the metastable, semi-coherent η' phase [11]. At 200°C, this phase transforms into the stable η phase. It is well known that the main strengthening precipitates are the GP II Zones and the η' phase [11].

The large quantities of heat input during welding will cause these sensitive particles to coarsen or be destroyed, resulting in softening of the alloy and a reduction in mechanical performance. This is one reason why welding aluminum has remained such a challenge.

2.2 Common Weld Defects in Aluminum Welding

The high-strength heat treatable aluminum alloys – specifically, the 2xxx and 7xxx series wrought alloys – have always presented a host of difficulties when subjected to fusion welding methods [5], to the extent that they are generally considered un-weldable by traditional means [1]. The other heat treatable wrought aluminum alloys are the 6xxx series, which generally exhibits good weldability, so long as the welding technique and filler metal are chosen carefully to avoid weld metal compositions prone to solidification cracking [2]. The drawback is that the 6xxx alloys are not able to provide the same strength or damage tolerance as the 2xxx and 7xxx alloys [1]. The 3xxx and 4xxx series of aluminum alloys are traditionally used as filler metals when fusion welding aluminum components due to their high Si content and good flowability [1], however they are generally too weak for serious structural applications and are not always successful in creating defect-free joints when used in conjunction with

7xxx series alloys. The use of filler metals will also add weight to the structure, which is not desirable. Problems known to occur during fusion welding of these aluminum alloys include: weld porosity, solidification cracking in the fusion zone (FZ), liquation cracking in the partially melted zone (PMZ) and severe softening in the heat-affected zone (HAZ) [2].

Porosity in fusion welding occurs due to the ionization of diatomic gasses, O_2, N_2 and H_2, into smaller single molecules at high temperatures, and the absorption of these molecules into the liquid metal [2] [12]. In the case of aluminum, porosity caused by hydrogen absorption is a particular concern, because the solubility of hydrogen being much higher in liquid aluminum than in solid aluminum – this means that during fusion welding, hydrogen will migrate from the solid material *into* the molten weld pool along the advancing solid-liquid interface. The number of sources of H_2 gas is also larger where aluminum welding is concerned, as the aluminum surface oxide is known to absorb moisture from the air. Other sources of hydrogen are from moisture in the shielding gas, or grease on the workpiece or electrode. Hydrogen porosity has been shown to reduce the strength, ductility, and fatigue performance of joints in aluminum parts [2].

Solidification cracking is a problem that can occur in welding of all metals, but is especially common with aluminum [12]. It describes intergranular cracks caused by internal stresses that result from shrinkage and contraction of solidifying weld metal [2]. The most critical factor that influences the formation of solidification cracks is the composition of the base metal and weld metal. For moderately-alloyed grades of aluminum, it has been shown that a small amount of low-melting-point eutectic liquid is forced into the grain boundaries during welding, which, upon solidification, creates a thin intergranular film that increases susceptibility to solidification cracks [2]. By contrast: low-alloy (nearly pure) aluminum will not have as much of the eutectic solution, and will therefore not form the same intergranular film; while highly alloyed compositions will have an abundance of liquid with the eutectic

composition that can fill incipient cracks before they develop further [2]. Unfortunately, these alloys do not always provide the required mechanical performance of the more moderately alloyed aluminum materials. More often, these are used as a filler metal when welding an alloy that is more prone to solidification cracking; however this can also produce a relatively weak joint and will add weight to the overall structure, which could defeat the purpose of using an advanced heat-treatable aluminum alloy in the first place.

Liquation cracking is an issue that is seen almost exclusively in aluminum welding – arising because of the significantly different melting points amid phases in an aluminum alloy system. It will occur in the partially melted zone (PMZ) of the weld, where temperatures fall between the eutectic temperature (T_E) and the liquidus temperature of the alloy. This process is schematically shown by the images in Figure 4, taken from the work of Kou [2].

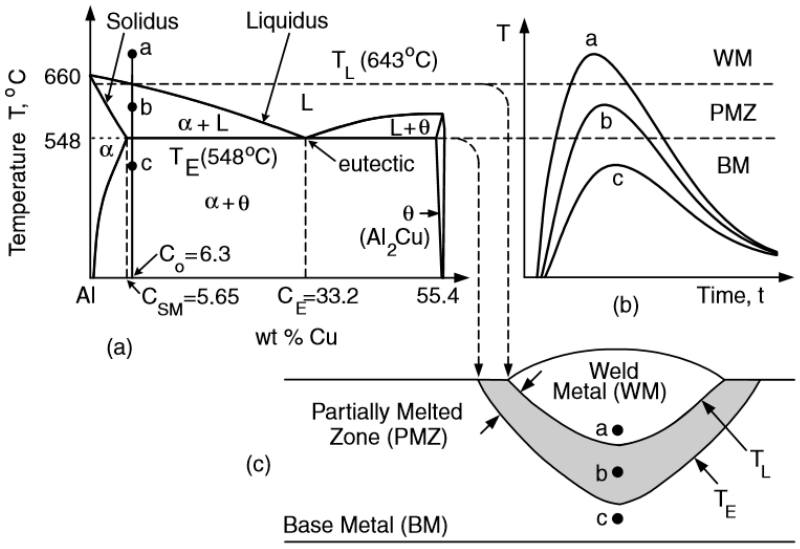

Figure 4: Phase diagram of a AA2219 alloy given in context to the different zones of the fusion weld – (a) shows the phase diagram with important temperatures labeled; (b) shows the corresponding thermal cycles; (c) a transverse cross-section of the weld [2]

During welding, temperatures will first reach T_E, and a mixture of solid α phase Al and liquid with eutectic composition will form; then as temperatures increase above T_E (point *b* in Figure 4), the α-phase will begin to melt as well, diluting the eutectic liquid and producing a hypoeutectic liquid. Upon cooling, the solute-depleted α phase will solidify first, creating areas of soft α-phase around large solute-rich eutectic particles [2]. Cracks that propagate through these softer regions along the grain boundaries are known as liquation cracks, and are notorious in fusion welding of aluminum. Figure 5 is also taken from the Kou text [2], and helps in visualizing the microstructural evolution of the PMZ in an aluminum fusion weld.

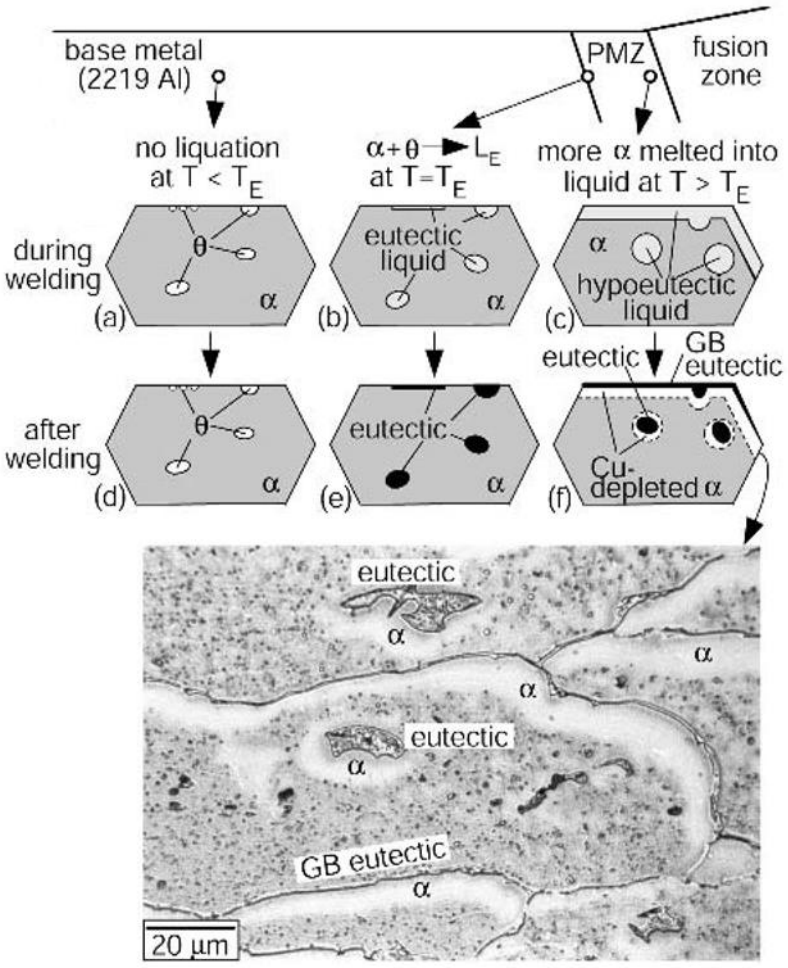

Figure 5: Diagram showing the microstructural evolution in an aluminum fusion weld (top) alongside an optical micrograph image of the actual grains in the PMZ of an aluminum fusion weld (bottom) [2]

All welded joints experience a degree of softening in the heat affected zone (HAZ) of the weld. In the case of aluminum, HAZ softening occurs because temperatures in this region are elevated enough to cause either coarsening (i.e.: overageing) or complete dissolution of the precipitate particles that provide strength to the alloy system [6]. In either case, the careful heat treatment that was applied to the base metal of the workpiece before welding is undone, and the metal will rarely maintain the desired strength or hardness.

Based on these issues, it is clear that the main challenges in fusion welding aluminum stem from the heat applied to the workpieces during joining. Firstly, there is the issue of porosity, which forms upon cooling of the molten aluminum in the weld pool. Second, there are the problems of solidification cracking and liquation, which arise during the re-solidification of the molten aluminum. Thirdly, the overageing and softening in the HAZ is a result of the thermal cycles that this area of the workpiece is subjected to during welding. The techniques that exist to reduce the occurrence of these defects involve changing the material composition – either by using certain types of alloys or by the addition of specific filler metals – which is significantly restrictive to the design process in that it limits the available materials, adds weight to the component, or complicates the manufacturing practices. Friction stir welding, by virtue of being a solid-state joining method, is able to avoid many of the challenges inherent to fusion welding, and easily create strong bonds between aluminum components [5].

The next section will describe the FSW process in detail, and outline the major welding parameters and microstructural characteristics of the joints.

3.0 Background Information II – Friction Stir Welding

Friction stir welding is an autogenous solid-state welding process (or "cold-welding" process), meaning that it is able to create a joint without melting the base metal or using molten filler metal [6]. A friction stir weld is created by plunging a non-consumable rotating cylindrical tool between two workpieces, as shown in Figure 6.

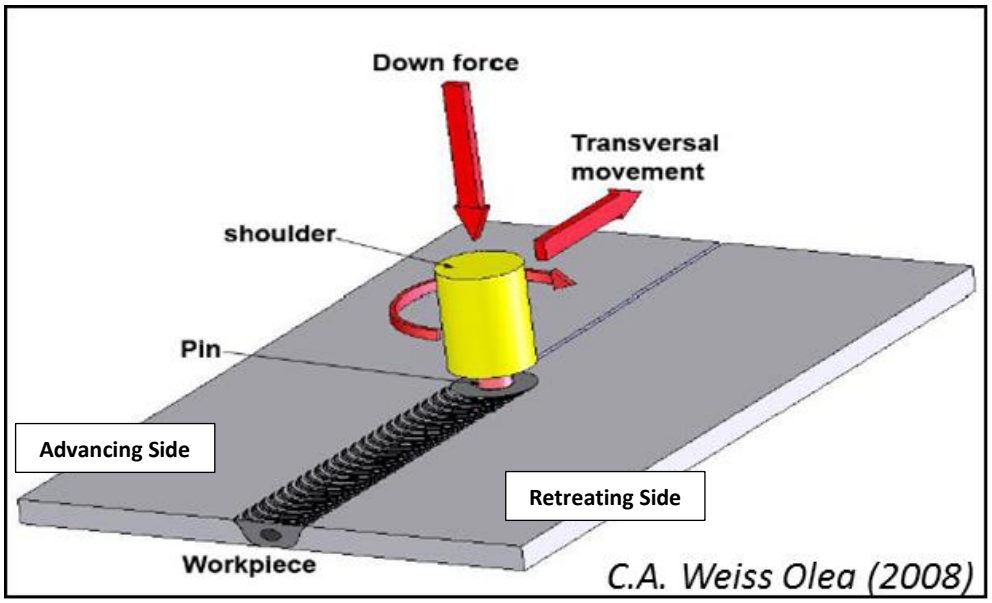

Figure 6: Schematic of the FSW process [10]

The rotational movement will generate frictional heat and plastic deformation, softening and stirring the materials together; while the applied downward pressure of the tool acts as a forging force, consolidating the softened material into a single location [6]. If the rotating tool is moved laterally across the workpieces, a linear friction stir weld is made. FSW can be used to make butt welds and lap welds in steel, copper, aluminum, magnesium and titanium of thicknesses of up to 25mm in a single pass for the case of aluminum [7].

3.1 Microstructural Regions of the FSW Joint

It is necessary to have an understanding of the characteristics of a friction stir weld in order to comprehend the existing literature. The three main areas of a finished weld (moving outwards from the center): the stir zone (SZ), the thermo-mechanically affected zone (TMAZ), and the heat affected zone (HAZ). Outside of the HAZ is the unaffected base metal (BM). The FSW process also produces slightly asymmetric welds due to the combined rotation and transverse movement of the tool. The side of the weld on which the rotational movement vector and transverse movement vector are in the same direction is referred to as the advancing side (AS) and the side of the weld on which the vectors are opposite is referred to as the retreating side (RS) (this is also depicted in Figure 6). A diagram showing the location of the weld zones is shown in Figure 7.

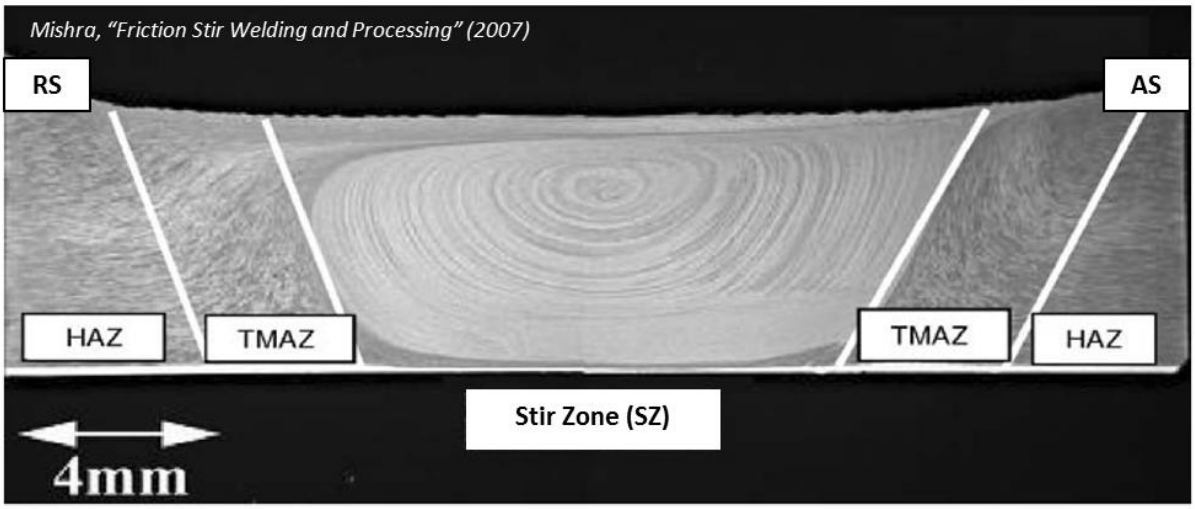

Figure 7: Typical FSW joint cross section showing distinct microstructural zones [5]

The stir zone (SZ) is typically an oval-shaped area at the center of the weld. It is here where the pin of the FSW tool has passed through and mixed the material together. This area of the weld is subjected to the highest temperatures [13]. The combination of high temperatures and large mechanical strain results in a phenomenon known as geometric dynamic recrystallization of the grain structure in

the metal [5]. This dynamic recrystallization of grains results in an ultra-fine grain structure, with sizes usually ranging from 1 to 10 μm [5] [14] [15].

The thermo-mechanically affected zone (TMAZ) is a narrow area that lies just outside the SZ. In this region, the metal has also been subjected to high temperatures, though slightly lower than the SZ. The grain structure has also been altered due to mechanical deformation, however in this zone there has been no dynamic recrystallization, and instead the grains are elongated and typically of a different orientation than those in the base metal [5]. This area of the weld will typically be softer than the SZ and the base metal, since there is sufficient heat to promote precipitate dissolution but no dynamic recrystallization. Some studies have measured temperatures in this region to be between 450^{o}C and 550^{o}C for aluminum FSW [15] [16], though the temperature will vary greatly depending on the welding parameters and workpiece material.

The heat affected zone (HAZ) is the region between the TMAZ and the unaffected base metal. In this zone, the metal was heated to temperatures far lower than those experienced in the SZ [13]. The temperatures across the HAZ decrease with distance from the weld center. This region experiences no mechanical deformation from the welding process [5]. While there is no significant change in grain size or orientation, the temperatures in this area are still high enough to result in precipitate evolution, often making this zone the softest region of welded heat treatable alloys [5]. According to the literature, temperatures in the HAZ of aluminum friction stir welds can reach up to 350^{o}C [16] [17], and decrease rapidly with distance from the weld centerline. Some HAZ regions have been observed to extend more than 30mm from the weld centerline [16] [17], however the size of the HAZ and the temperature gradient is highly dependent on the welding parameters and dimensions of the tool and workpiece materials.

The side of the FSW on which the direction of tool travel and the direction of tool rotation are in the same direction is known as the advancing side (AS); whereas the side on which they are opposite one another is called the retreating side (RS), seen schematically in Figure 6. Temperatures in the FSW are generally slightly higher on the AS compared to the RS; and the boundary between the SZ and the TMAZ is noticeably more abrupt and more well defined on the AS [5]. Voids that form during FSW are typically located on the AS near the bottom corner of the SZ, and occurring in this region when the deformed material is unable to fill the void produced by the tool that passes through the workpiece [5]. The selection of welding parameters can do much to reduce the formation of voids, and is discussed in the following section.

3.2 Parameters in FSW

The major parameters in FSW are the following: joint configuration, workpiece and tool material, tool travel speed, tool rotational speed, tool plunge depth, tool tilt angle, tool geometry and features. These parameters will be discussed in detail in the subsections below.

Joint configuration refers to the arrangement of the workpieces. FSW can be performed in either a butt or lap configuration. In a butt configuration, the two workpieces are arranged end-to-end; the tool is plunged into the faying interface between the two workpieces and moved along the interface to create a welded connection. A concern in butt FSW is the clamping force used to restrain the workpieces in the lateral directions (the plane perpendicular to the tool) – sufficient force must be applied so that the workpieces do not shift or spread apart during the FSW process. In a lap configuration, the two workpieces are arranged on top of one another, with a specified overlap distance. The tool is plunged into the workpieces – penetrating the top sheet completely and partially penetrating the lower sheet – and then moved laterally in the desired direction of welding. Clamping is also a concern in lap FSW, as there must be sufficient downward force to ensure that the workpieces do

not laterally slide during welding. Additionally, the pin length, plunge depth and thickness of the workpieces must be carefully measured and monitored, so that under- and over-penetration is avoided. A final issue that presents itself during lap FSW is the formation of a flaw known as a “hook feature” – which refers to a hook-shaped extension of the sheet interface into the upper workpiece caused by the vertical movement of metal during welding, and is shown in Figure 8 [13]. The extension of the interface reduces the effective thickness of the top sheet, decreasing the strength of the joint. This flaw will be discussed in more detail in the literature review, since this has become a key issue with lap FSW.

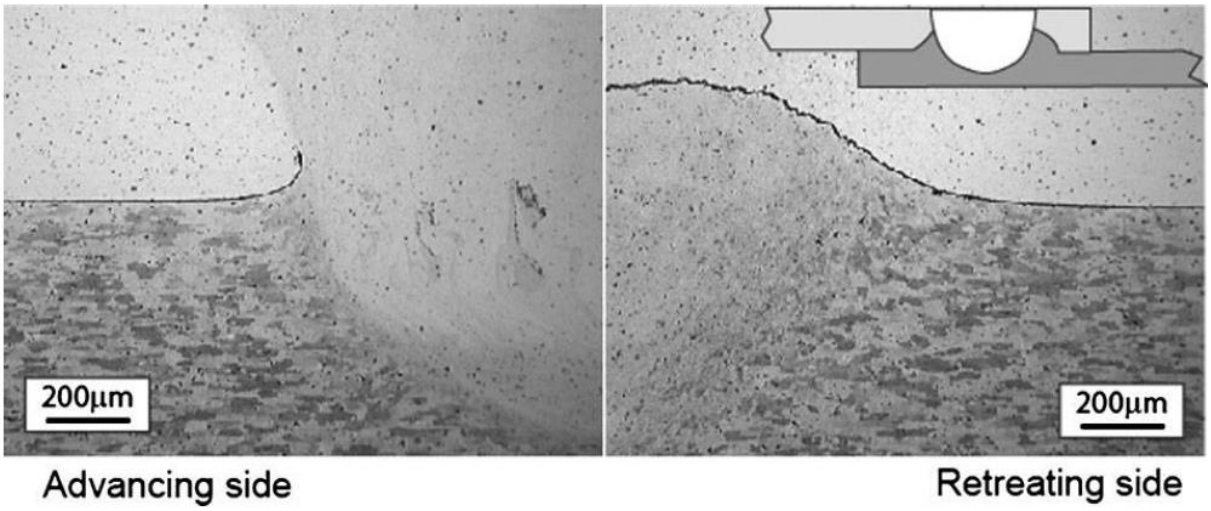

Figure 8: Example of the hook feature or hooking flaw that is inherent to lap FSW [13]

The workpiece and tool materials go hand-in-hand, and must be selected carefully to avoid any problems. The tool material must have sufficiently high hardness, toughness, and high-temperature properties to withstand the temperatures and forces during FSW, which will differ depending on the materials that are being welded. Simple tool steels such as H13 high temperature die steel can be used for softer workpiece materials like aluminum, magnesium and copper; but for stainless and low-alloy steels, nickel alloys and titanium alloys, more exotic tool materials are required [18] [19]. These must be able to maintain their properties at very high temperatures and are therefore made from materials like: nickel and cobalt superalloys, refractory metals (molybdenum, niobium, tantalum), carbides, and

polycrystalline cubic boron nitride [18]. These materials are very expensive and have limited lifespans for welding hard workpieces, so a thorough cost analysis is required when selecting a material. Since the present study focuses on aluminum workpieces; a simple and inexpensive H13 steel was used for the tooling.

Travel speed, or welding speed, refers to the speed at which the tool is moved through the workpiece. It is an important parameter as it will affect the heat input to the weld. The literature indicates a trend of faster welding speeds producing a colder weld and a narrower HAZ, which typically results in greater joint strengths [6] [7] [20] – this further benefits the use of FSW in an industrial setting, as manufacturers are interested in faster turnover times to increase production. A travel speed that is too rapid, however, may not generate enough heat, leading to insufficient mixing of the workpiece metal and the formation voids in the stir zone [5] [13]. The maximum possible travel speed that will produce an acceptable weld is also dependent on a number of other parameters, such as the size and shape of the tool, the rotational speed, as well as the thickness and material of the workpiece. Travel speeds in FSW can range from 20mm/min [21] to as fast as 6m/min [22] in some industrial settings. In general, FSW speeds in single pass welds of thin sheets (as thin as 0.5mm) are comparable to fusion welding speeds [13]; and for thicker workpieces can be even faster than fusion welding, since only a single pass is required for FSW. During FSW of thin sheet aluminum alloys, typical speeds of up to around 1m/min have been reported [23], with most studies considering speeds which fall in the rage of 100 to 500mm/min [16] [24] [25] [26] [27] [28].

The tool rotational speed is another major parameter that influences heat input to the FSW. In general, the existing literature shows that a faster rotational speed leads to increased heat input and a larger degree of deformation and mixing in the weld [7] [20]. Higher temperatures in the FSW are typically not desirable, as they will lead to an enlarged HAZ and more precipitate dissolution in

aluminum alloys. More mixing, on the other hand, is desired in the FSW, as it will yield a larger weld nugget and stronger joint. The rotational speed will vary greatly depending on the size of the tool, the workpiece material and the desired travel speed, but common values in existing studies of aluminum FSW lie between 500 and 1500 rpm [16] [24] [25] [26] [27] [28], with the majority of studies using speeds around 1200 rpm [7] [20].

A balance must be found between rotational speed and travel speed, so that a sufficiently large stir zone is created while minimizing the size of the HAZ and preventing voids in the weld. The ratio of tool rotations to tool travel speed is called the pitch, usually expressed at the distance of tool advanced per rotation, and it is used to describe the amount of mixing in the FSW. Excessively high pitch will result in wormhole formation at the base of the weld and inadequate flow of softened metal, but has also been shown to produce narrower softened regions in the HAZ [13].

Tool angle refers to the small degree of tilt, backward from the vertical axis (or upward from the horizontal plane of the workpiece), normally imposed on the FSW tool. The chosen angle is typically between 1^{o} and 3^{o} [6] [18], so that the rear of the tool contacts the workpiece before the leading edge of the tool. It has been shown that this small angle provides increased pressure slightly behind the tool, which helps to consolidate the softened metal of the workpiece as the tool passes through [5].

The plunge depth refers to the vertical distance that the tool is driven into the workpiece before it begins to travel laterally. This parameter is highly dependent on the geometry of the workpieces and the tool. Typically, the tool is designed so that the shoulder will contact the top surface of the workpiece when the tip of the pin is around 80% to 90% through the thickness of the workpiece (for lap welds this refers to the total thickness of both sheets) [7]. From the point at which the shoulder makes contact with the workpiece, it is typically plunged another 0.1mm into the surface, so that it will generate frictional heat and apply axial pressure during welding. Using insufficient plunge depth will result in large

gaps of unconsolidated metal in the weld (as there was insufficient force applied to forge the softened workpieces), while too high a plunge depth can result in sheet thinning and excessive flash formation as the metal in front of the tool is pushed out to either side; or in the worst case, plunging the pin completely through the workpiece entirely and creating a hole.

Perhaps the most complex welding parameter for FSW is the geometry of the welding tool – comprising the size, shape and features of the shoulder and the pin. A FSW tool can be divided into two sections: a larger diameter shoulder and a smaller diameter pin that protrudes from the end of the tool. The purpose of the shoulder is to contact the workpiece, generating frictional heat and providing forging pressure during welding. The pin protrudes from shoulder and is driven into the workpiece to deform and stir the workpiece material. Over years of experimentation with FSW, it has been found that the majority of results have been obtained with a shoulder to pin diameter ratio of approximately 2.6 [18] [19], though this can vary slightly depending on workpiece material and other features on the tool. The actual diameter of the shoulder and pin are chosen based on the size and material of the workpieces – thicker sheets and stronger alloys will require more heat input, so larger diameters are used; as well as the desired travel speed – faster travel speeds will generally require more heat input in order to achieve sufficient mixing. Features on the shoulder and pin can significantly affect the material behaviour during welding and the final joint properties. The shoulder geometry can broadly be broken down into three categories: outer-surface shape, end-surface shape and end-surface features, illustrated in Figure 9 [18].

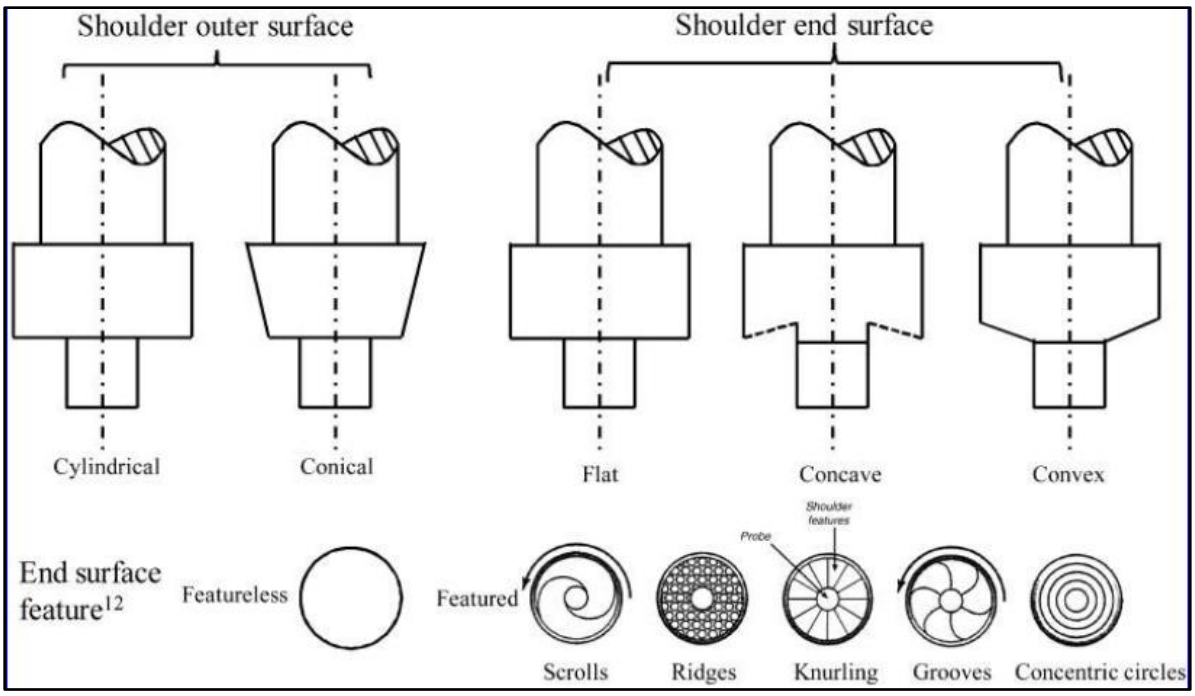

Figure 9: Examples of different designs for the FSW tool shoulder [18]

The shape of the end-surface can be flat, concave or convex. While the flat surface is easy to manufacture, it may create excessive flash during welding since it pushes the softened material away from the tool. A concave shoulder design is advantageous because it is able to trap the flowing metal during welding while still applying the requisite forging pressure to the weld. As the tool moves forward, new material fills the reservoir created by the shoulder, and the existing material is pushed down into the FSW [18]. A convex shoulder is vulnerable to the same problems as a flat shoulder because it will push material away from the pin; however, it can be advantageous in some sheet combinations where the workpieces have differences in thickness or surface roughness, as the narrowing shape will allow the tool to make sufficient contact with the workpiece. End-surface features refer to any shapes or designs on the underside of the shoulder, such as: scrolls, ridges, grooves, concentric circles, etc. Typically, these features are included to improve the flow of the metal or increase the frictional heating during welding [18]. Scrolls that spiral toward the tool center are perhaps the most common feature, and are used to promote material flow from the edge toward the central pin. These scrolls have also been shown to

reduce flash and suppress the undercut defect [18]. There are a great number of different features that incorporated into the geometry of the pin. The most common include: a domed tip; a taper angle (giving a conical or frustum shape); flutes or threads along the surface; flats ground into the sides of the pin. These, along with many others, are shown in Figure 10 [18].

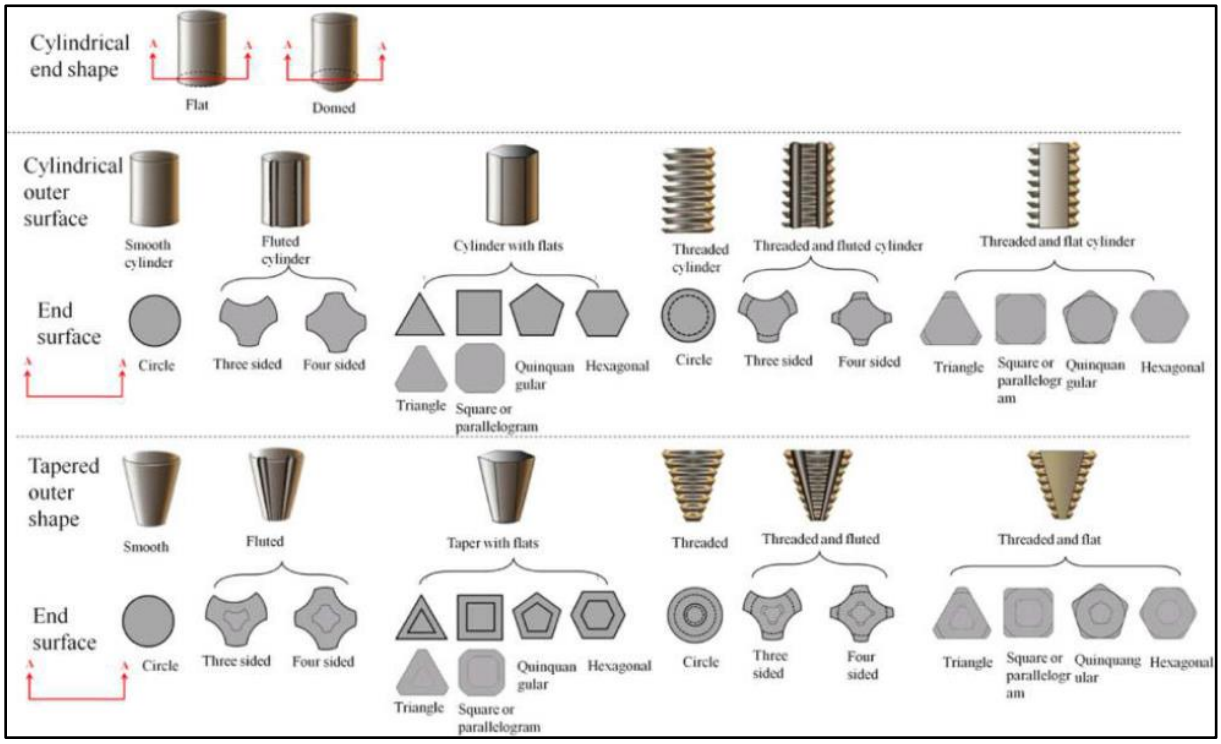

Figure 10: Examples of different designs for the FSW tool pin [18]

A domed tip is used to reduce the forces on the tool during plunging and subsequent welding, which improves the longevity of the tool. A tapered tool profile (rather than a simple cylinder) is advantageous when joining thick workpieces because of increased frictional heating as a result of the larger contact area between the pin and the workpiece [18]. Some studies have also shown that a tapered pin shape creates high hydrostatic pressure in the weld zone, which improves plastic deformation and mixing. Flats, threads and flutes are all commonly used features that increase the "swept volume" of the weld – that is: the ratio of the volume displaced by the pin to the volume of the pin itself – for which a higher value is desirable because it represents better material mixing and

dispersion of surface oxides through the weld area [13]. Threads and flutes achieve this by trapping the softened material and drawing it downward to be circulated and deposited behind the tool; while flats act as paddles that increase turbulence and push more material behind the tool. Flats have also been shown to decrease the transverse force acting on the tool during welding, improving tool life; however they also create higher temperatures in the weld area [18]

Notable to the work discussed in this thesis, is the fact that special tool designs have been considered for use in lap FSW because of the challenges inherent to this joint configuration – namely: the formation of the hook defect, and the difficulty in breaking up surface oxides at the sheet interface [18]. The unique tool geometries that have been developed for lap FSW are shown in Figure 11. A flared pin uses an outward taper angle to give a pin that is wider at the tip than at the base (the opposite of the tapered profile described previously), and a "skewed" pin places the center-axis of the pin at an inclined angle with respect to the center-axis of the tool shoulder and the machine spindle [18].

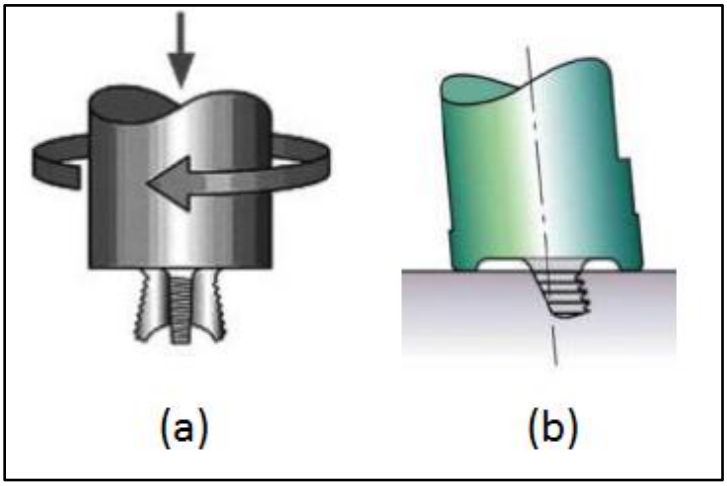

Figure 11: Flared pin (a) and skewed pin (b) geometries designed for overlap FSW applications [18]

The purpose of these designs are to generate a larger swept volume near the center and bottom of the weld area – which promote breakup and mixing of surface oxides at the sheet interface, and yield a larger weld nugget, thereby reducing the detrimental effects of the hook defect. Some researchers

have also explored using non-helical threads (in essence, concentric grooves along the outer surface of the pin) in order to reduce the vertical motion of material during welding and minimize the size of the hook. There are many other tool geometry designs that exist, for both lap and butt FSW, however they are not directly related to the work in this study, and will not be discussed for the sake of brevity.

3.3 Review of FSW Lap Joining of Thin Sheets

The FSW process has existed for 25 years, however there is relatively little published literature due to patents on the process that have limited academic research. In recent years these patents have begun to expire and there have been a large number of studies on FSW – the majority of which examine welding of popular aluminum alloys (AA6061, AA2024, AA7075, etc.) welded in the butt configuration, as this is most common in industry and therefore of greater concern. There are far fewer articles that relate directly to the present work – i.e.: ones that discuss lap FSW, joining of very thin sheets, and FSW of dissimilar aluminum alloys. Mishra [6] summarized the dissimilar FSW studies available in published literature in a review paper, and this is shown in Table 1.

Table 1: Summary of published studies on dissimilar FSW of aluminum alloys [6]

Material Combination	Plate Thickness (mm)	Rotation Rate (rpm)	Travel Speed (mm/min)	Reference
AA2024 to AA6061	6.0	400-1200	60	Li et al. [29] [30]
AA6061 to AA2024	12.7	637	133	Ouyang [31]
AA2024 to AA1100	0.65	650	60	Murr et al. [32]
AA5052 to AA2017	~5.3, 3	1000, 1250	60	Kazi et al. [5] [33]
AA7075 to AA2017	~5.3, 3	1000, 1250	60	Kazi et al. [5] [33]
AA7X1X (Sc) to AA7X5X (Sc)	~5.3	1000	60	Murr et al. [33]
AA7075 to AA2017	3	1250	60	Kazi et al. [5]
AA7075 to AA1100	3	1250	60	Kazi et al. [5]
AA5083 to AA6082	5.0	-	170-500	Larsson et al [34]
AA2024 to D357	-	-	-	Lederich et al. [5]
AA6061 to A356	4.0	1600	87-267	Lee at al. [35] [36] [37]
AA2024 to AA7075	25.4	150-200	76.2-127	Baumann et al. [35]
AA6016-T4 to AA5182-H111	1	1120	320	Leitao et al. [38]

Of the studies that have been published, the focus is typically on material flow and how the dissimilar materials interact rather than the optimization of parameters, and therefore much of the work listed above presents welds riddled with defects. Furthermore, it should be noted that the majority of the existing literature examines FSW in the butt configuration, rather than the lap configuration; and there are currently no papers that specifically examine lap FSW of thin sheet AA7075-T6 to AA6022-T4. That being said, these papers are still relevant to the work discussed in this thesis as they provide a starting point for the selection of some welding parameters and help to validate some preliminary experimental results. Additionally, they present general trends of weld microstructure, precipitation behaviour, and joint performance when process parameters are changed.

The following section will review some literature that is of particular relevance to this project. The types of alloys, measurements, and observations presented in these papers all help to explain the results from experiments carried out in this thesis

3.1.1 Relevant literature in FSW of AA6xxx series alloys

A 1999 study [17] examined AA6022 using differential scanning calorimetry (DSC) to monitor the precipitation evolution of the alloy. While not directly related to FSW, the results are helpful in understanding the behaviour of the 6022 alloy used for the experiments in this thesis. The suggested precipitation sequence in the AA6022 alloy is the following [17]:

SSSS -> GP Zones -> needle-like β'' -> rod-like β' + lath-like precipitates -> β + Si of various morphologies

A temperature of 95^{o}C corresponded to the formation of GP zones; 240^{o}C to the precipitation of β''; 290^{o}C to the precipitation of β'; and 335^{o}C to the precipitation of β and Si; with β'' acting as the primary strengthening phase [17]. The researchers also examined the effects of an artificial ageing process that would imitate a paint-bake cycle commonly used in the automotive industry – heating the

samples to 175°C for 20 minutes. Specimens that were naturally aged before the paint-bake cycle yielded a lower hardness than the samples that were not naturally aged before the paint-bake cycle, though both groups showed an increase in hardness after undergoing the paint-bake cycle, and neither group reached a peak-aged condition [17].

One group [39] studied an AA6005-T6 alloy that was FSW and naturally aged for 4 different lengths of time – 1 hour, 1 day, 4 weeks, and 6 months. Temperatures in the weld ranged from 200 to 360°C in the HAZ; 360 to 480°C in the TMAZ, and 480 to 520°C in the SZ. Temperatures in the SZ were high enough to cause dissolution of all precipitates. Thermal cycles in the TMAZ resulted in the dissolution of metastable β' and Q' phases (which provide small amounts of strengthening), and the precipitation of stable β particles [39]. In the HAZ, the elevated temperatures caused coarsening and dissolution of the existing β'', as well as the precipitation of Q' and β'. The post-weld natural ageing process showed that a longer ageing time resulted in a higher degree of hardness recovery in the weld. The minimum hardness values were observed in the TMAZ and the HAZ nearest to the stir zone boundary (approximately 4mm from the weld centerline). The hardness minima are located in this region because temperatures here were ideal for the formation of the stable β phase, which is known to provide little strengthening [39]. Since most of the solute in this area is in a stable phase, very little re-precipitation of strengthening particles is achieved through natural ageing. In the SZ, the dissolution of all particles allows for solute to re-precipitate as β'' and β' phases over the course of natural ageing. In the HAZ, lower peak temperatures coarsened the ideal strengthening particles and formed secondary strengthening particles, yielding a moderate hardness that is less than the peak-aged hardness of the base metal [39]. Table 2 and Figure 12 show the temperatures experiences in each zone of the FSW and how they correspond to the precipitation evolution temperatures typical of Al-Mg-Si systems. Note that in Figure 12, the temperatures at the weld centerline (0 on the x-axis) are not actual data points, but interpolations based on other measurements around the weld.

Table 2: Precipitate evolution in AA-6005A compared to temperatures in experienced in different FSW zones

---------> Increasing Temperature (°C) --------->					
HAZ			**TMAZ**		**SZ**
220 – 250°C	250 – 320°C	~290°C	400 - 480°C	~480°C	~502°C
β'' coarsening and dissolution	β'' -> β' transformation	Q' precipitation	β' and Q' dissolution	Stable β precipitation	Stable β dissolution

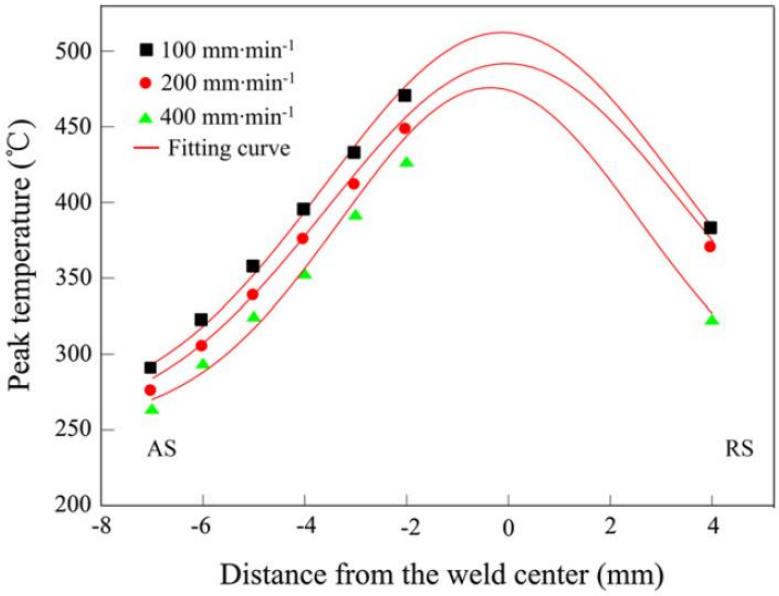

Figure 12: Temperature profiles through the FSW at different welding speeds [39]

Figure 13 shows a comparison between the SZ and the HAZ of the FSW AA6005 alloy. An absence of strengthening particles is observed in the SZ after welding, which corresponds to the temperatures that were recorded in this zone. In the HAZ, there was no dissolution of precipitates, but coarsening and the formation of Q' and β' particles is clearly observed.

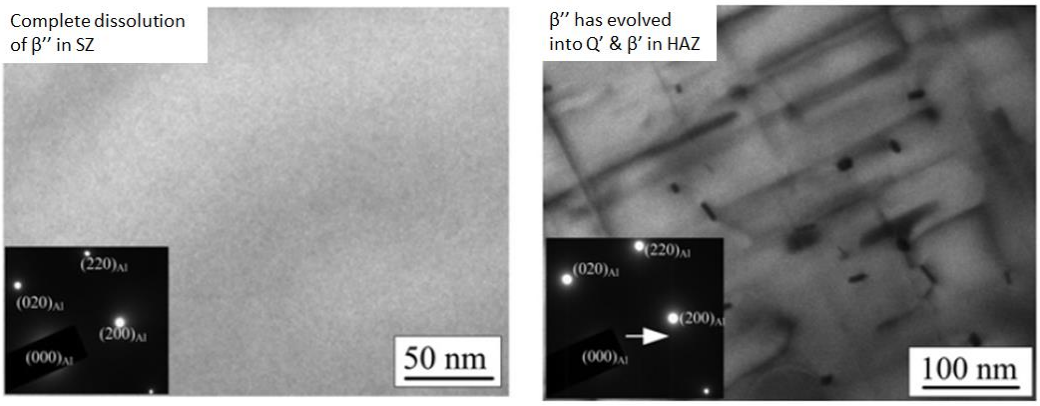

Figure 13: Comparison of precipitate evolution in the SZ (left) to the HAZ (right) [39]

Another study [27] considered the effect of a post-weld heat treatment (PWHT) on the microstructures of AA6061-T6 alloy. They performed welds on the alloy in annealed (O) and peak-aged (T6) temper conditions and found that hardness values increased by ~13 HV in non-PWHT samples (i.e.: brief natural age) and by ~70 HV in PWHT samples [27]. Figure 14 shows the hardness profiles of the welds in both temper conditions before and after the PWHT.

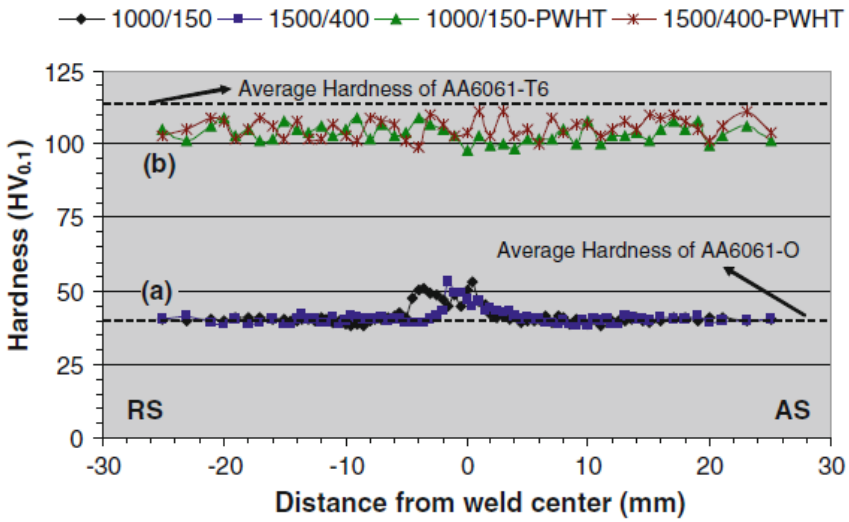

Figure 14: Hardness profiles across the FSW for AA6061-O and AA6061-T6 [27]

A study by C. Jonckheere et al in 2012 studied butt FSW of AA6061-T6 to AA2014-T6 [28]. The tool used had a 15mm diameter shoulder with a scroll end-feature, 5mm diameter straight pin with

threads and 3 flats. The workpieces were relatively thick at 4.7mm. The rotational speeds used were 500rpm and 1500rpm, and the welding speed was set at 90mm/min. Temperatures in the weld zone were recorded, and it was found that higher rotational speeds of the tool led to higher temperatures in the weld; with a maximum temperature of ~425^{o}C at 6mm from the centerline at 500rpm, and a maximum temperature of ~475^{o}C at 6mm from the centerline at 1500rpm. The minimum hardness value (~60HV) was located ~7.5mm from the weld centerline in the samples that were welded at 1500rpm. The hardness returned to the base metal value (~120HV) at ~20mm from the weld center, and the average hardness through the SZ was measured as ~80VH [28]. The softest areas of the weld were those areas that were subjected to temperatures that correspond to the dissolution temperatures of the major strengthening precipitates [28]. The temperature and hardness profiles in Figure 15 and Figure 16 for the various FSW conditions illustrate the direct correlation between peak temperatures and softening in the HAZ.

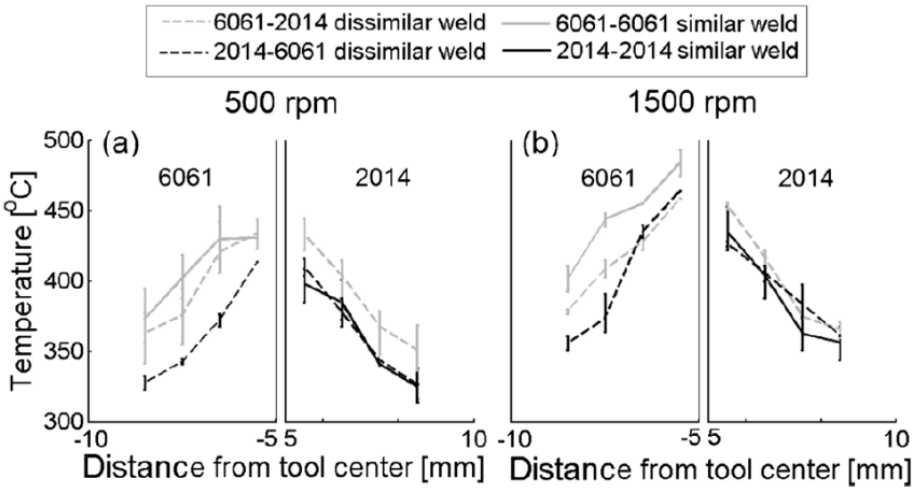

Figure 15: Temperature measurements through the FSW for AA6061 and AA2014 alloys [28]

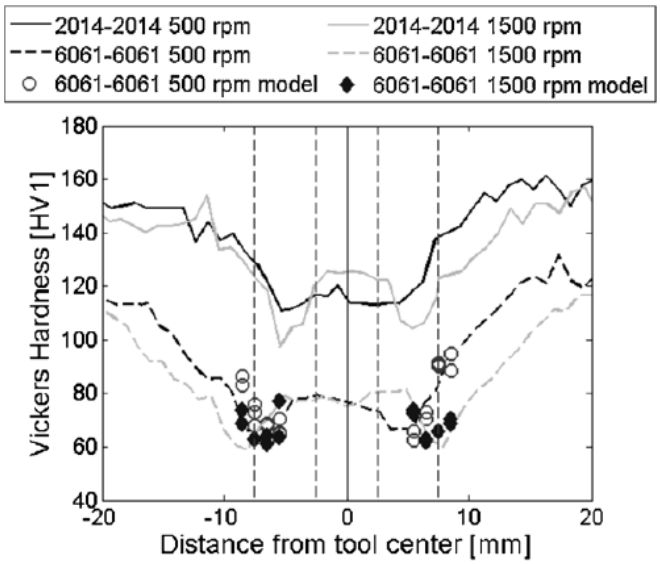

Figure 16: Hardness profiles through the FSW for AA6061 and AA2014 alloys [28]

Relatively few studies have looked at the overlap shear properties of FSW joints. In general, the published work shows that joint strength is evaluated through overlap shear pull tests [23] [40], in which thin strips are cut from the weld and pulled using a tensile testing machine. An example of this is shown in Figure 17.

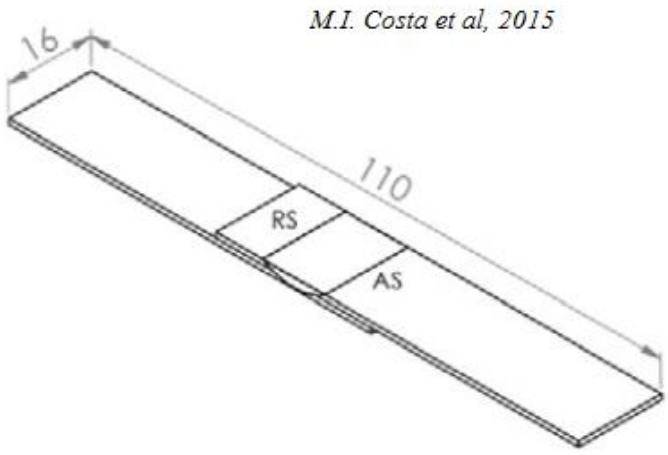

Figure 17: Example of an overlap shear test specimen cut from a long FSW joint [40]

Joint strengths are quantified by the maximum force at fracture, but this is highly dependent on the width of the specimens, the composition of material, and the thickness of the sheet. One study of AA6082 [23] showed a trend of stronger joints when faster travel speeds and tools with fewer features were used. A different study [40] showed that altering the width and profile of the pin (cylindrical vs. conical) will affect the joint strengths, with their results indicating that a larger diameter conical pin produced the strongest FSW joints.

3.1.2 Relevant literature in FSW of AA7xxx series alloys

A recent study [41] examined the effects of FSW on the well-known AA7075-T6 alloy and obtained data on weld thermal cycles and microhardness. Temperatures were measured at 2mm and 5mm from the weld centerline on either side of the weld. The temperature at 2mm from the weld reached a maximum value of 440°C, while temperatures 5mm from the weld reached a maximum of 340°C. It is known that temperatures above 450°C rapidly lead to complete dissolution of strengthening precipitates [41]. Slightly lower temperatures (in the range of 400 to 500°C) result in coarsening and dissolution of only some precipitates [41], where the base metal microhardness was measured as 170HV, while the highest hardness value across the weld profile was located in the SZ (172HV) and the lowest hardness value was located in the TMAZ (121HV) [41]. The authors attribute the high hardness value in the SZ to the dissolution of precipitates followed by the re-precipitation of strengthening particles during natural ageing following the FSW process [41]. The softening observed in the TMAZ and HAZ is attributed to the coarsening of particles with negligible dissolution, meaning that little solute is available to re-precipitate any fine strengthening particles during natural ageing [41]. Figure 18 shows the thermal cycle for one of the many welds performed during the research, with the A1 and A2 corresponding to thermocouple locations of 2mm and 5mm, respectively, on the advancing side of the weld; while R1 and R2 correspond to thermocouple locations of 2mm and 5mm, respectively, on the

retreating side of the weld. Figure 19 shows an optical micrograph of the base metal which reveals evidence of coarser strengthening precipitates.

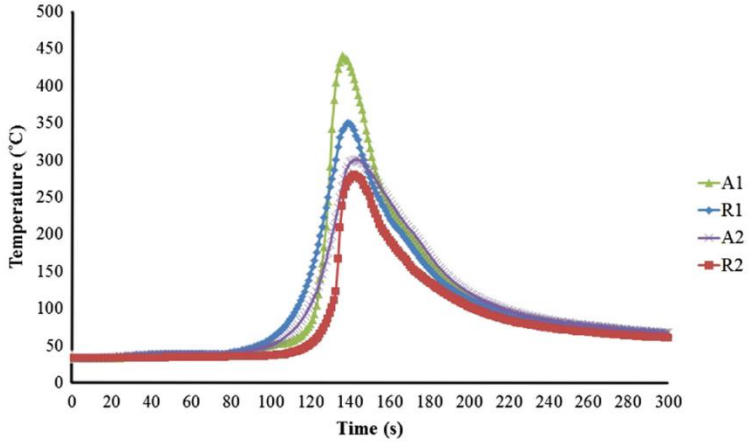

Figure 18: Thermal cycle for an AA7075-T6 FSW sample. The different curves correspond to thermocouples in different locations in the weld [41]

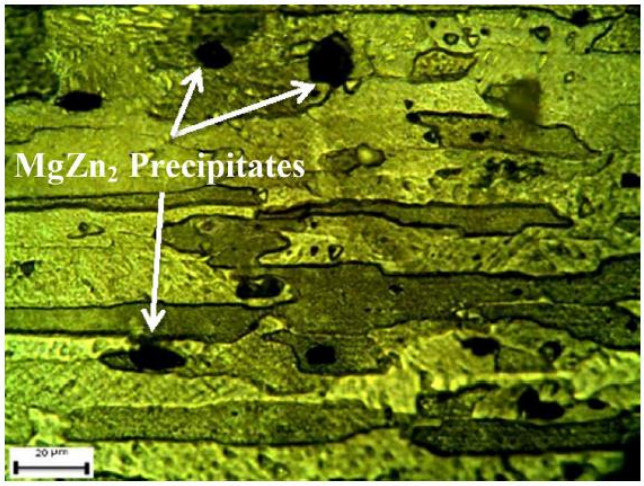

Figure 19: Microstructure of the 7075-T6 base metal with visible precipitates of η' phase [41]

A different study [11] performed experiments on AA-7039 alloy in initial temper conditions of T6, W, and O conditions (peak-aged, naturally aged and annealed, respectively). It was found that the $MgZn_2$ particles (η') responsible for strengthening were more numerous in the TMAZ of welds performed in the -T6 temper, while conversely, the HAZ of -T6 welds contained fewer η' particles than in the other two conditions [11]. Furthermore, the particles in the HAZ of the -T6 weld were coarser than

in the other welds. Hardness measurements shown in Figure 20 were used to assess the precipitate evolution after FSW. The -T6 welds showed the highest average hardness both in the base metal (135HV) and the SZ (115HV); however the -O joints exhibited a significant hardness increase after welding, from a base metal value of 65HV to a SZ value of 104HV. The hardness minimum in the -T6 joint was observed in the HAZ (89HV); the hardness minimum in the -W joint was observed in the SZ (93HV); and the hardness minimum in the -O joint was observed in the base metal (75HV) [11]. In all cases, the maximum hardness was observed in the TMAZ (~140VH for -T6 and ~125 for -O and -W), which is very different from the trend in 6xxx alloys. These results are attributed to the fact that existing η' particles in a peak-aged alloy will be dissolved by the heat input and subsequently re-precipitate as strengthening particles during natural ageing. On the other hand, during FSW of 7xxx Al in the -W condition, the existing GP(II) zones are simply transformed into stable η precipitates and then coarsened, resulting in a lower hardness and without a chance to re-precipitate upon subsequent natural ageing. The sharp drop in hardness in the HAZ is explained by the coarsening of η precipitates [11].

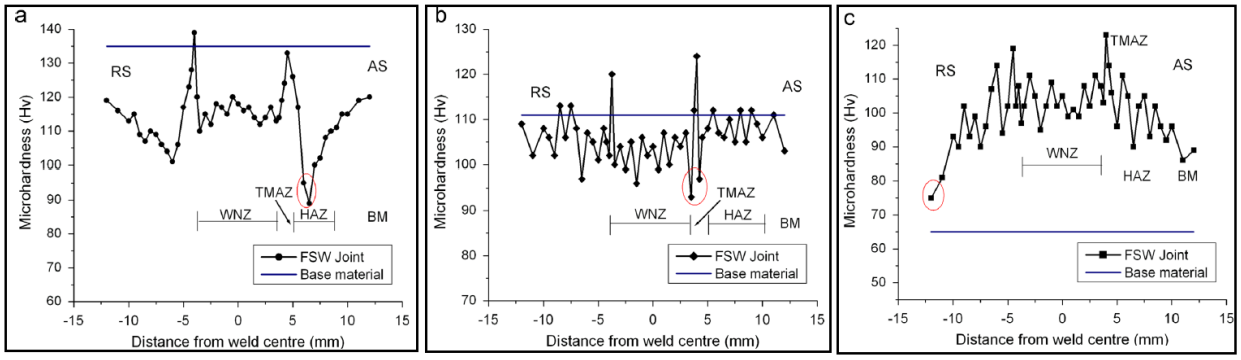

Figure 20: Hardness profiles for the FSW of AA7039 in the (a) T6 (b) W and (c) O temper conditions [11]

The existing studies of FSW for 6xxx and 7xxx alloys have examined the evolution of strengthening particles during welding and subsequent PWHT by the use of TEM microscopy and microhardness profiles. Some thermal measurements have also been made, though typically these measurements provide limited and scattered information. This is likely due to the fact that it is difficult

to embed thermocouples in the rotating tool, and nearly equally difficult to embed thermocouples in the weld metal without damaging them during the FSW process. In general, the trends show that the temperatures in the SZ are high enough to cause dissolution of major strengthening precipitates; and temperatures in the HAZ are sufficient to cause coarsening of these particles, or the precipitation of the stable phase. The hardness distribution in joints made between alloys in the -T6 temper condition exhibited a W-shaped profile, with the hardness minima in the TMAZ and or interface between the SZ and HAZ regions, and an intermediate hardness value observed across the SZ. The majority of existing literature focuses on butt FSW involving the common AA6061 and AA7075 alloys, with only a few individual studies examining more niche 6xxx and 7xxx alloys, and even fewer studies focusing on FSW performed in the lap configuration.

4.0 Experimental Methods

This research investigates the effect of different tool geometries and travel speeds on the properties of the resulting friction stir weld. FSW was performed on aluminum alloy sheets in the lap configuration with 5 unique tool geometries. A preliminary study was first carried out on similar FSW of AA7075-T6 material. The main focus of the research was the study of dissimilar FSW between AA7075-T6 and AA6022-T4.

4.1 Materials

The compositions of the alloys were confirmed using x-ray fluorescence (XRF) with the values given in Table 3.

Table 3: Composition of the AA7075-T6 and 6022-T4 sheet base material

Alloy	Zn	Mg	Cu	Fe	Cr	Si	Mn	Ti	Al
AA7075-T6	5.41	2.38	1.51	0.25	0.19	0.07	0.02	0.02	Balance
AA6022-T4	<0.01	0.56	0.06	0.13	0.03	0.66	0.07	0.03	Balance

For the similar FSW, two 610mm long x 76mm wide x 2mm thick sheets of AA7075-T6 were joined by FSW in a lap configuration with the joint along the transverse direction. For the dissimilar FSW, one 610mm long x 76mm wide x 2mm thick sheet of AA7075-T6 and one 610mm long x 76mm wide x 0.9mm thick sheet of AA6022-T4 were joined by FSW in a lap configuration with the joint along the transverse direction. The base metal properties were characterized by colleagues at Queen's University [42] and are summarized in Table 4 and Table 5.

Table 4: Base metal properties of AA7075-T6 sheet

AA7075-T6	Rolling Direction	Transverse Direction	45° to Rolling Direction
Elastic Modulus (GPa)	70.4	70.2	65.6
0.02% Yield Strength (MPa)	529.1	499.3	472.1
Considère Strain	0.112	0.116	0.103

Table 5: Base metal properties of AA6022-T4 sheet

AA6022-T4	Rolling Direction	Transverse Direction	45° to Rolling Direction
Elastic Modulus (GPa)	67.3	64.4	66.9
0.02% Yield Strength (MPa)	140.6	129.2	134.6
Considère Strain	0.193	0.183	0.233

4.2 Parameter Selection

Five different tool designs were used for this research. The major dimensions were kept identical between each tool design, with small alterations being made to the shape and features on the pin of each tool, as shown in Figure 21 (full drawings of the tools can be seen in Appendix A – FSW Tool Drawings). For the remainder of the thesis, the tools will be referred to as Tool1 through Tool5. Tool1 has a straight cylindrical pin with an M6 thread. Tool2 has a 10° tapered cylindrical pin with an M6 thread. Tool3 has a 10° tapered cylindrical pin with an M6 thread and three flat faces. Tool4 has a 10° tapered cylindrical pin and three flat faces (no threads). Tool5 has a 10° tapered pin and straight grooves that follow the profile of an M6 thread, but are non-helical. A shoulder diameter of 15mm, shoulder concavity of 8°, pin length of 2.8mm, and maximum pin diameter of 6mm is the same for all 5 tools. The major dimensions of the shoulder and pin were selected based on tool geometries that are common in existing FSW [5] [7] as these are known to produce welds without defects such as internal weld voids. The pin geometries on Tool1, Tool2, and Tool3 are also commonly seen in the literature [13] [18] for butt FSW of aluminum alloys. There is a limited amount of available literature on lap FSW of thin

aluminum sheets, so this work compares these three common designs for their effectiveness in lap FSW. While there are some studies that examine the use of more complex tool geometries (such as skewed or flared pins, as described in the previous section) to improve the quality of lap FSW, it was decided that the equipment available in the lab was unsuited to using these types of designs, as the resulting forces on the FSW machine would be too great. The Tool4 and Tool5 pin geometries were designed to explore ways to reduce the size of the hook feature that is common in lap FSW. Other welding parameters were also selected based on values commonly seen in the literature that have been shown to produce good quality FSW joints. Travel speeds of 125, 180, 250, 355, 500mm/min were used – which encompassed a wide range of the values seen in the literature (see Table 1). Tool tilt angle and rotational speed were kept constant at 2.5^{o} and 1120rpm, respectively, due to these being commonly used settings in the literature (see Table 1). While many studies vary the travel speed as well as the rotational speed, time constraints only allowed for the variation of travel speed and tool geometry in this research.

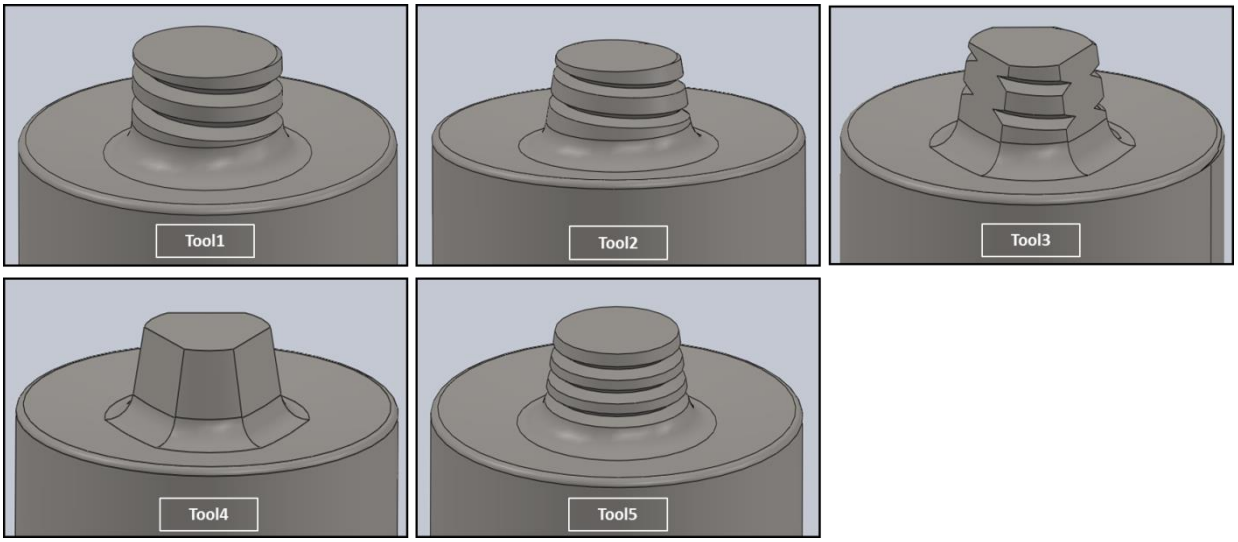

Figure 21: Tool geometries examined in the present work.

4.3 Equipment and Test Setup

For the preliminary study of similar AA7075-T6 FSW, initial welds were made with Tool1, Tool2, and Tool3 using a travel speed of 125mm/min. Further welds were made at speeds of 180mm/min and 250mm/min, but Tool2 was withdrawn from testing at these travel speeds due to severe defect formation. Welds at higher speeds were not attempted for similar FSW. For the main study of dissimilar AA7075-T6/AA6022-T4 FSW, welds were made with all 5 tools at speeds from 125 mm/min to 500 mm/min. Only Tool4 and Tool5 showed severe defect formation at faster speeds. Overlap between the two work-pieces was approximately 20mm. Metal specimens were secured during welding by use of specially designed clamps, shown in Figure 22.

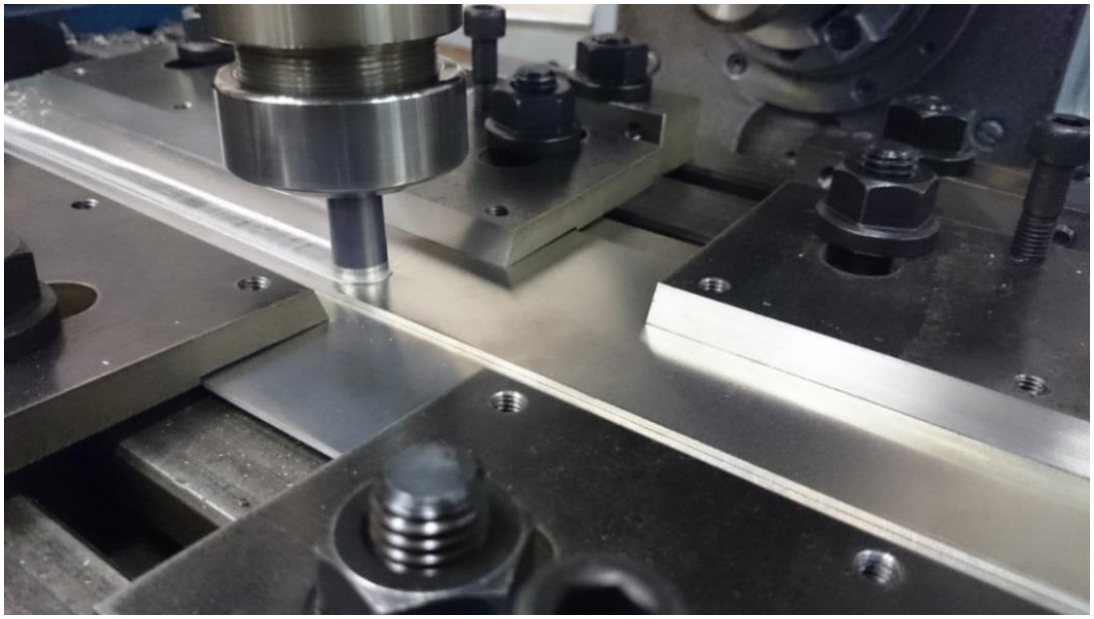

Figure 22: Clamping configuration during FSW.

Table 6 summarizes the welding conditions used during experimentation. In this table, the welds with “severe defects” are welds that showed large voids and lack of mixing on the surface of the material that was visible to the naked eye, and in some cases, would fall apart when removed from the clamping system. A “successful” weld refers to a weld that appeared to be defect-free upon visual

inspection, though there remained a potential that there could be internal defects which required cross-sectioning to verify.

Table 6: Summary of welds made

		Welding Speed (mm/min)				
		125	180	250	355	500
Similar FSW: AA7075-T6 / AA7075-T6	Tool1	Successful	Successful	Successful	Not Attempted	Not Attempted
	Tool2	Successful	Severe Defects	Severe Defects	Not Attempted	Not Attempted
	Tool3	Successful	Successful	Successful	Not Attempted	Not Attempted
	Tool4	Not Attempted	Not Attempted	Not Attempted	Not Attempted	Not Attempted
	Tool5	Not Attempted	Not Attempted	Not Attempted	Not Attempted	Not Attempted
Dissimilar FSW: AA7075-T6 (top) / AA6022-T4 (bottom)	Tool1	Successful	Successful	Successful	Successful	Successful
	Tool2	Successful	Successful	Successful	Successful	Successful
	Tool3	Successful	Successful	Successful	Successful	Successful
	Tool4	Successful	Successful	Successful	Successful	Severe Defects
	Tool5	Successful	Successful	Successful	Successful	Successful

Standard metallographic techniques were used to prepare joint cross-sections, using a polishing procedure of: 9um diamond suspension for 10 minutes on an MD-Largo polishing pad; followed by 3um diamond suspension for 5 minutes on an MD-Mol polishing pad; and final polishing with 0.3 um colloidal silica media on an MD-Chem polishing pad. Microstructures of the AA7075 alloy were revealed by etching with Keller's reagent (50mL 2% HF, 1.5mL HCl, 10mL nitric acid, 58.5mL distilled water), and observed using an Olympus BX51 microscope.

In the preliminary study of AA7075-T6 similar FSW, Vickers micro-hardness profiles were measured across the top sheet of the weld, approximately 0.5mm above the interface of the two sheets

using a load of 200gf and a 10s dwell time. In the main study of AA7075-T6/AA6022-T4 dissimilar welds, Vicker's micro-hardness profiles were measured across the bottom sheet of the weld, approximately 0.7mm below the interface of the two sheets (within the bottom sheet) using a load of 200gf and a 10s dwell time. The reason for the difference is that the AA6022 material was of interest in the dissimilar study, as the joint would fail consistently in this sheet. This will be discussed in detail in the results.

Overlap shear test specimens of the welds were water-jet cut to a 30mm width in the similar study; and to a 25mm width in the dissimilar study; and gripped using two additional spacer shims, as shown in Figure 23. The similar weld shear test specimens were deformed at a constant cross-head speed of 1mm/min until fracture using an Instron 8874 tensile test machine. The dissimilar weld shear test specimens were deformed at a constant cross-head speed of 1mm/min until fracture using a Tinius Olsen (H10KT) tensile test machine. Three repeat specimens were tested for each combination of tool geometry and travel speed.

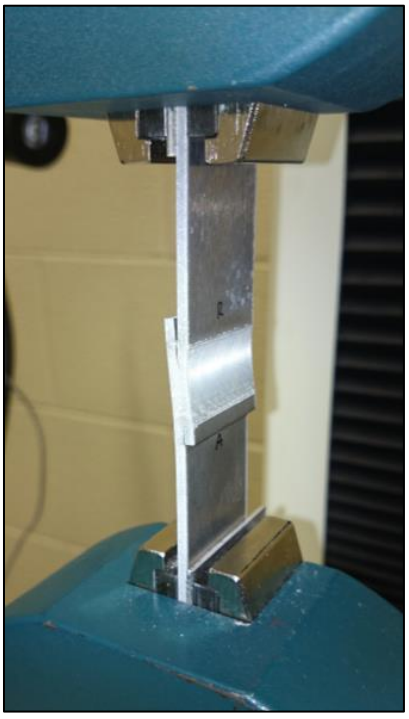

Figure 23: Overlap shear fracture testing configuration.

Temperature measurements from the weld area were obtained for the dissimilar material combination only. Omega k-type thermocouples (diameter 0.08mm) were inserted into shallow grooves that were ground into the underside of the upper workpiece. The embedded thermocouples were adhered to the workpiece using a small amount of epoxy so that they would not move during welding. Thermocouples were positioned such that there were 4 embedded in each workpiece, equally spaced, at distances of 4mm, 8mm, 12mm, and 16mm from the weld centerline. Data was collected from 4 thermocouples at a time, at a rate of 60Hz, using a National Instruments DAQ-9171 data acquisition system and National Instruments Signal Express software. A schematic diagram of the thermocouple placement is shown in Figure 24.

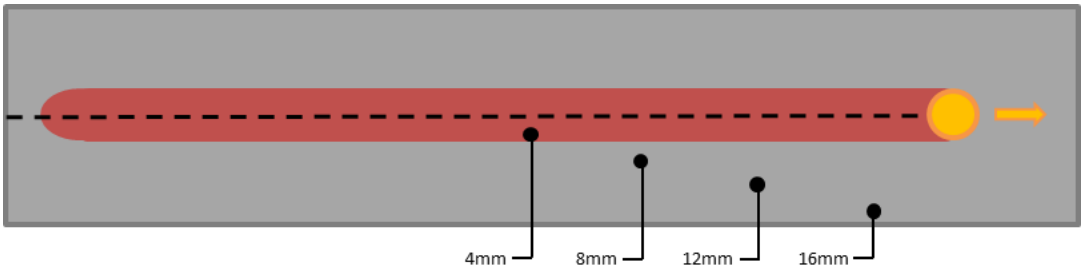

Figure 24: Schematic showing the path of the tool and positions of the thermocouples used for temperature measurements during FSW

Temperature measurements from the center of the tool were obtained for the dissimilar material combination only, and only for welds made with Tool3. A single omega k-type thermocouple (diameter 0.25mm) was inserted into a 0.3mm hole that was bored through the center of the FSW tool. The end of the thermocouple was secured using Omegabond 600 high temperature chemical set cement. An MSR 145-B wireless data acquisition system was fastened to the spindle of the FSW machine, and data was recorded at a rate of 1 Hz (the maximum of the hardware). Images of the setup are shown in Figure 25.

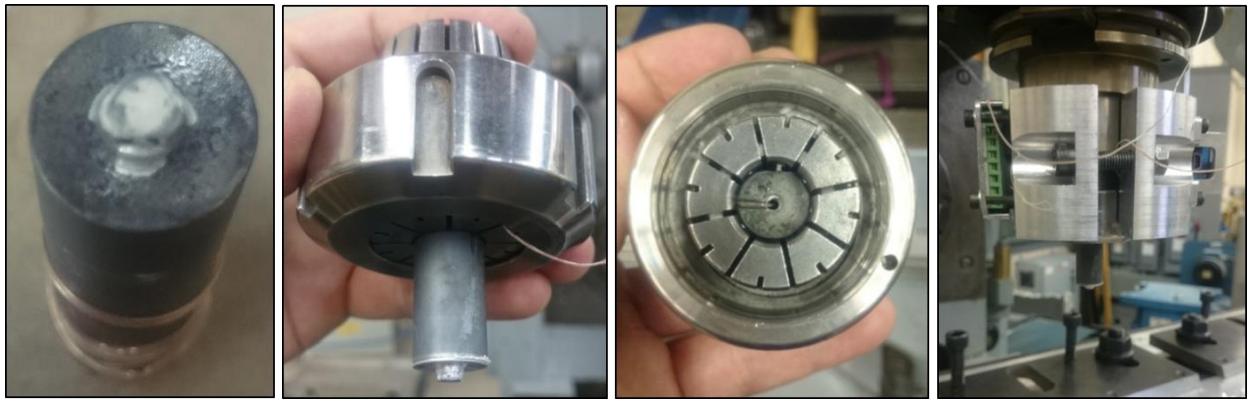

Figure 25: Tool-embedded thermocouple setup

5.0 Results and Discussion

The results and discussion will be divided into two sections: first, the results of the similar FSW; and second, the results for the dissimilar FSW.

5.1 Similar FSW

FSW was performed in the lap configuration with Tool1, Tool2, and Tool3 at 125mm/min for a layup of similar AA7075-T6; with a total workpiece thickness of 4mm (2mm per sheet). These welds were made as part of preliminary work to the main focus of the research, which would be on dissimilar welds of AA7075-T6 to AA6022-T4 (sheet thicknesses of 2mm and 1mm, respectively).

5.1.1 Optical Microscopy and Weld Microstructure

Optical micrographs of the FSW joints are shown for all three tools at a welding speed of 125mm/min in Figure 26.

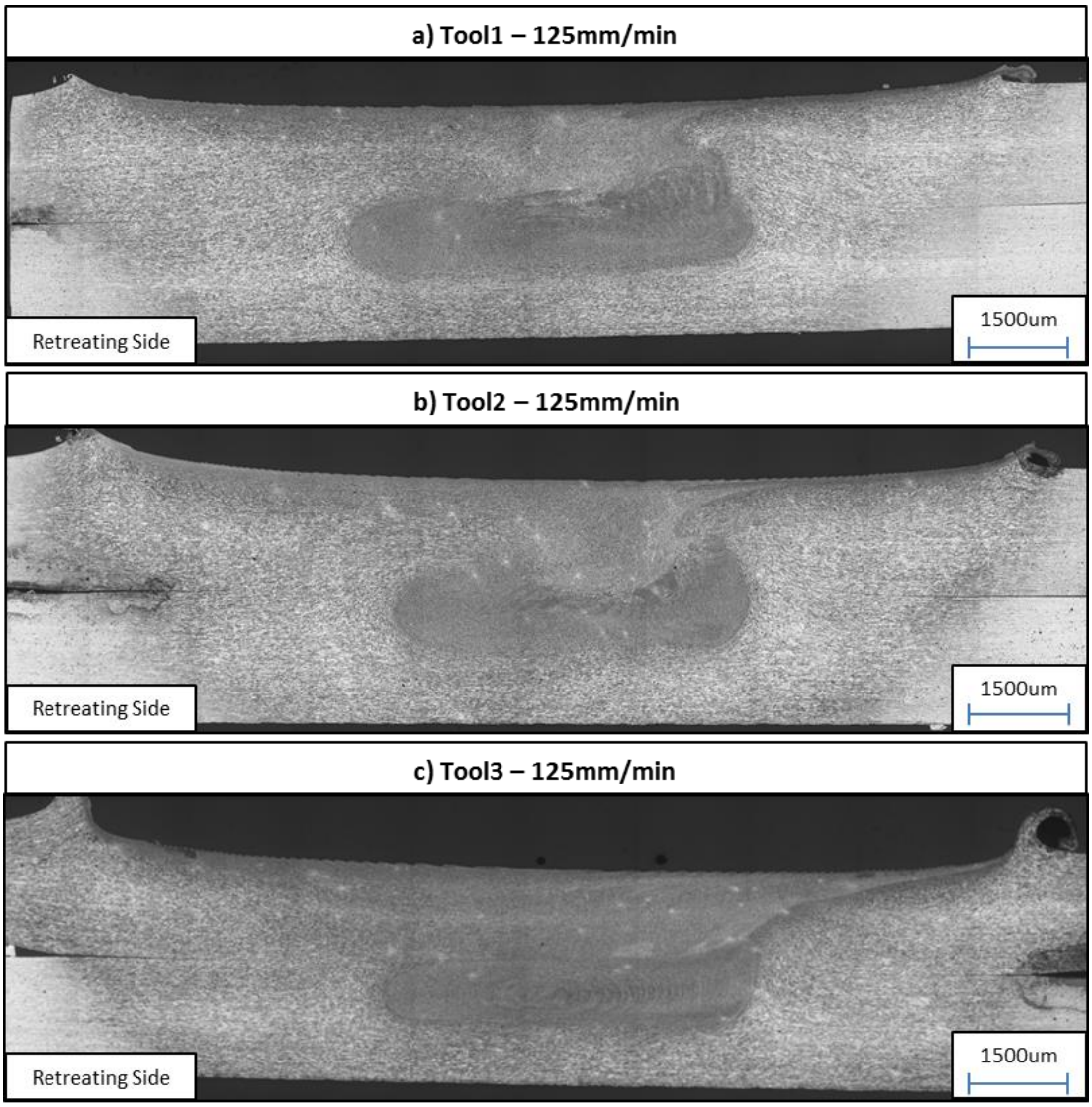

Figure 26: Cross-sectional optical micrograph images of a similar AA7075 FSW made at the following conditions: (a)Tool1-125mm/min (b)Tool2-125mm/min (c)Tool3-125mm/min

The stir zone of the FSW is the darker area that can be seen in the center of each image. This area appears darker due to the large number of refined grains that result from the geometric dynamic recrystallization process that occurs during welding. The area on either side of the stir zone that is slightly lighter in colour is indicative of the thermo-mechanically affected zone, in which the grains have undergone deformation but not dynamic recrystallization. The heat affected zone can be seen as the very light material located at the edges of each micrograph. A small amount of flash is seen in the upper

sheet, caused by the downward force applied by the tool during welding. Also notable is the presence a small gap at the interface of the two sheets that extends into the TMAZ. This interface gap ends in a 'hooking' flaw that it characteristic of lap FSW welds, and has been well documented in existing literature [21] [23]. A high magnification image of the end of the hooking flaw is shown in Figure 27, and the size of the hook in relation to the rest of the joint is revealed more clearly in images that have been etched to a lesser extent, shown in Figure 29.

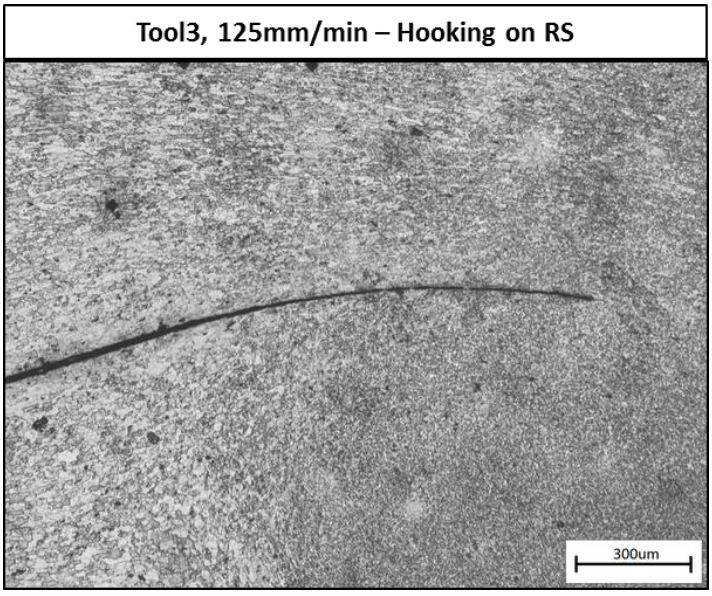

Figure 27: Image of the hooking flaw as seen on the retreating side of the similar AA7075/AA7075 FSW made under welding conditions of Tool3-125mm/min

The stir zone geometries were comparable when using Tool1 versus Tool2, since only the tool taper slightly changed between these two designs. The average grain sizes in the stir zones were measured using the line intercept method and contained equiaxed grains with average sizes measured from 4.5 to 5.5 µm, whereas the base material had pancaked shaped grains which averaged 106x28x31 µm along the normal, transverse, and rolling directions, respectively. Figure 28 shows the grain structure in the SZ, the TMAZ, and the start of the HAZ on the advancing side of a FSW. Note the drastic and immediate change in grain size and orientation as the SZ (left of the image) transitions to the TMAZ

(center of the image) and finally to the HAZ (right side of the image). The microstructural appearance of the joint is in agreement with the existing FSW literature [14] [15].

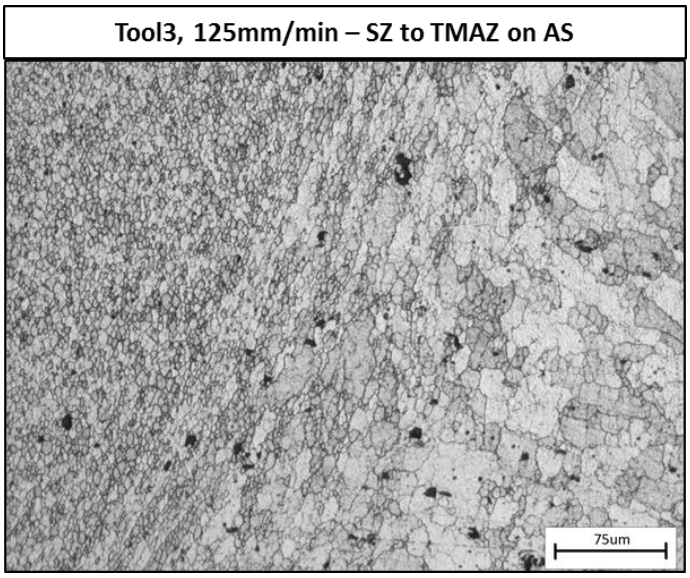

Figure 28: Image of grain structure of the advancing side of the similar AA7075/AA7075 FSW at the transition between SZ and TMAZ. Welding conditions: Tool3-125mm/min

There is a slight increase in grain refinement when the 3 flats are added to the tool that is likely related to the increased strain rate that occurs near these features, as shown in modeling work by Colegrove and Shercliff [43]. The grain size values in the weld nugget are comparable to the size ranges from 3 to 6 μm previously reported for FSW butt welds in AA7075 [14] [15] [44]. This grain refinement in the stir zone is a result of dynamic recrystallization in which even finer equiaxed grains nucleate and grow to the sizes observed in the stir zone, and this has been widely studied in prior work [45].

Similar AA7075-T6 lap FSW was performed again with Tool1, Tool2 and Tool3 at increased welding speeds of 180mm/min and 250 mm/min. When travel speeds exceeded 125 mm/min using Tool2, voids, porosity, and long sections of wormhole defects were consistently produced within the stir zone. Consequently, Tool2 was withdrawn from further study at these speeds and no optical micrograph

images were obtained. Figure 29 compares only optical micrograph images of the cross-sections of similar AA7075-T6 FSW made with Tool1 and Tool3 at speeds of 180mm/min and 250mm/min.

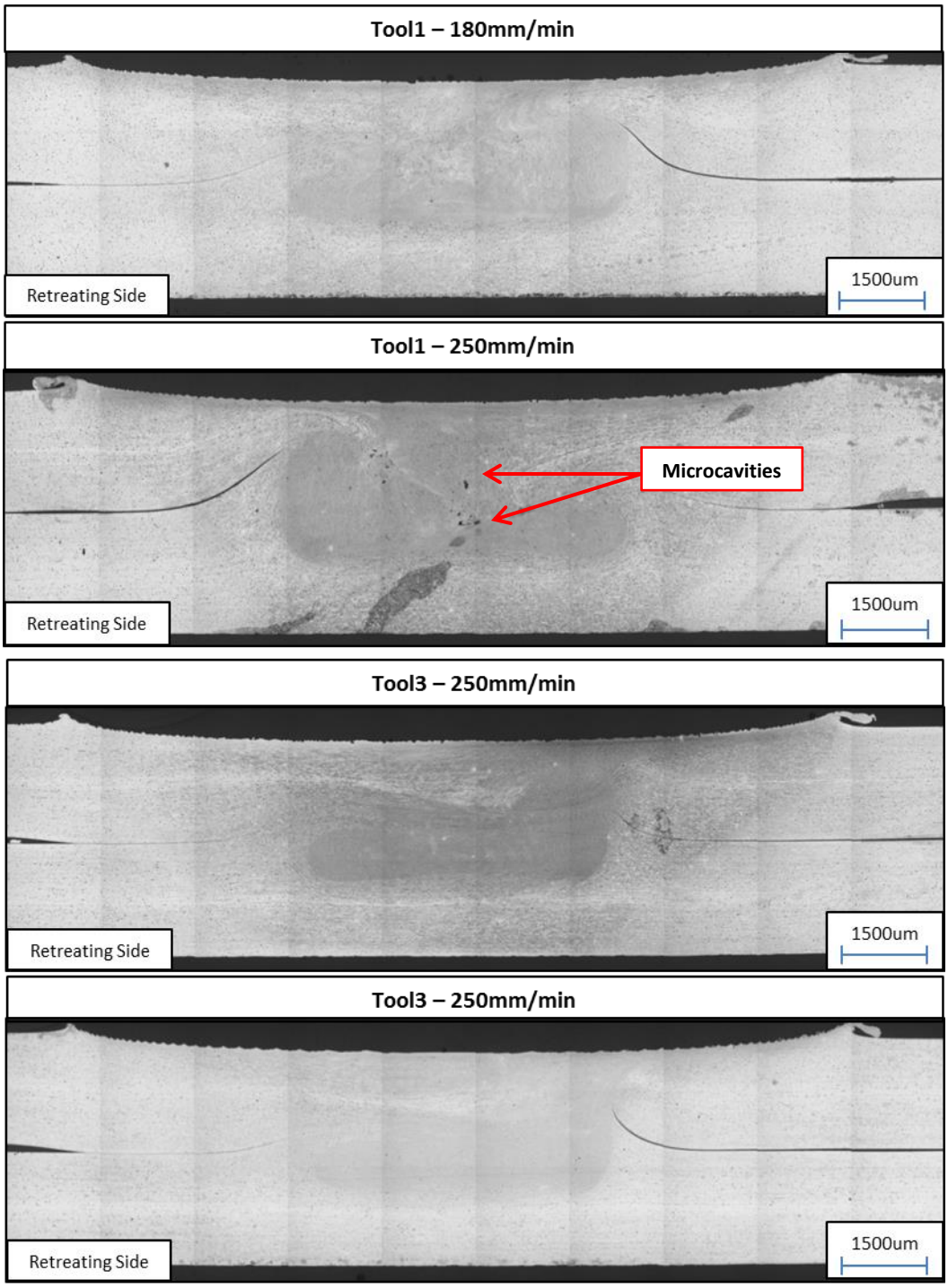

Figure 29: Optical micrograph images of a similar AA7075 FSW made at the following conditions: (a)Tool1-180mm/min (b)Tool1-250mm/min (c)Tool3-180mm/min (d)Tool3-250mm/min

In general, the SZ and TMAZ in the welds made at faster speeds are similar in size and shape to those that were seen in Figure 26. In the center of the SZ in Figure 29b, the small black features (identified by the arrows) are evidence of micro-cavities that were formed during FSW with Tool1 at 250mm/min. By contrast, Tool3 was able to form fully consolidated welds at travel speeds of both 180mm/min and 250mm/min.

The images shown in Figure 29 have been etched to a lesser degree than those shown in Figure 26, and so it is possible to clearly see the unbonded sheet interface or 'hook' feature, which extends from the workpiece interface into the upper sheet. In the case of Tool1, the hook extends to more than 1 mm into the upper sheet (see Figure 29a, Figure 29b), and this feature has been discussed in recent work [23] [21]. In the case of the Tool3 welds, the unbonded sheet interface only extends upwards by approximately 0.5 mm when 180 mm/min is applied (Figure 29c), which increases to approximately 0.85 mm when 250 mm/min is applied (Figure 29d). The projection of this unbonded interface up towards the surface of the upper sheet may facilitate premature fracture during overlap shear testing, and so there have been attempts to tailor the tool pin geometry in order to maintain a nearly flat, aligned interface across of overlapping sheets [46]. Consequently, the mechanical properties were compared in order to assess the influence of the tool geometry on joint strength.

5.1.2 Joint strength testing

Overlap shear fracture tests were performed to determine the maximum load that the FSW joints could sustain before failing. A tensile test frame was used to carry out these experiments; however, these tests differ from ordinary tensile tests because the samples were not cut into the traditional dog-bone shape. Instead, the lap welds were cut into samples of a 30mm width. Due to the shape of the lap welded joints, the applied stress during testing was not purely tensile across the welded

area. This test procedure is similar to the industry test used for resistance spot welds [47]. Three samples were tested for each welding condition; the average breaking force is shown in Figure 30.

The lap shear pull test was carried out with three repetitions on similar AA7075 lap FSW samples made with Tool1 at 125, 180 and 250mm/min; with Tool2 at 125mm/min; and with Tool3 at 125, 180 and 250 mm/min. Recall that welding with Tool2 at 180 and 250mm/min produced very poor quality joints, so these data points were not plotted. The results of the lap shear fracture tests are summarized in Figure 30, with the error bars representing 1 standard deviation at each welding condition.

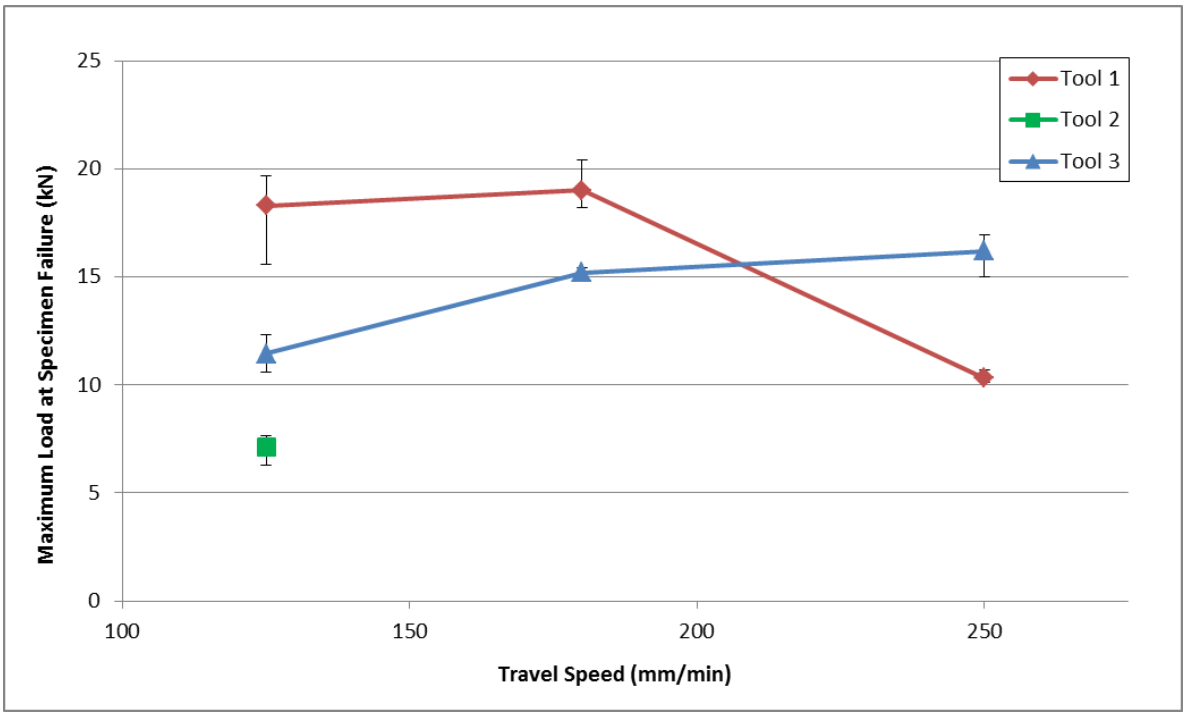

Figure 30: Maximum load at failure for pull test specimens of similar AA7075 lap FSW using Tool1 and Tool3 at 125, 180, 250mm/min; and Tool2 at 125mm/min.

Joint strength is expressed as a breaking force in Figure 30, but can also be expressed as a linear strength (in N/m) by dividing by the width of the specimen (30mm for the similar samples) to allow for an easy comparison to the dissimilar FSW samples (which will be shown later in this thesis) or other lap joining methods. At a travel speed of 125 mm/min, Tool1 exhibited the best strength performance with

a maximum load of 19.71 kN (0.657N/m), while Tool2 exhibited the poorest performance with a maximum load of 7.63 kN (0.254N/m), and Tool3 provided intermediate performance with a maximum load of 12.35 kN (0.412N/m). As a brief comparison, studies that have examined the overlap shear strength of resistance spot welded joints for aluminum samples of similar size demonstrate maximum loads of between 2kN and 5kN [48]; and studies of adhesive bonded samples demonstrate maximum strengths between 4kN and 10kN [49] [50].The low strength of joints made with Tool2 is likely due to excessive thinning of the upper sheet; as well as a more severe hooking defect, which results in a smaller effective plate thickness (based on the distance between the tip of the hook flaw and the surface of the sheet). Increasing the travel speed to 180 mm/min resulted in an increase in strength for welds made with Tool1 and Tool3. Applying a speed of 250 mm/min, the strength of welds made with Tool3 increases further; however, overlap shear loads in welds made with Tool1 decrease significantly at this highest travel speed. This decrease in joint strength can be explained by the observation of voids in the welds noted in Figure 29b. The trend of higher strength at faster travel speeds is also commonly observed in other FSW studies using other heat treatable alloys such as AA7075-T6 [51] [15] [44], and is attributed to the fact that faster travel speeds produce lower heat input to the weld, which results in less softening of the heat-treatable material, producing a stronger joint overall. The highest joint strength of 20.45kN was achieved with Tool1 at a speed of 180 mm/min.

The tensile specimens failed consistently through the SZ region in the upper sheet, with the fracture originating from the hooking defect at the sheet interface on the retreating side and propagating upwards. An optical micrograph of a specimen which was strained to approximately 80% of the maximum load during overlap testing is shown in Figure 31, which clearly shows that the interface begins to spread apart from the retreating side before it propagated upwards to sheet top surface. It is possible that further optimization of the tool geometry to align the sheet interface horizontally towards

the middle of the weld may improve overlap shear strengths further. Figure 32 shows a photograph of the typical fracture location of the test specimens.

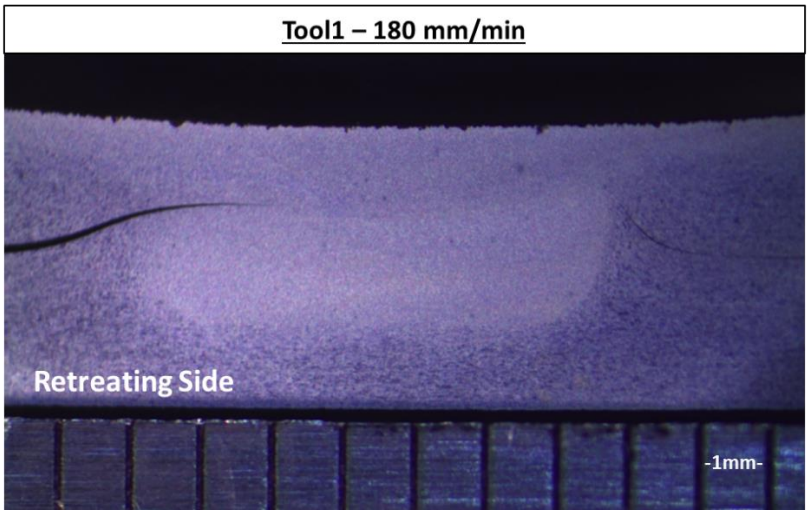

Figure 31: Overlap shear pull test specimen strained to ~80% of the average maximum load reached for the parameters applied in this weld (180 mm/min travel speed)

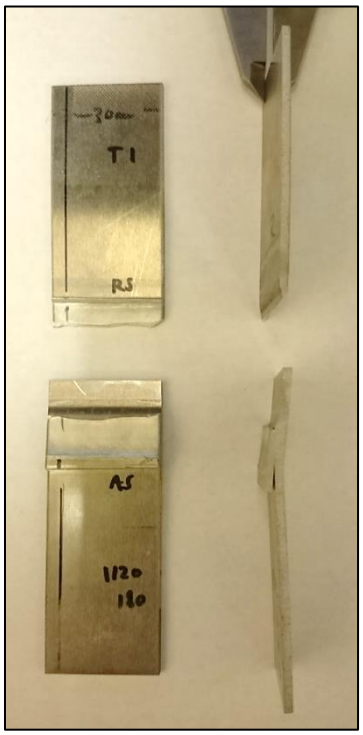

Figure 32: Typical fracture location for samples of similar AA7075 lap FSW. Shown in the figure are pulled samples of a weld made with Tool1 at 180mm/min

5.1.3 Weld Microhardness Profiles

The microhardness profiles measured for Tool1, Tool2, Tool3 at 125mm/min are shown in Figure 33, and microhardness profiles for Tool1 and Tool3 at faster speeds are shown in Figure 34 and Figure 35. The weld metal exhibited softening since hardness values were all below that of the base metal hardness of 175 HV (which is the maximum for the peak aged temper in this AA7075). The hardness values were all comparable for each tool, as noted by the overlapping scatter in Figure 33. Since the specimens for the hardness measurements were only 20 mm wide based on the overlapping areas of the sheet, it was not possible to identify the location where the minimum hardness value occurs, or where the thermal softening would dissipate and allow hardness values to return to that of the base material. Based on these results, it would seem that the heat applied near the tool surface would have readily exceeded the coarsening and dissolution temperatures for the precipitates in this alloy.

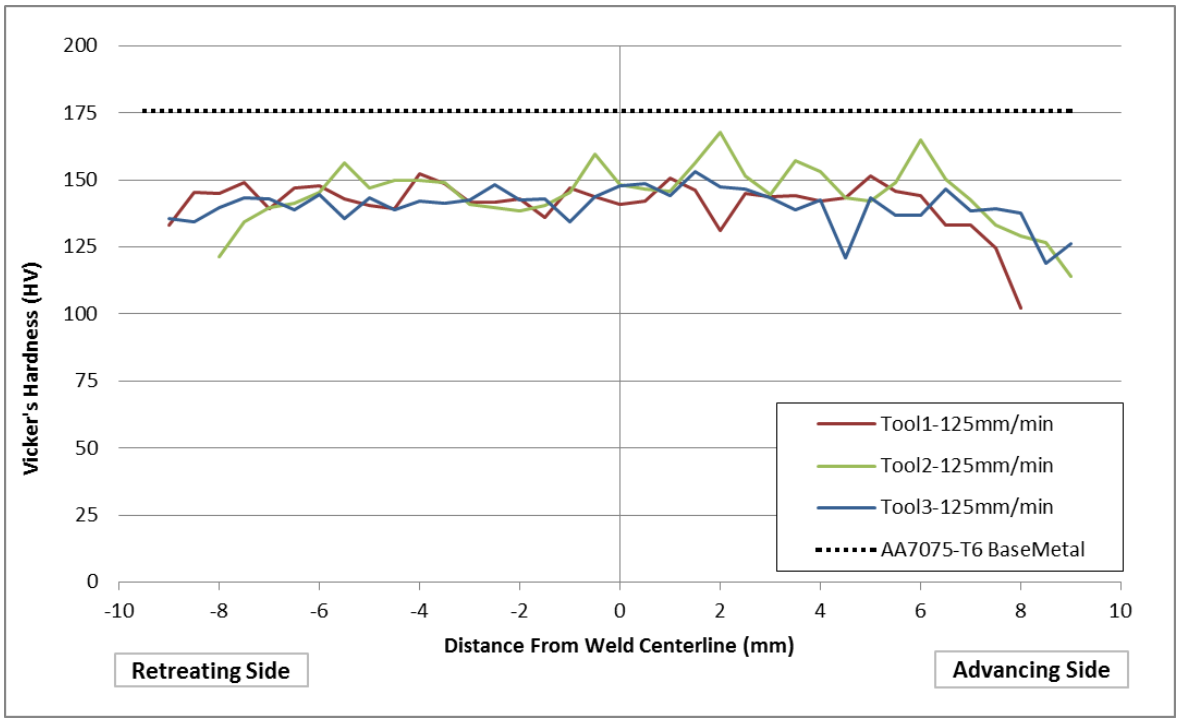

Figure 33: Weld microhardness profiles across the FSW for Tool1, Tool2, Tool3 at 125mm/min

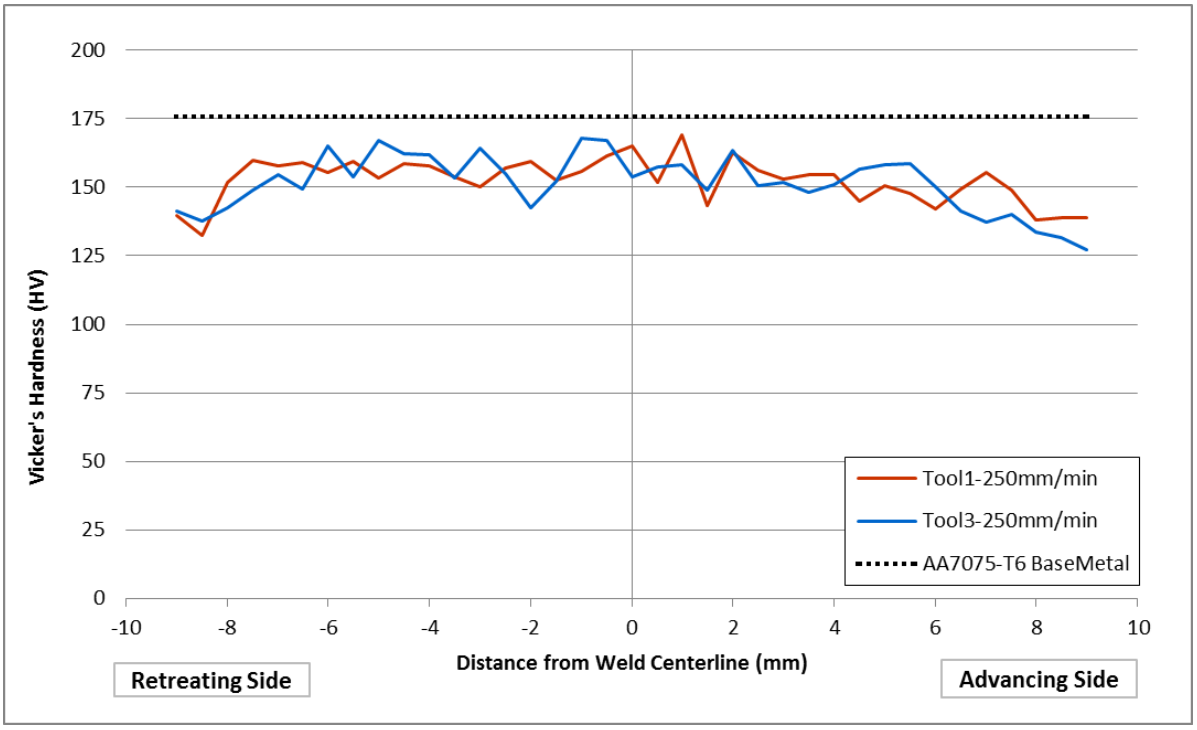

Figure 34: Weld microhardness profiles across the FSW for Tool1, Tool3 at 250mm/min

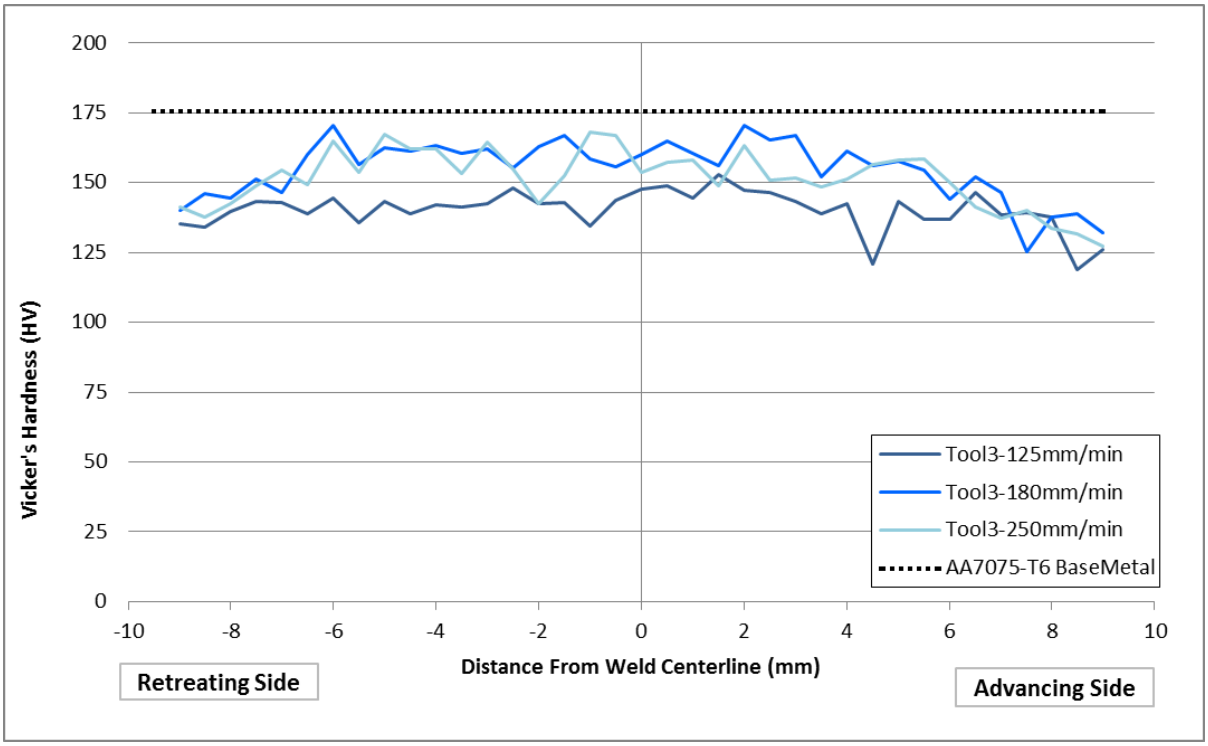

Figure 35: Weld microhardness profiles across the FSW for Tool3 at 125, 180, 250mm/min

The application of higher travel speeds was successful in maintaining higher hardness values across the weld as indicated in Figure 34 and Figure 35. The hardness remained on average greater than 150 HV when the travel speeds increased to 180 and 250 mm/min using both Tool1 and Tool3. However, it should be noted that the softened region could still not be completely captured within the 20 mm wide specimen used for hardness measurement. The differences in the hardness values between different tools and traveling speeds are difficult to compare due to the overlapping scatter, and so the average hardness values only about a region +/- 2 mm from the centerline of the joint were compared and summarized in Table 7. The data points shown in Figure 34 would indicate that the difference in pin geometry between Tool1 and Tool3 does not significantly affect the hardness of the resulting weldment.

Table 7: Average microhardness values through the SZ in similar AA7075 lap FSW

Average Vicker's Hardness Through Stir Zone [HV] (+/- 2mm about the weld centerline)		**Welding Speed (mm/min)**		
		125	**180**	**250**
Similar FSW: AA7075-T6 / AA7075-T6	**Tool1**	142	158	153
	Tool2	150	Unsuccessful Weld	Unsuccessful Weld
	Tool3	145	162	157

It can be noted that each tool produced similar hardness value when travel speeds are 125 mm/min; however the hardness increases when higher travel speeds are applied. While temperatures were not measured while making these welds, much of the literature indicates that slower welding speeds result in higher heat inputs to the FSW [6] [7] [20]. The lower hardness values that are observed at 125mm/min could therefore be a result of higher temperatures and slower cooling rates causing coarsening and/or dissolution of the strengthening precipitates of the AA7075-T6. As the travel speeds increase, the dissolution times decrease, which would suppresses the dissolution and coarsening process. However, since the minimum hardness values were produced well outside of the stir zone (see

Figure 33, Figure 34, and Figure 35), it is possible that all the stir zone microstructures underwent complete dissolution of precipitates, suggesting temperatures were well above 400°C. Hardness values were measured at least 2 weeks after FSW was performed, and therefore can be attributed to a combination of natural aging and grain refinement. This would be consistent with prior work showing that high tool rotation speeds could produce stir zone temperatures near 525°C [43]. Furthermore, average hardness values from 5mm to 9mm on both sides of the weld centerline were used to compare the hardness of the advancing and retreating sides, see Figure 36.

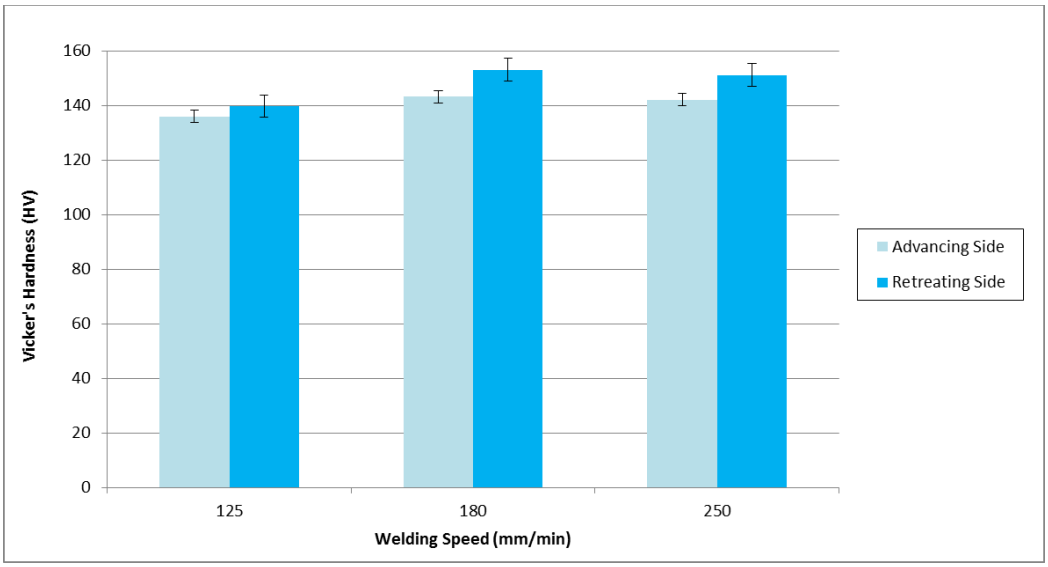

Figure 36: Average hardness values in the HAZ (between 5mm to 9mm from the weld centerline) on the advancing and retreating sides of similar AA7075-T6 lap FSW produced with Tool3

The values seen above are averages of hardness values taken between 5mm and 9mm on the advancing and retreating side of the weld, for each set of welding parameters that was attempted. A trend of higher hardness on the retreating side is easily seen, in this graph, and was is also seen when comparing welds made with Tool1 and Tool3 at the various welding speeds. This observation is consistent with prior studies which indicate that a higher temperature occurs on the advancing side during FSW [52]. Again, it is possible that the lower heat input on the retreating side would suppress the effects of the dissolution and coarsening process in the same way as it did for faster travel speeds.

5.2 Dissimilar FSW

As stated in the background information section, one of the great strengths of the FSW process is its ability to join dissimilar alloys or completely different metals together. Of particular interest to the automotive industry is the joining of 6xxx and 7xxx aluminum alloys. It is often desirable to construct more critical components from the stronger but difficult-to-weld 7xxx series; and less structurally important components from the weaker but more formable 6xxx series. Traditional fusion welding processes struggle to create a strong joint between different series of aluminum alloys, since the mixing of certain alloying elements will result in solidification defects and poor mechanical properties. Mechanical joining methods are time and money intensive, and add weight to the final structure. FSW shows promise as a technique that can create strong joints between these two alloys, consequently, this thesis investigates the properties of FSW joints between thin sheets of AA7075-T6 and AA6022-T4

FSW was performed with Tool1, Tool2, Tool3, Tool4 and Tool5 at speeds of 125, 180, 250, 355, and 500mm/min for a layup of dissimilar AA7075-T6/AA6022; with sheet thicknesses of 2mm and 0.9mm, respectively. In these dissimilar welds, the AA7075 is the upper sheet, and the AA6022 is the lower sheet. Keller's etchant was used to reveal the grain structure of the AA7075 sheet, but it had no effect on the AA6022, which remains un-etched in these images.

5.2.1 Optical Microscopy and Weld Microstructure

Optical micrograph images were obtained for the dissimilar welds made with Tool3 at all welding speeds, as shown in Figure 37. The striking contrast between the two alloys is evident, which results in the difference in etching rate, since the AA6022 alloy is a more dilute composition and more corrosion resistant.

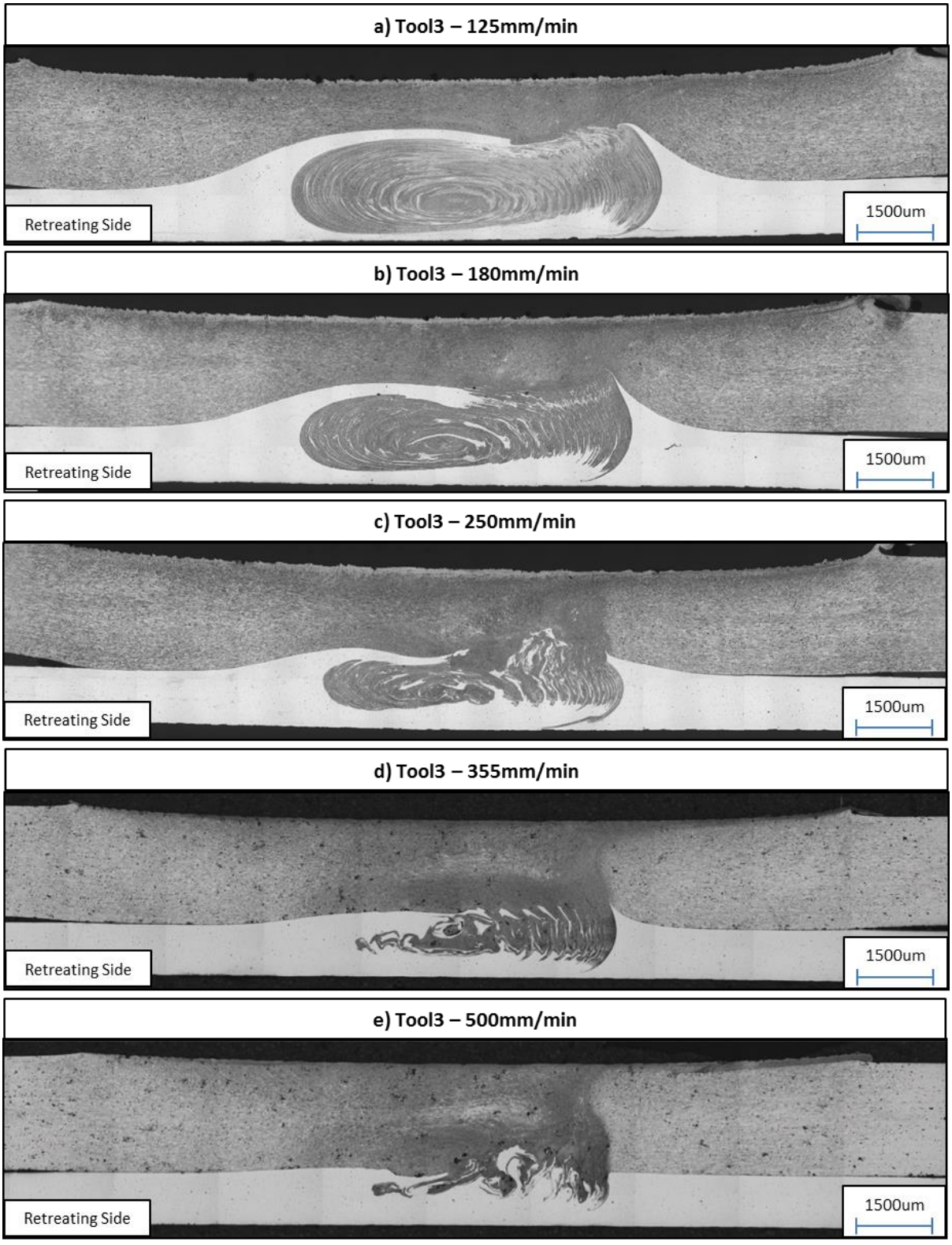

Figure 37: Optical micrograph images of a dissimilar AA7075/AA6022 FSW made at the following conditions: (a)Tool3-125mm/min (b)Tool3-180mm/min (c)Tool3-250mm/min (d)Tool3-355/min (e)Tool3-500mm/min. In each image, AA7075 is on top (darker) and AA6022 is on the bottom (lighter).

The stir zone of the weld is clearly visible at the center of each image. During the FSW process, the dissimilar materials experience a large degree of mixing, as evidenced by the thin bands of material which etches differently in each alloy to produce light (AA6022) and dark (AA7075) contrast within the SZ of the weld. At faster travel speeds, the size of the stir zone decreases. This is not surprising, since passing the rotating tool through a given area more quickly would leave less time for mixing to occur. The most significant difference in the shape of the SZ occurs between the travel speeds of 250mm/min and 355mm/min (Figure 37c and Figure 37d, respectively). At the slower travel speeds (125, 180, 250mm/min), the SZ maintains an oval shape with a large amount of AA7075 material that is displaced underneath the sheet interface on both the advancing and retreating sides of the weld. However, at faster travel speeds (355, 500mm/min) there is a noticeable decrease in the amount of AA7075 that has been mixed into the lower sheet. Recall that the rotational speed of the tool was held constant for these welds. The change is SZ shape above a certain travel speed could therefore be the result of the tool passing through a given location in the workpiece before it is able to complete the number of rotations that are required for sufficient mixing. This suggestion is based on the intermixing mechanism that has been described in detail in prior work which revealed similar lamellar structures for FSW joints [53].

Figure 38 shows three high magnification images (at 100x, 200x, and 500x) taken at the edge of the SZ on the retreating side for a weld made with Tool3-125mm/min. These images reveal that the grain sizes of the AA7075-T6 alloy are nearly the same for the dissimilar FSW as for the similar FSW (shown previously in Figure 28). A very fine lamellar pattern can be observed at the lower travel speeds, suggesting very good mixing of the two materials.

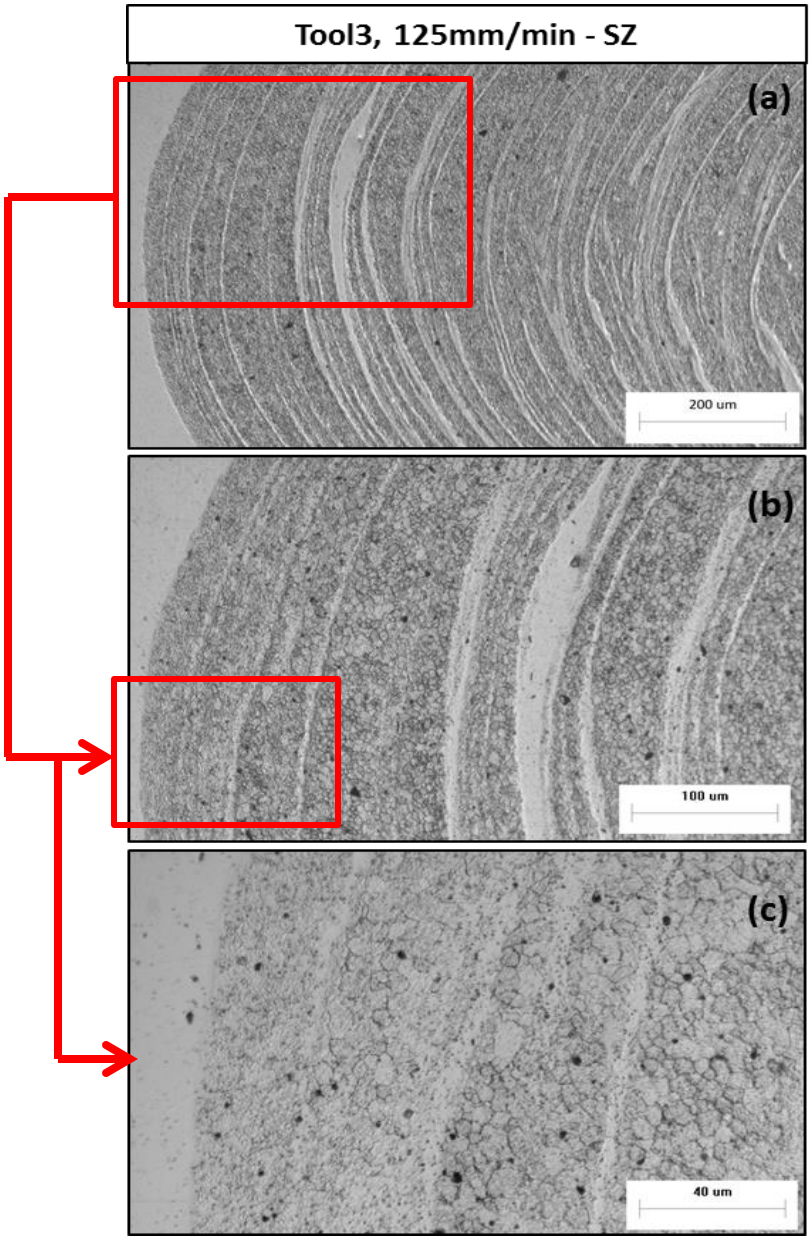

Figure 38: Optical microscope images of the SZ on the retreating side of FSW made with Tool3 at 125mm/min at magnifications of: (a) 100x; (b) 200x; (c) 500x for the dissimilar material combination (AA7075-T6 / AA6022-T6)

The majority of the dark spots that are visible in Figure 37d and Figure 37e are due to small amounts of pitting that occurred because of slight over-etching of the samples during preparation. It was observed, however, that at speeds of 355 and 500mm/min, there were some micro-cavities formed in the SZ of the weld. These are distinguished by being slightly larger and rounder than the pitting

features, and occur near the boundaries between the 7075 and 6022 materials. High magnification images of the microcavities are shown in Figure 39. Note the scale of these images, and that the cavities are very small in size.

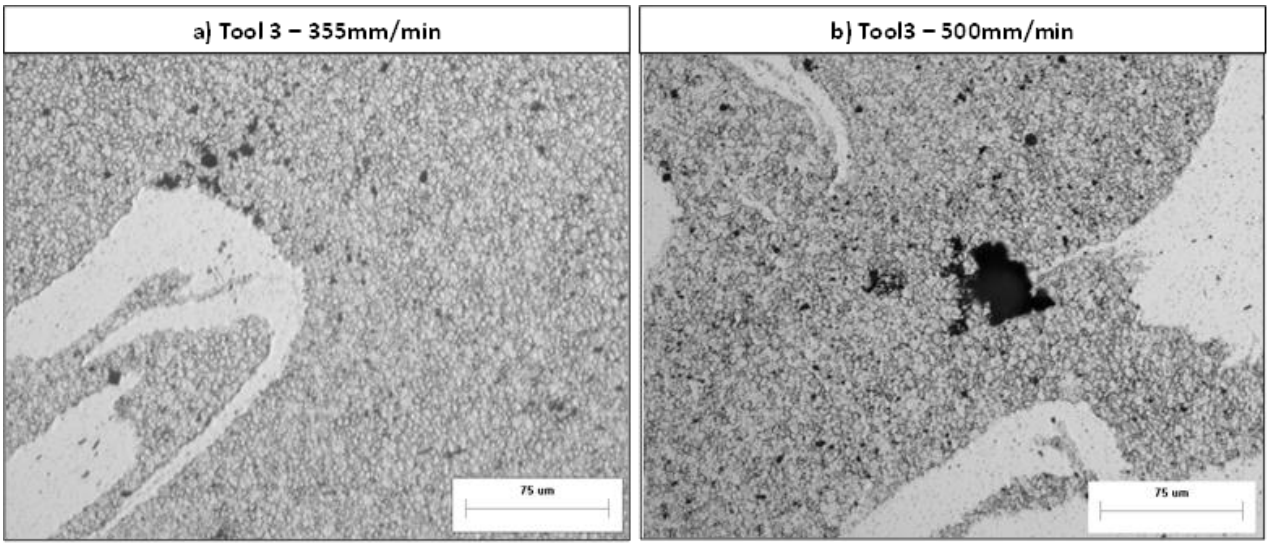

Figure 39: High magnification images of microcavities formed in the SZ of dissimilar welds at 355mm/min and 500mm/min.

As with the micrograph images of the similar welds, the hook feature is visible in the dissimilar welds as well. The hook is most noticeable in the welds made at slower travel speeds (Figure 37a, Figure 37b). At faster travel speeds (Figure 37d, Figure 37e) the sheet interface remains relatively flat right into the SZ. This behaviour is expected, as it is known that the hook feature is caused by the vertical movement of material during the welding process. Since there is significantly less mixing at faster travel speeds, the hook will inherently be smaller.

The geometry of Tool4 was designed in an attempt to reduce the vertical motion of material during FSW, thereby reducing the size of the hook. The Tool4 design is nearly identical to Tool3 (which is the tool geometry that has performed best in the tests so far) and uses a 10^{o} tapered pin, 3 flat sides, but no thread feature on the pin. FSW with Tool4 was accomplished at speeds of 125, 180, 250, and 355mm/min, but was unsuccessful at 500mm/min. Furthermore, the welds made at 250 and

355mm/min contained very large wormhole defects that ran through the interior of the entire weld. Optical micrograph cross-section images of these FSW are shown in Figure 40.

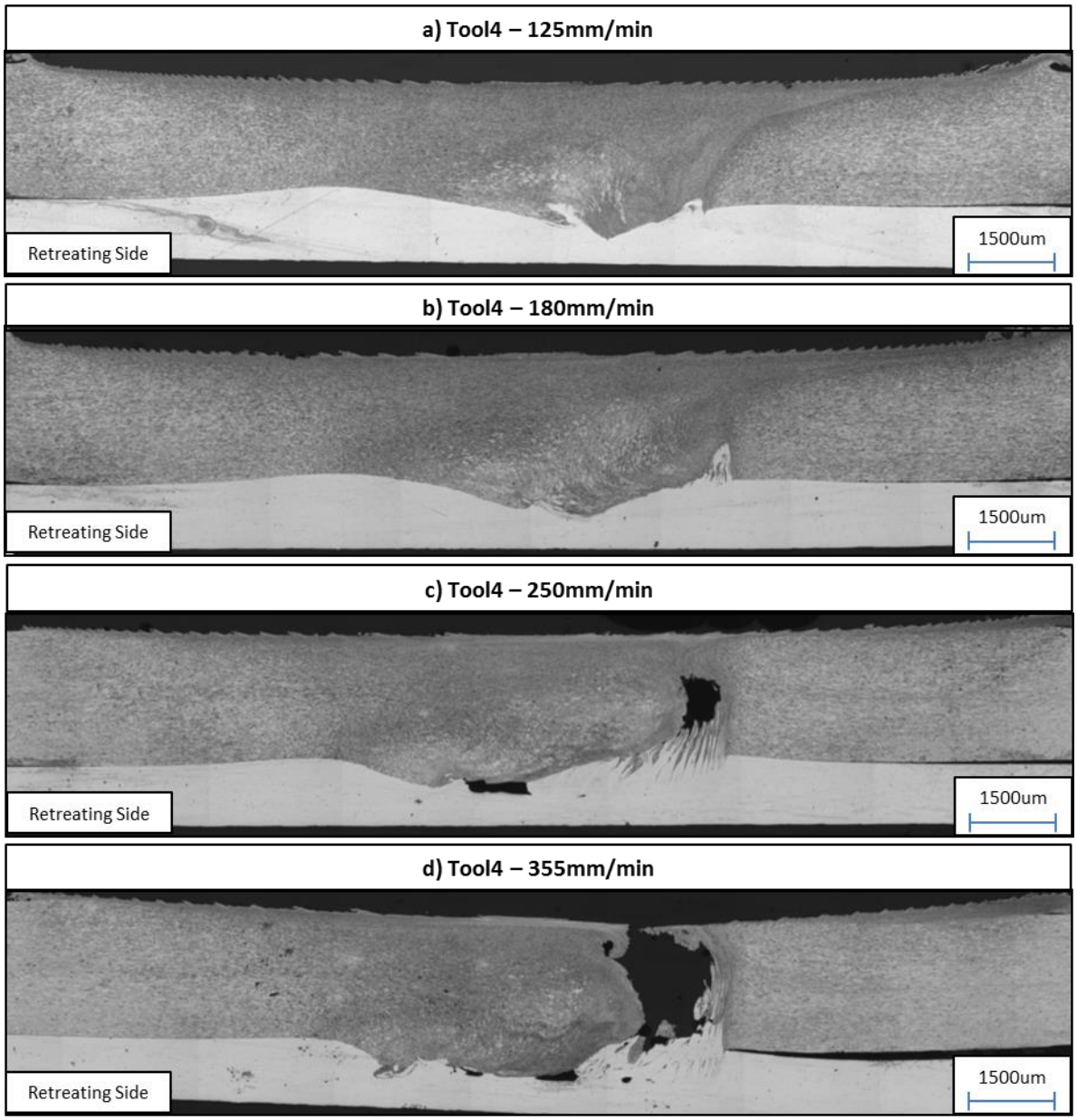

Figure 40: Optical micrograph images of a dissimilar AA7075/AA6022 FSW made at the following conditions: (a)Tool4-125mm/min (b)Tool4-180mm/min (c)Tool4-250mm/min (d)Tool4-355/min

From the images, it is clear that the welds made with Tool4 experience much less mixing than those made with Tool1, Tool2, and Tool3. The most obvious difference is the absence of a weld nugget

in the center of the weld. In Figure 37, it was possible to see a large mixed area in the center of the weld where Tool3 had mixed the materials to form a finely lamellar structure. In contrast, the images in Figure 40a and Figure 40b reveal that only a small amount of the more lightly-coloured AA6022 has was mixed into the AA7075; otherwise, the sheet interfaces appear nearly undisturbed. At faster travel speeds of 250 and 355mm/min (seen in Figure 40c and Figure 40d), voids and wormholes that have formed within the weld are evidenced by the large black areas seen on the advancing side. These are likely a result of insufficient mixing and movement of material due to the lower temperatures that are generated at faster travel speeds. Tool4 appears to be successful, however, in reducing the degree of the hooking flaw that was present in the joints produced with Tool3. The interface between the sheets is quite flat at the low speeds of 125 and 180mm/min. Even at the higher speeds of 250 and 355mm/min, the interface on the advancing side remains smooth; although the development of large voids on the retreating side at these speeds is likely more harmful to the weld mechanical properties than would be a hooking flaw.

Based on the welds resulting from the welds made with Tool4, a new geometry, Tool5, was designed with the goal of increasing material mixing while still maintaining a small degree of vertical flow. To accomplish this, Tool5 was created with straight grooves that have the same pitch and shape as an M6 thread, but are not helical. Flats were also removed from the design in order to better asses the effects of the straight grooves on their own. The hypothesis was that the non-helical grooves would promote better deformation and mixing than a tool with only flats (Tool4), while keeping the hook size to a minimum. FSW with Tool5 was accomplished at speeds of 125, 180, 250, 355, and 500mm/min, however all the welds made contained wormhole defects that ran through the interior of the entire weld, near the bottom of the SZ on the advancing side. Optical micrograph cross-section images of welds at three different speeds are shown in Figure 42.

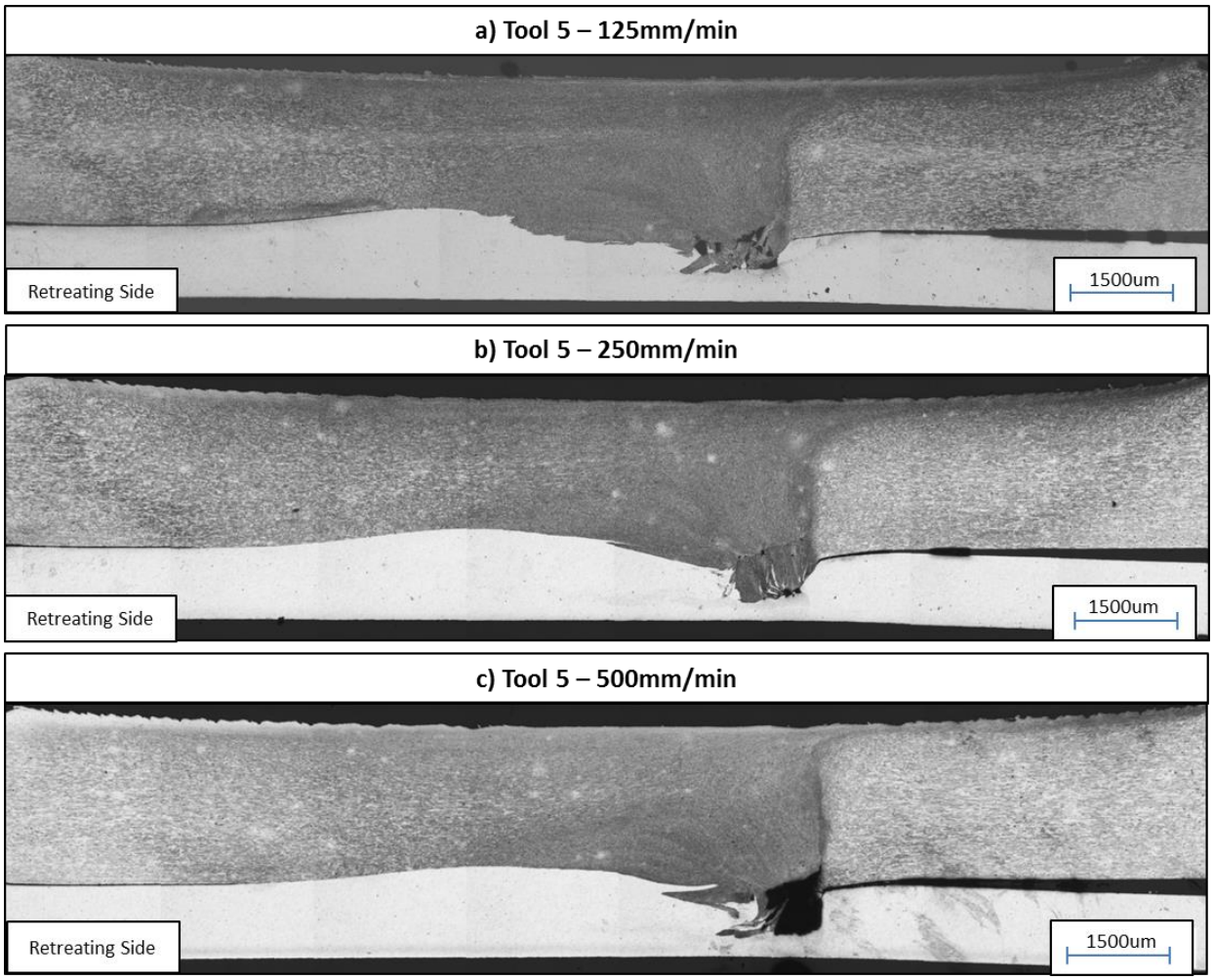

Figure 41: Optical micrograph images of a dissimilar AA7075/AA6022 FSW made at the following conditions: (a)Tool5-125mm/min (b)Tool5-250mm/min (c)Tool5-500mm/min

Similarly to the welds made with Tool4, these images show that the welds made with Tool4 lack a defined SZ, suggesting that this tool design also promotes much less mixing than Tool1, Tool2, and Tool3. In fact, when comparing Figure 40 and Figure 41, Tool5 appears to provide even less mixing than Tool4, as Figure 41 shows that none of the lighter coloured AA6022 material was mixed into the AA7075, even at low speeds. Tool5 still results in large wormhole defects through the weld SZ, in roughly the same position as those seen in the Tool4 welds in Figure 40. The difference is that the wormholes were slightly smaller, and so welding was still technically possible at speeds of 500mm/min, though the quality of the joint is still quite poor. At a glance, Figure 41 might also appear to show that

Tool5 has reduced the size of the hooking defect; however upon closer inspection it should be noticed that the hook is still present, but it hooks slightly *downward* into the AA6022 sheet, on the advancing side. Due to the difference in alloy strength and sheet thickness, the change in hook direction will reduce the strength of the joint, as will be discussed in the following section.

5.2.2 Joint Strength Testing

Lap shear pull tests were performed on the AA7075/AA6022 dissimilar welds made with all 5 tools at speeds of 125, 180, 250, 355 and 500mm/min. The setup was identical to that used for the similar AA7075 welds, however the sample width was changed from 25mm instead of 30mm, in order to provide a more direct comparison to prior work and an emerging test standard [47]. Three samples were pulled for each condition, and the maximum force at joint failure (breaking force) was recorded for each. The average breaking force values and error bars representing 1 standard deviation are displayed in Figure 42, with very narrow scatter ranges (with the exception of Tool5). It should be noted that Tool4 was unsuccessful in producing a weld at 500mm/min, so this data point is not included in the figure.

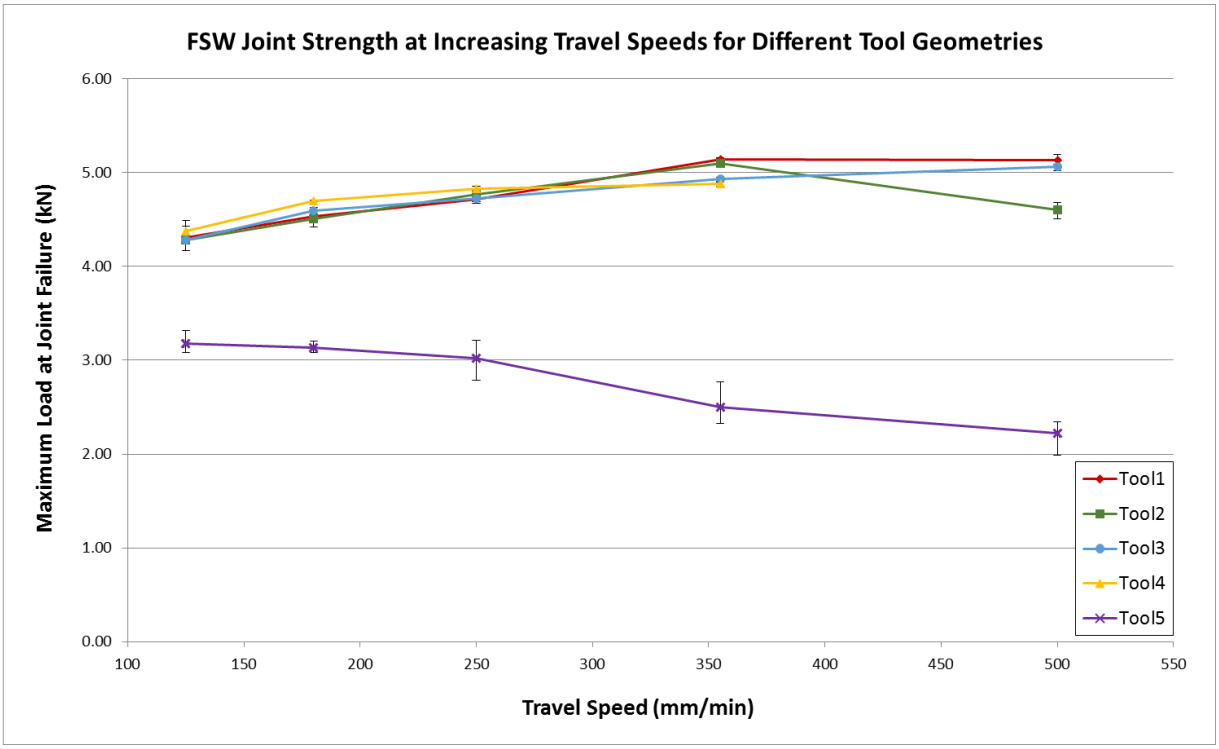

Figure 42: Maximum load at failure for pull test specimens of dissimilar AA7075/AA6022 lap FSW using Tool1, Tool2, Tool3, Tool4 and Tool5 at 125, 180, 250, 355, 500mm/min

Firstly, it should be noted that the breaking force values for the dissimilar joints are much lower than those of the similar joints for the same welding speed. Joint strength is expressed as a breaking force in Figure 42, but can also be expressed as a linear strength (in N/m) by dividing by the width of the specimen (25mm for the dissimilar samples) to allow for an easy comparison to the similar FSW samples or other lap joining methods. The best overall dissimilar joint performance of 5.14kN (0.206N/m) was observed in Tool1 at 355mm/min (compared to a maximum of (0.657N/m) in the similar FSW study, also seen with Tool1) and the strongest joint made by Tool3 measured 5.06kN (0.202N/m) (compared to a maximum strength of 0.412N/mm in the similar FSW study). If Tool5 is ignored, the lowest dissimilar joint strength of 4.28kN (0.171N/m) is observed in Tool2 (compared to a minimum joint strength of 0.254N/m in the similar FSW study, which was also seen with Tool2).

The maximum breaking force values do show a trend of higher joint strength at faster welding speeds for all tools except Tool5. This is consistent with the results of the similar FSW study, where faster travel speeds also resulted in a stronger joint, though recall that the fracture in these samples occurred in the SZ of the FSW. Contrarily, fracture in the dissimilar FSW samples made with Tool1, Tool2, Tool3 and Tool4 occurred in the HAZ of the AA6022 material – approximately 7mm – 8mm from the weld centerline. It is therefore likely that the parent metal, not the quality of the weld, is controlling the fracture of the samples. The reason that Figure 42 shows an opposite relationship for Tool5 can be explained by further comparing the fracture locations of the dissimilar FSW samples, and will be discussed in detail at the end of this section.

If the Tool5 data points are ignored, the dissimilar FSW study also reveals two trends that are contrary to the similar FSW study. Firstly, the measured values for Tool1, Tool2, Tool3 and Tool4 show that there is no significant difference in joint strength when different tool geometries are used for welding. This is different from the results observed in the preliminary study of similar FSW, as Tool1 was observed to promote stronger joints than either of the other tools. Additionally, the presence of weld defects does not appear to severely degrade the joint strength of the dissimilar welds, as can be seen when comparing the breaking force values of the Tool4 welds (which are known to contain very large defects) to the welds made with the other tools (which are known to produce fully consolidated welds). This is in contrast to the similar FSW study, where it was observed that any cavities present in the weld had a significant negative impact on the overall joint strength.

The differences between the two studies can be largely attributed to the fact that one of the materials being joined in the dissimilar study is a 0.9mm thick sheet of AA6022-T4, which is inherently much softer and weaker than a 2mm thick sheet of AA7075-T6. Recall also that the specimen width for the dissimilar FSW study was decreased to 25mm from 30mm in the preliminary study. The change in

workpiece thickness, coupon size and material strength explains the severe decrease in the magnitude of the joint strength for welds in all conditions. It can also explains why the weld defects no longer appear to have a negative effect on the joint strength – because the joint no longer fractures through the TMAZ and SZ of the weld, but rather through the HAZ of the softer and thinner sheet of AA6022. Some examples of fractured samples can be seen in Figure 43.

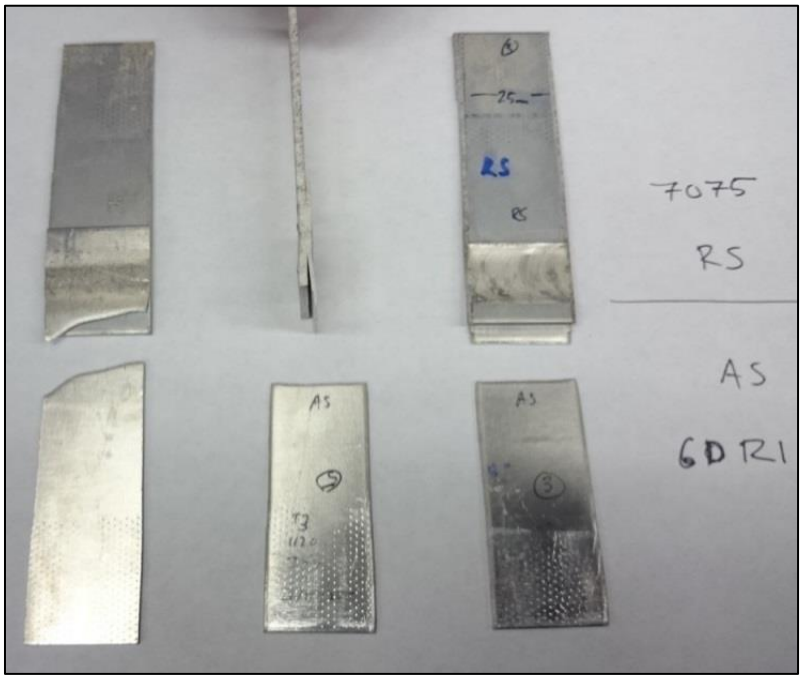

Figure 43: Location of fracture during the lap shear pull tests of dissimilar lap FSW of AA7075-T6 to AA6022-T4. Welding conditions are, from left to right: Tool3-250mm/min, Tool3-355mm/min, Tool3-500mm/min.

Recall that 3 samples were tested for each permutation of tool design and travel speed. For Tool1, Tool2, Tool3 and Tool4, all samples fractured through the AA6022 sheet approximately 8mm from the weld centerline. The fracture locations of the samples suggest that the presence of defects within the SZ of the weld – which were observed at 500mm/min with Tool1, Tool2, and Tool3, and at 250 and 355mm/min with Tool4 – have no real effect on the overall joint strength, since the joint is failing far away from the SZ.

Tool 5, however, does not agree with any of the trends noted in the previous paragraphs. The reason for this is a combined effect from the difference in material strengths and the downward hooking defect that was shown in Figure 41. When the hook moves downward into the already thinner and weaker AA6022 material, it further reduces the strength of that sheet, making it very susceptible to fracture during overlap shear testing. The result is that the 15 joints produced with Tool5 all fractured through the base of the SZ on the advancing side (through the wormhole defect), and were the only samples that fractured this way in all the overlap shear tests that were performed. This fracture behaviour explains why the Tool5 welds shows much lower joint strength than those made with the other tools, and also why the Tool5 joints are the only ones that seem to be negatively affected by larger defects – since these are the only specimens that fail close to the weld. An example of a fractured specimen made with Tool5 is shown in Figure 44.

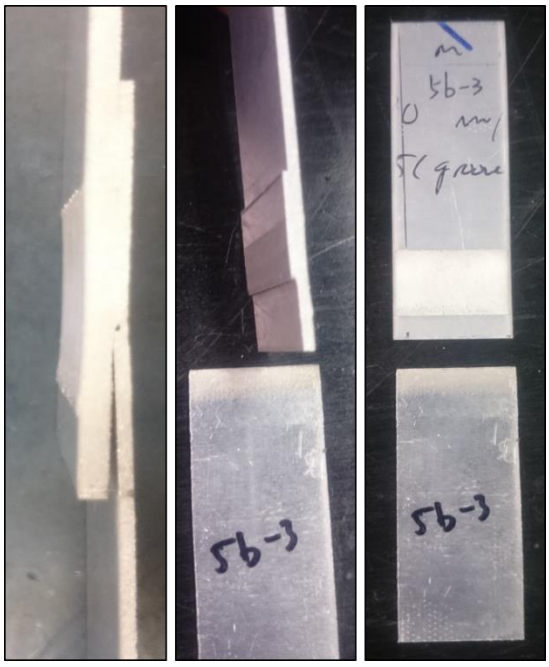

Figure 44: Location of fracture during the lap shear pull tests of dissimilar lap FSW of AA7075-T6 to AA6022-T4 under a welding condition of Tool5-250mm/min

5.2.3 Weld Microhardness Profiles

Microhardness profiles across the FSW were obtained for welds made with Tool3 at speeds of 125, 180, 250, 355 and 500mm/min. The AA6022 was of greatest interest, as joint failure occurred consistently through this material; therefore the indentations were made slightly below the midplane of the 0.9mm sheet (approximately 0.5mm to 0.6mm below the interface). Indentations were made every 0.5mm, to a distance of 20mm on either side of the weld centerline. A plot of the Vickers hardness values is shown in Figure 45.

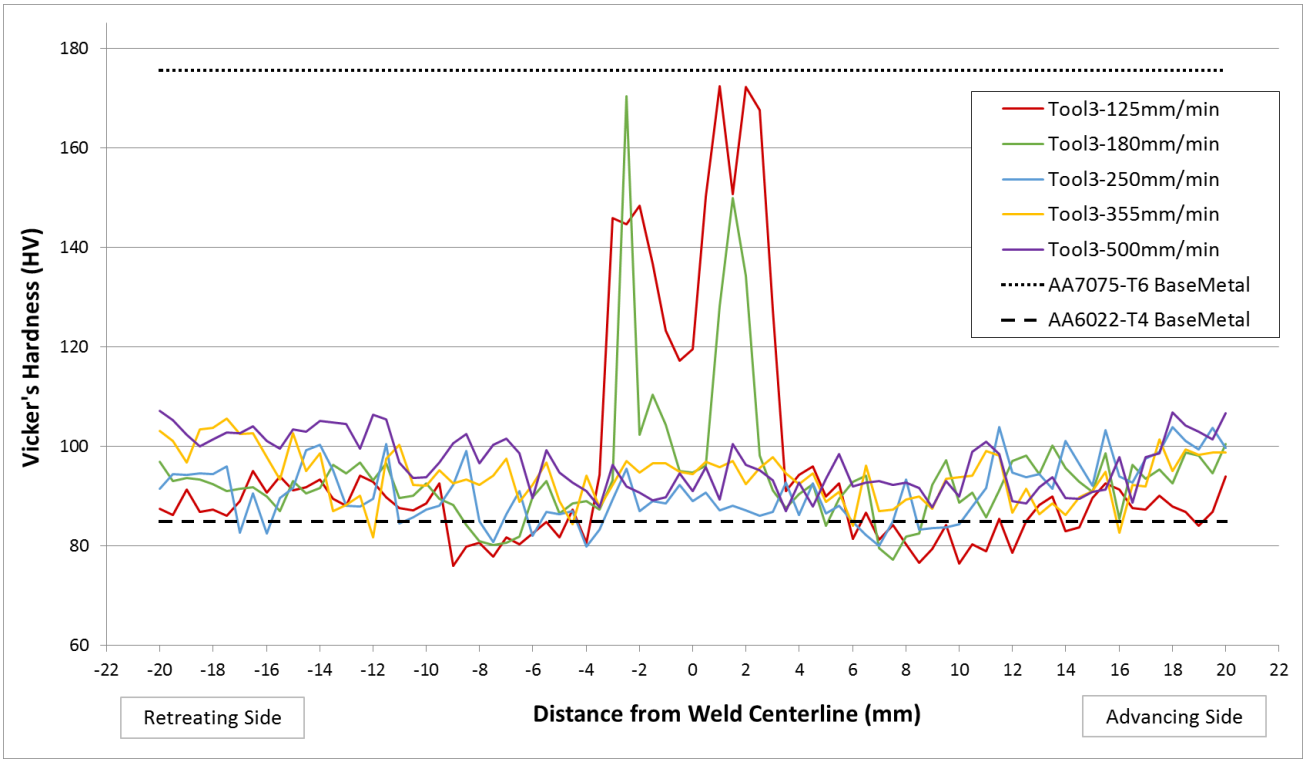

Figure 45: Microhardness values through the AA6022 sheet of dissimilar lap FSW of AA7075/AA6022 made with Tool3 at 125, 180, 250, 355, 500mm/min

The large peaks in hardness that occur at the center of the weld (between +/-4mm) in the hardness profiles for Tool 3 at 125 and 180 mm/min are due to the indentations being made inside or partially inside of the lamellar regions of AA7075 that was mixed into the lower sheet during welding. These few points indicate that the microhardness of the AA7075 material in the SZ is only slightly lower

than the base metal hardness of AA7075-T6. Existing literature suggests that temperatures within the FSW can be high enough to cause coarsening of strengthening precipitates in 7xxx alloys, and sometimes reach values even higher than the dissolution temperature of these precipitates [41] [11] [54] – this would suggest that the observed hardness recovery is largely due to grain refinement during welding and some natural ageing that occurred between the time of welding and the time of the hardness indentations.

Within the region of 7mm to 10mm on either side of the weld centerline, the AA6022 material is softened to below the base metal hardness values. These areas are the HAZ of the friction stir weld – where temperatures are high enough to cause coarsening (and perhaps dissolution) of strengthening precipitates, but where no mechanical deformation or grain refinement occurs [41] [11] [54]. Beyond the +/-10mm mark on either side of the centerline, the hardness values begin to rise above the AA6022-T4 base metal hardness. At this distance from the FSW tool, temperatures are elevated but not sufficient to result in significant precipitate coarsening. Instead, the metal appears to be slightly hardened – anywhere from 5 to 20 HV depending on the welding parameters – which could be indicative of mild artificial ageing at these distances as a result of the thermal cycles resulting from the FSW process.

The microhardness profiles for different welding conditions indicate that increasing the welding speed is successful in decreasing the size and severity of the HAZ. For the slower welding speeds of 125, 180 and 250mm/min there is a drop in hardness at approximately +/-8mm from the weld centerline, and recovery to base metal hardness values at around 15mm from the centerline. This is in agreement with the results seen in the lap shear pull tests, where samples showed a trend of higher joint strength at faster travel speeds, and were observed to fail in the softer AA6022 sheet at a distance of 7mm to 8mm from the weld centerline.

When welding is performed at 355mm/min and 500mm/min (the yellow and purple lines, respectively, in Figure 45) the microhardness values remain above the AA6022-T4 base metal hardness across the SZ, dropping only slightly at around +/-7mm from the centerline. Hardness values greater than the base metal values are unexpected, since the existing literature indicates that β'' particles (the primary strengthening particle in 6xxx alloys) will precipitate at ~240^{o}C and dissolve at ~290^{o}C [17]. The measured hardness values suggest that the temperatures in this area during FSW at fast speeds are not high enough to cause dissolution of β'' particles, but instead are within a temperature range that would encourage artificial ageing of the alloy. This will be explored further in the next section, where temperature measurements were obtained at various distances from the weld.

5.2.4 In-weld Temperature Measurements

In order to better correlate the hardness measurements with the effects of precipitate coarsening, thermocouples were embedded between the AA7075-T6 and AA6022-T4 sheets at distances of 4mm, 8mm, 12mm, and 16mm from the weld centerline to measure the temperature history in these locations. FSW was performed on this workpiece with Tool3 at speeds of 125mm/min, 250mm/min and 500mm/min in order to observe the temperatures reached during the welding process. The measured thermal cycles are shown in Figure 46 for each travel speed (with (A) corresponding to 125mm/min; (B) to 250mm/min; and (C) to 500mm/min).

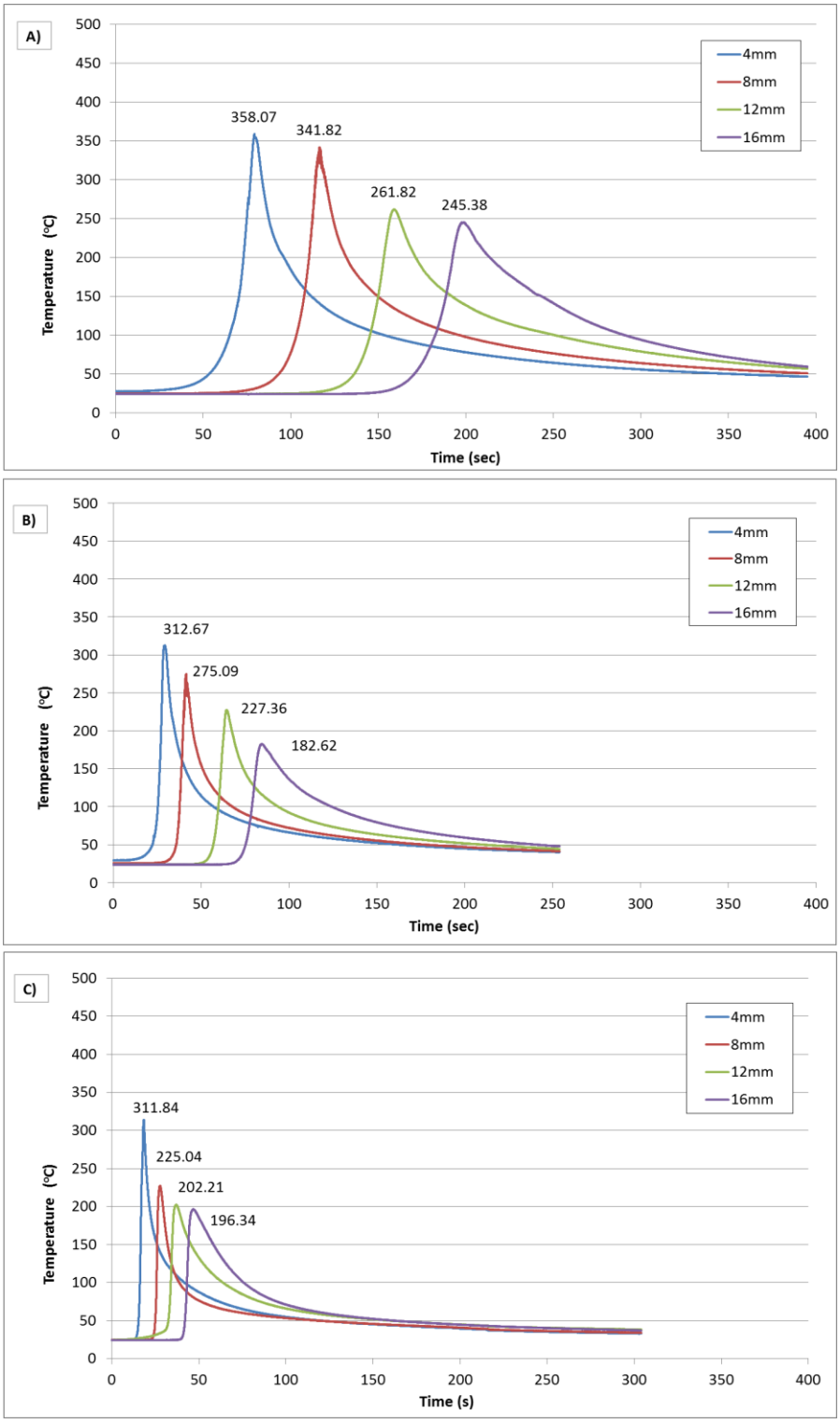

Figure 46: Temperature measurements vs. time taken at various distances from the weld centerline during FSW with Tool3 at the following travel speeds: (a) 125mm/min; (b) 250mm/min; (c) 500mm/min

From the plots in Figure 46 one can immediately note a trend between faster cooling rates and lower maximum temperatures when the travel speed is increased. There is a significant drop in maximum temperatures at all distances from the centerline when the speed is increased from 125mm/min (Figure 46a) to 250mm/min (Figure 46b). The decrease in maximum temperatures between the 250mm/min (Figure 46b) and 500mm/min (Figure 46c) travel speeds is less severe, but still present.

At 4mm from the centerline, the measured temperatures at 250mm/min and 500mm/min (313^{o}C and 312^{o}C, respectively) are nearly identical, whereas the measurement at 125mm/min (358^{o}C) is significantly higher. The cooling rate, however, maintains the trend of being quicker with a faster travel speed. This suggests there may be a minimum critical temperature that must be met in the weld in order to create a successful FSW between these two materials. It has already been shown that a model for the peak temperature at the tool surface during FSW is strongly correlated to the rotation speed and weakly correlated to travel speed [55] [56].

Based on the results of the microhardness and joint strength tests, one location of interest in the weld area lies at around 8mm from the centerline, as this is where minimum hardness and joint fracture were observed. Recall that the previous tests showed a higher hardness and greater joint strength when the travel speed was greater. From the temperature measurements at the 8mm location, the observed peak temperatures were: 342^{o}C at 125mm/min; 275^{o}C at 250mm/min; and 225^{o}C at 500mm/min. This comparison seems to show that a lower peak temperature results in less softening of the material, resulting in higher joint strength, which is in agreement with the trends presented in much of the existing literature [6] [13] [57].

In the case of the joints made with a speed of 500mm/min, the hardness tests showed that the values across the entire weld were higher than the AA6022-T4 base metal values. The maximum recorded temperature of 225^{o}C at 8mm is below the β’’dissolution temperature of 290^{o}C, and even

below the precipitation temperature of 240°C suggested in the literature [17] [58]. This lends more credibility to the relatively high hardness values measured across the welds made at 500mm/min, indicating that such rapid welding speeds might only result in temperatures high enough to cause mild artificial ageing of the AA6022 alloy.

Temperatures were also measured from the center of the FSW for welds made with Tool3 at speeds of 125, 250 and 500mm/min. The full experimental setup was quite complicated and is explained in detail in the experimental methods section. In essence, a thermocouple was inserted through a hole drilled through the center of the tool, and held in place with cement. Figure 47 shows the measured temperatures during one long FSW (2 feet long) during which the speed and plunge depth were changed several times. Temperatures were recorded this way first because it was found that inserting and extracting the tool several times would damage the embedded thermocouple.

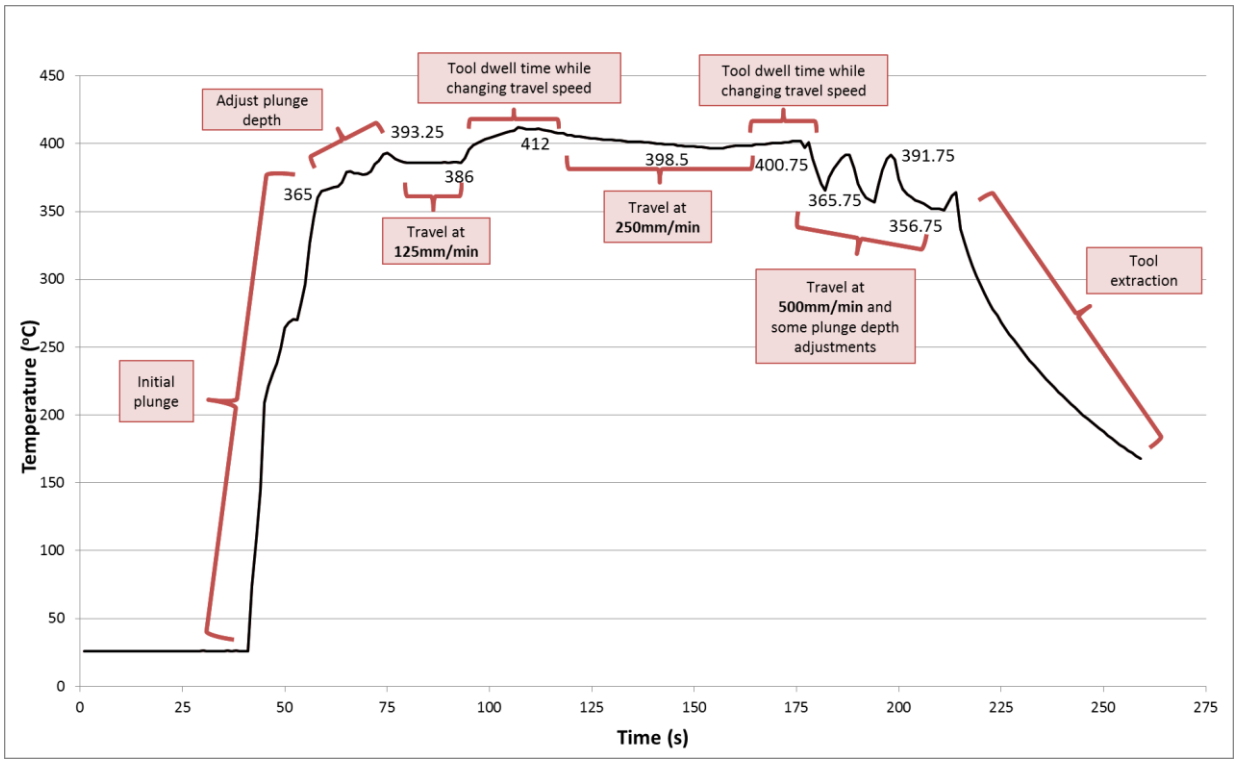

Figure 47: In-tool temperature measurements for a FSW performed at various speeds with Tool3. Speed changes, plunge-depth changes, and corresponding temperature measurements are labeled.

The process was given time to reach a steady state at each welding speed before the parameter was changed – these can be seen as the longer periods of relatively constant temperature. The steady temperature for the 125mm/min weld was recorded as 386°C; for 250mm/min as 398°C; and for 500mm/min as ~365°C, although at this point there was limited space remaining on the workpiece and the tool was to be removed. As the specialized tool was still intact, individual experiments were performed to obtain measurements for long welds at each of the three welding speeds. The results are shown below in Figure 48. Unfortunately, the specialized thermocouple instrumented tool broke only a few seconds after starting the weld at 500mm/min.

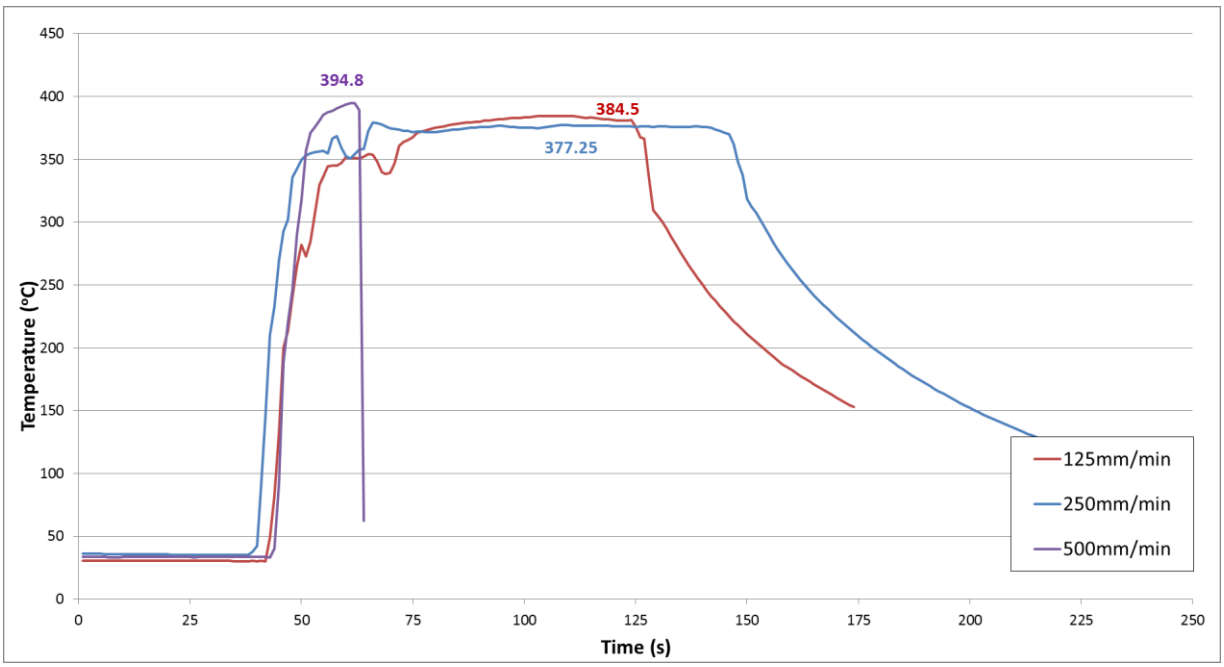

Figure 48: In-tool thermocouple measurements for long welds under the conditions of Tool3-125mm/min, Tool3-250mm/min, Tool3-500mm/min.

From these two data sets, 125mm/min shows a steady state temperature of 386°C and 384°C; 250mm/min a steady state temperature of 398°C and 377°C; and 500mm/min shows temperatures of 365°C and 396°C. The range of temperatures is relatively small, and no clear trend is discernable between welding speed and temperature, indicating perhaps that the travel speed does not have an

effect on the maximum temperature near the center of the weld. This would be in line with the results of the temperature measurements at the 4mm mark in the workpiece, which were nearly equal at faster travel speeds of 250mm/min and 500mm/min (see Figure 46b and Figure 46c). These measurements also show that the temperatures in the center of the weld are far higher than the 290^{o}C dissolution temperature of the strengthening β'' precipitates in AA6022, but right around the 375^{o}C precipitation temperature of coarser β and Si precipitates, as suggested in the literature [17] [58].

5.2.5 Influence of Post-weld Heat Treatment on Joint Strength

Welds made with Tool3 were subjected to a post-weld heat treatment of 30 minutes at 180^{o}C, followed by cooling in still air. The heat treatment process was designed to mimic the paint bake cycle that the aluminum sheets would be subjected to during manufacturing [47]. The welded samples were left to rest at room temperature for a minimum of 4 weeks prior to heat treatment, and then were left to rest at room temperature again for a minimum of 4 weeks before any mechanical testing was performed. These waiting periods allowed the material to undergo any natural ageing processes and reach a stable state. The joint strength of the post-weld heat treated samples was tested with an overlap shear fracture test, under the same conditions that were used previously.

The results of heat treating are shown in Figure 49, with the dashed line representing the joint strength after the post-weld paint bake heat treatment. The Tool3 data points are identical to those seen in Figure 42, and are shown for easy comparison. Recall that the joint strengths made with other tools are very similar to those made with Tool3 (with the exception of Tool5). An image of the fracture location in the pulled samples can be seen in Figure 50.

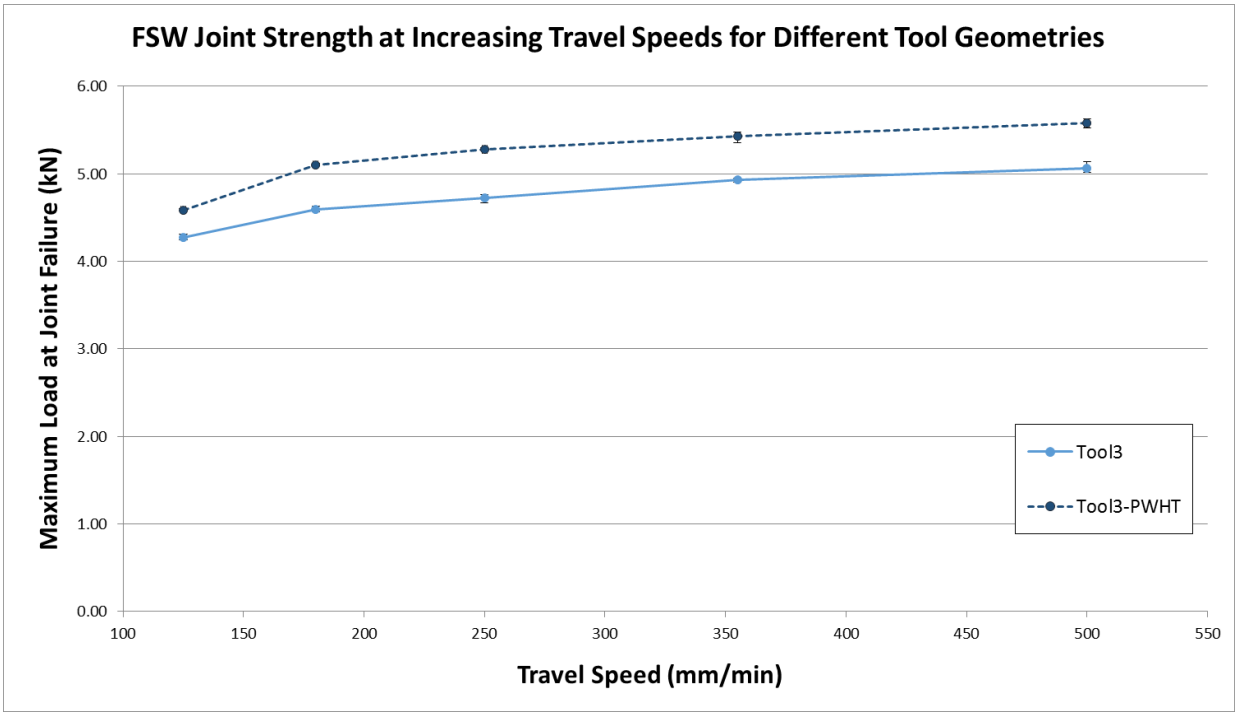

Figure 49: Comparison of maximum load at failure between as-welded and post-weld heat treated pull test specimens of dissimilar AA7075/AA6022 lap FSW Tool3 at 125, 180, 250, 355, 500mm/min

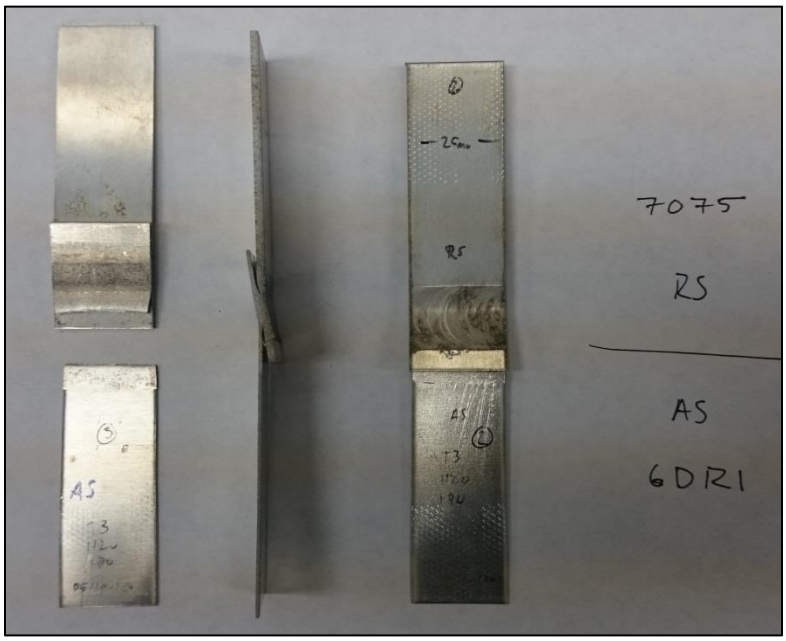

Figure 50: Location of fracture during the lap shear pull tests of post-weld heat treated dissimilar lap FSW of AA7075-T6 to AA6022. The welding condition for all samples is Tool3-180mm/min.

The post-weld heat treatment of 180^{o}C for 30 minutes resulted in approximately a 10% increase in joint strength at each travel speed. The increase in strength is thought to be the product of artificial ageing that takes place in the AA6022 at 180^{o}C, as the results suggest that this temperature promotes the precipitation of strengthening particles in the material. This is in line with existing literature which showed a slight increase in the strength of friction stir spot welds of a similar alloy AA6111 after a paint bake heat treatment [59]

The location of fracture within the test specimens remained the same as what was observed in samples that had not been subjected to a post-weld heat treatment. This would indicate that the AA6022 is not peak-aged, but has experienced only enough artificial ageing to marginally increase the hardness in the HAZ.

6.0 Conclusions

The objectives of the thesis were stated at the beginning as the following; firstly: identify process parameters of tool geometry and travel speed that will produce FSW joints between the given materials; secondly: compare the mechanical properties between FSW joints made with these process parameters; thirdly: determine a tool geometry that will provide good quality welds across a wide operating window. Based on the results presented above, the goals were achieved. The research presented in this thesis has explored the effect of processing parameters on FSW overlap joints between similar materials (2mm thick AA7075-T6 sheets), as well as dissimilar materials (2mm thick AA7075-T6 and 0.9mm thick AA6022-T4). Five welding speeds were used: 125, 180, 250, 355, and 500mm/min; and 5 different tool shapes were attempted: Tool1 – straight pin with threads; Tool2 – tapered pin with threads; Tool3 – tapered pin with threads and 3 flats; Tool4 – tapered pin with 3 flats; Tool5 – tapered pin with straight horizontal grooves. Welds were characterized using optical microscopy, overlap shear pull tests, microhardness profiles, and temperature measurements.

Of the tool designs that were attempted, the most robust geometry proved to be Tool3, which was able to produce good quality welds across all speeds, in both material combinations. Other tool designs were prone to producing welding defects. The tool geometries of Tool1, Tool2 and Tool3 were all capable of creating welds with large mixed areas, but also produced an upward hooking defect that is common in lap FSW. The Tool4 design was able to eliminate the hooking defect, but resulted in much less mixing of the materials. The Tool5 design resulted in a hooking defect down into the lower sheet, and also resulted in negligible mixing of the materials.

Of the welding speeds that were attempted, there are two that have merit. A speed of 250mm/min proved to be the most robust – creating welds with a large mixed area, good mechanical properties, and no signs of defects. The strongest dissimilar FSW produced at this speed was made with

Tool3 and showed a linear strength of 1.90N/m. On the other hand, a welding speed of 500mm/min proved to be most effective – producing the overall strongest and hardest welds at the fastest rate; though they had smaller mixed areas and showed evidence of small weld defects. The strongest dissimilar FSW produced at this speed was made with Tool3 and showed a linear strength of 0.206N/m. Note that the speed of 355mm/min is not suggested because it appears to have the worst of both cases – it produces a noticeably smaller mixed area and is prone to defects, but still creates welds at a slower rate than 500mm/min. In the specific case of a dissimilar material combination of 2mm thick AA7075-T6 joined to 0.9mm thick AA6022-4, the results show that the size of the mixed area and the presence of defects is not significant, as the joint will fail in the HAZ of the softer, thinner sheet of AA6022-T4.

Temperature measurements during FSW of the dissimilar material combination in the center of the weld and the surrounding area allowed for a direct comparison to existing literature on the precipitation evolution of AA6022. This further suggested that the temperatures in the HAZ at slow welding speeds were high enough to cause coarsening and dissolution of the β'' phase, whereas those at faster speeds were not.

7.0 Recommendations for Future Work

It is recommended that microhardness profiles of the post-weld heat treated samples be obtained. It is possible to draw some conclusions from only the temperature measurements and overlap shear test results, but having thorough microhardness data of the samples after PWHT would better characterize the FSW joint.

The use of transmission electron microscopy (TEM) would be useful to reveal differences in the precipitates in pre-weld workpiece material and post-weld joint. While there are many comparisons that can be made to the existing literature on precipitate evolution based on the temperature measurements obtained in the current research, it would be best to examine the precipitates of the welded specimens firsthand. The best way to do this is through TEM before and after the welding process.

A corrosion study is recommended so that the mechanical properties of the FSW joints can be examined after being subjected to a corrosive environment. It is possible that the specimens that perform well under a quasi-static load condition even though they show evidence of defects in the stir zone will experience significant degradation of joint quality due to corrosion. It would also be wise to examine the corrosion behaviour of the dissimilar material combination. As corrosion is always a concern in automotive applications, this is an area that merits some study.

A fatigue loading study is recommended so that the mechanical properties of the FSW joints can be examined under cyclic loading conditions. As stated above, it is possible that the specimens that perform well under a quasi-static load condition even though they show evidence of defects in the stir zone will experience significant degradation of joint quality due to fatigue. It would also be wise to examine the effects of the hooking defect on the fatigue performance of the joints. Since cyclic loading is an important load case in automotive parts, it is an area that merits some study.

References

[1] F. Campbell et al., Elements of Metallurgy and Engineering Alloys, Ohio: ASM International, 2008.

[2] S. Kou et al., Welding Metallurgy, Hoboken: John Wiley & Sons, 2003.

[3] J. Lancaster et al., Metallurgy of Welding, William Andrew, 1999.

[4] W.M. Thomas et al., "Friction Stir Butt Welding". Great Britain Patent 9125978-8, 1991.

[5] R. S. Mishra et al., Friction Stir Welding and Processing, ASM International, 2007.

[6] R. S. Mishra et al., "Friction Stir Welding and Processing Review Journal," *Materials Science and Engineering R,* no. 50, 2005.

[7] R. Nandan et al., "Recent advances in friction stir welding process, weldment structure and properties," *Progress in Materials Science,* vol. 53, no. 6, 2008.

[8] D. A. Porter et al., Phase Transformations in Metals and Alloys, Boca Raton: Taylor & Francis Group, 2009.

[9] M. Epler et al., "Structures by Precipitation from Solid Solution," in *ASM Handbook*, vol. 9, Ohio, ASM International, 2004.

[10] C. W. Olea et al., "Influence of Energy Input in Friction Stir Welding on Structure Evolution and Mechanical Behaviour of Precipitation-Hardening in Aluminium Alloys (AA2024-T351, AA6013-T6 and Al-Mg-Sc)," GKSS Forschungszentrum Geesthacht, Geesthact, 2008.

[11] C. Sharma et al., "Influence of pre-weld temper conditions of base metal on microstructure and mechanical properties of friction stir weld joints of Al–Zn–Mg alloy AA7039," *Materials Science and Engineering A,* vol. 620, 2014.

[12] J. Lippold et al., Welding Metallurgy and Weldability, Hoboken: John Wiley & Sons, 2015.

[13] P. Threadgill et al., "Friction stir welding of aluminium alloys," *International Materials Reviews,* vol. 54, no. 2, 2009.

[14] Y. Uematsu et al., "Fatigue behaviour of friction stir welded A7075-T6 aluminium alloy in air and 3% NaCl solution," *Welding International,* vol. 27, no. 6, 2013.

[15] J. F. Guo et al., "Friction stir welding of dissimilar materials between AA6061 and AA7075 Al alloy effects of process parameters," *Materials and Design,* vol. 56, 2013.

[16] H. J. Aval et al., "A study on microstructures and residual stress distributions in dissimilar friction-stir welding of AA5086–AA6061," *Journal of Materials Science,* vol. 47, 2012.

[17] W. Miao et al., "Precipitation Hardening in Aluminum Alloy 6022," *Acta Metallurgica,* vol. 40, no. 7, pp. 873-878, 1999.

[18] Y. Zhang et al., "Review of tools for friction stir welding and processing," *Canadian Metallurgical Quarterly,* vol. 51, no. 3, 2012.

[19] R. Rai et al., "Review: Friction Stir Welding Tools," *Science and Technology of Welding and Joining,* vol. 16, no. 4, 2011.

[20] B. Givi et al., Advances in Friction Stir Welding and Processing, Cambridge: Woodhead Publishing, 2014.

[21] F. Fadaeirfard et al., "Investigation of Microstructure and Mechanical Properties of Friction Stir Lap Welded AA6061-T6 in Various Welding Speeds," *Journal of Applied Sciences,* vol. 14, no. 3, 2014.

[22] Y. Hovanski et al., *High Speed Joining of Dissimilar Alloy Aluminum Tailor Welded Blanks,* Richland: Pacific Northwest National Laboratory, 2014.

[23] K. Krasnowski et al., "Fatigue and static properties of friction stir welded aluminum alloy 6082 lap joints using triflute type and smooth tool," *Archives of Metallurgy and Materials,* vol. 59, no. 1, 2014.

[24] J. D. Backer et al., "Thermoelectric method for temperature measurement in friction stir welding," *Science and Technology of Welding and Joining,* vol. 18, no. 7, 2013.

[25] P. Cavaliere et al., "Mechanical response of 2024-7075 aluminium alloys joined by Friction Stir Weldin," *Journal of Materials Science,* vol. 40, 2005.

[26] G. Ipekoglu et al., "Effects of Initial Temper Condition and Postweld Heat Treatment on the Properties of Dissimilar Friction-Stir-Welded Joints between AA7075 and AA6061 Aluminum Alloys," *The Minerals, Metals and Materials Society and ASM International,* vol. 45A, 2014.

[27] G. Ipekoglu et al., "Investigation into the Influence of Post-Weld Heat Treatment on the Friction Stir Welded AA6061 Al-Alloy Plates with Different Temper Conditions," *Metallurgical and Materials Transactions A,* vol. 45, no. 2, 2014.

[28] C. Jonckheere et al., "Torque, temperature and hardening precipitation evolution in dissimilar friction stir welds between 6061-T6 and 2014-T6 aluminum alloys," *Journal of Materials Processing Technology,* vol. 213, no. 6, 2013.

[29] Y. Li et al., "Flow visualization and residual microstructures associated with the friction-stir welding of 2024 aluminum to 6061 aluminum," vol. 271, no. 1-2, 1999.

[30] Y. Li et al., "Solid-state flow visualization in the friction-stir welding of 2024 Al to 6061 Al," vol. 40, no. 9, 1999.

[31] J. Ouyang et al., "Material flow and microstructure in the friction stir butt welds of the same and dissimilar aluminum alloys," vol. 11, no. 1, 2002.

[32] L. Murr et al., "Fundamental Issues and Industrial Applications of Friction-Stir Welding," vol. 15, no. 1, 2000.

[33] L. Murr et al., "Aluminum 2001—Proceedings of the TMS 2001 Annual Meeting Aluminum Automotive and Joining Symposia," 2001.

[34] H. Larsson et al., "Proceedings of the Second International Symposium on Friction Stir Welding," Gothenburg, Sweden, 2000.

[35] R. S. Mishra et al., Friction Stir Welding and Processing II, Warrendale, PA: TMS, 2003.

[36] W. Lee et al., "The improvement of mechanical properties of friction-stir-welded A356 Al alloy," vol. 355, no. 1-2.

[37] S. Lim et al., "Tensile behavior of friction-stir-welded A356-T6/Al 6061-T651 bi-alloy plate," vol. 35, no. 9, 2004.

[38] C. Leitao et al., "Mechanical behaviour of similar and dissimilar AA5182-H111 and AA6016-T4 thin friction stir welds," vol. 30, no. 1, 2009.

[39] P. Dong et al., "Natural aging behaviour of friction stir welded 6005A-T6 aluminium alloy," *Materials Science and Engineering A,* no. 576, 2013.

[40] M. Costa et al., "Dissimilar friction stir lap welding of AA 5754-H22/AA 6082-T6 aluminium alloys: Influence of material properties and tool geometry on," *Materials and Design,* vol. 87, pp. 721-731, 2015.

[41] A. H. Lotfi et al., "Effect of Welding Parameters on Microstructure, Thermal, and Mechanical Properties of Friction-Stir Welded Joints of AA7075-T6 Aluminum Alloy," *Metallurgical and Materials Transactions A,* vol. 45, no. 6, 2014.

[42] O. Gopkalo, B. Diak and X. Liu, "Monthly update presentation - base material characterization," 2015.

[43] P. Colegrove et al., "Experimental and numerical analysis of aluminum alloy 7075-T7351 friction stir welds," *Science and Technology of Welding and Joining,* vol. 8, no. 5, 2003.

[44] S. A. Khodir et al., "Friction stir welding of dissimilar AA2024 and AA7075 aluminum alloys," *Materials Science and Engineering B,* vol. 148, 2008.

[45] W. Mahoney et al., "Properties of Friction Stir Welded 7075-T651 aluminum," *Metallurgical and Materials Trnasactions A,* no. 29, pp. 1955-1964, 1998.

[46] W. Thomas et al., "Friction stir welding - recent developments in tool and process technologies," *Advanced Engineering Materials,* vol. 5, no. 7, pp. 485-490, 2003.

[47] E. Hetrick and J. Forsmark, Interviewees, *Monthly progress meeting.* [Interview]. January 2015.

[48] L. Han et al., "A correlation study of mechanical strength of resistance spot welding of AA5754," *Journal of Materials Processing Technology,* no. 211, pp. 513-521, 2011.

[49] J. Na et al., "Effect of temperature on the joints strength of an automotive polyurethane adhesive," *Journal of Adhesion,* no. 92, pp. 52-64, 2014.

[50] S. Nunes et al., "Comparative Failure Assessment of Single and Double Lap Joints with Varying Adhesive Systems," *The Journal of Adhesion,* no. 92, pp. 610-634, 2015.

[51] G. Ipekoglu et al., "Investigation of the effect of temperm condition on the firction stir weldability of AA7075 Al-alloy plates," *Materials and Technology,* vol. 46, no. 6, 2012.

[52] J. Cho et al., "Modelling of strain hardening during friction stir welding of stainless steel," *Modelling and Simulation in Materials Science and Engineering,* vol. 15, no. 5, 2007.

[53] A. Gerlich et al., "Intermixing in Dissimilar Friction Stir Spot Welds," *Metallurgical and Materials Transactions A,* vol. 38, no. 3, pp. 584-595, 2007.

[54] N. Kamp et al., "Modelling of heterogeneous precipitate distribution evolution during friction stir welding process," *Acta Materialia,* vol. 54, no. 8, 2006.

[55] L. Commin et al., "Friction stir welding of AZ31 magnesium alloy rolled sheets: Influence of processing parameters," *Acta Materialia,* vol. 57, no. 2, pp. 326-334, 2009.

[56] A. R. Ilkhichi et al., "Establishing Mathematical Models to Predict Grain Size and Hardness of the Friction Stir-Welded AA 7020 Aluminum Alloy Joints," *Metallurgical and Materials Transations B,* vol. 46, no. 1, pp. 357-365, 2015.

[57] D. Lohwasser et al., Friction stir welding from basics to applications, New Delhi: Woodhead, 2010.

[58] J. Gracio et al., "Artificial aging and shear deformation behaviour of 6022 aluminum alloy," *International Journal of Plasticity,* no. 20, pp. 427-445, 2004.

[59] N. Blundell et al., "The Influence of Paint Bake Cycles on the Mechanical Properties of Spot Friction Joined Aluminium Alloys," 2006.

[60] M. Reza-E-Rabby et al., "Effect of tool pin features on process response variables during friction stir welding of dissimilar aluminum alloys," *Science and Technology of Welding and Joining,* vol. 20, no. 5, 2015.

[61] R. S. Mishra et al., Friction Stir Welding of Dissimilar Alloys and Materials, Oxford: Elsevier, 2015.

[62] M. H. Shahriyar et al., "Prospect of friction stir welding in automobile TWB production as alternative of laser welding," Blekinge Institute of Technology, Karslkrona, 2012.

[63] W. B. Lee et al., "Mechanical Properties Related to Microstructural Variation of 6061 Al Alloy Joints by Friction Stir Welding," *Materials Transactions,* vol. 45, no. 5, 2004.

[64] Y. Li et al., "Flow visualization and residual microstructures associated with the friction-stir welding of 2024 aluminum to 6061 aluminum," *Materials Science and Engineering A,* no. 271, 1991.

[65] N. Kumbhar et al., "Friction Stir Welding of AA5052 with AA6061 Alloys," *Journal of Metallurgy,* 2012.

[66] I. Shigematsu et al., "Joining of 5083 and 6061 aluminum alloys by friction stir welding," *Journal of Materials Science Letters,* no. 22, 2003.

[67] M. Mohammadtaheri et al., "The Effect of Base Metal Conditions on the Final Microstructure and Hardness of 2024 Aluminum Alloy Friction-Stir Welds," *Metallurgical and Materials Transactions B,* vol. 44, no. 3, 2013.

[68] H. Aydin et al., "An investigation on microstructure and mechanical properties of post-weld heat-treated friction stir welds in aluminum alloy 2024-W," *Journal of Mechanical Engineering Science,* vol. 227, no. 4, 2013.

[69] D. Burford et al., "Advances in Friction Stir Welding for Aerospace Applications," *American Institute of Aeronautics and Astronautics,* 2006.

[70] Y. Chen et al., "Precipitate evolution in friction stir welding of 2219-T6 aluminum alloys," *Materials Characterization,* vol. 60, no. 6, 2009.

[71] F. D. Geuser et al., "Microstructure mapping of a friction stir welded AA2050 Al–Li–Cu in the T8 state," *Philosophical Magazine,* vol. 94, no. 13, 2014.

Appendix A – FSW Tool Drawings

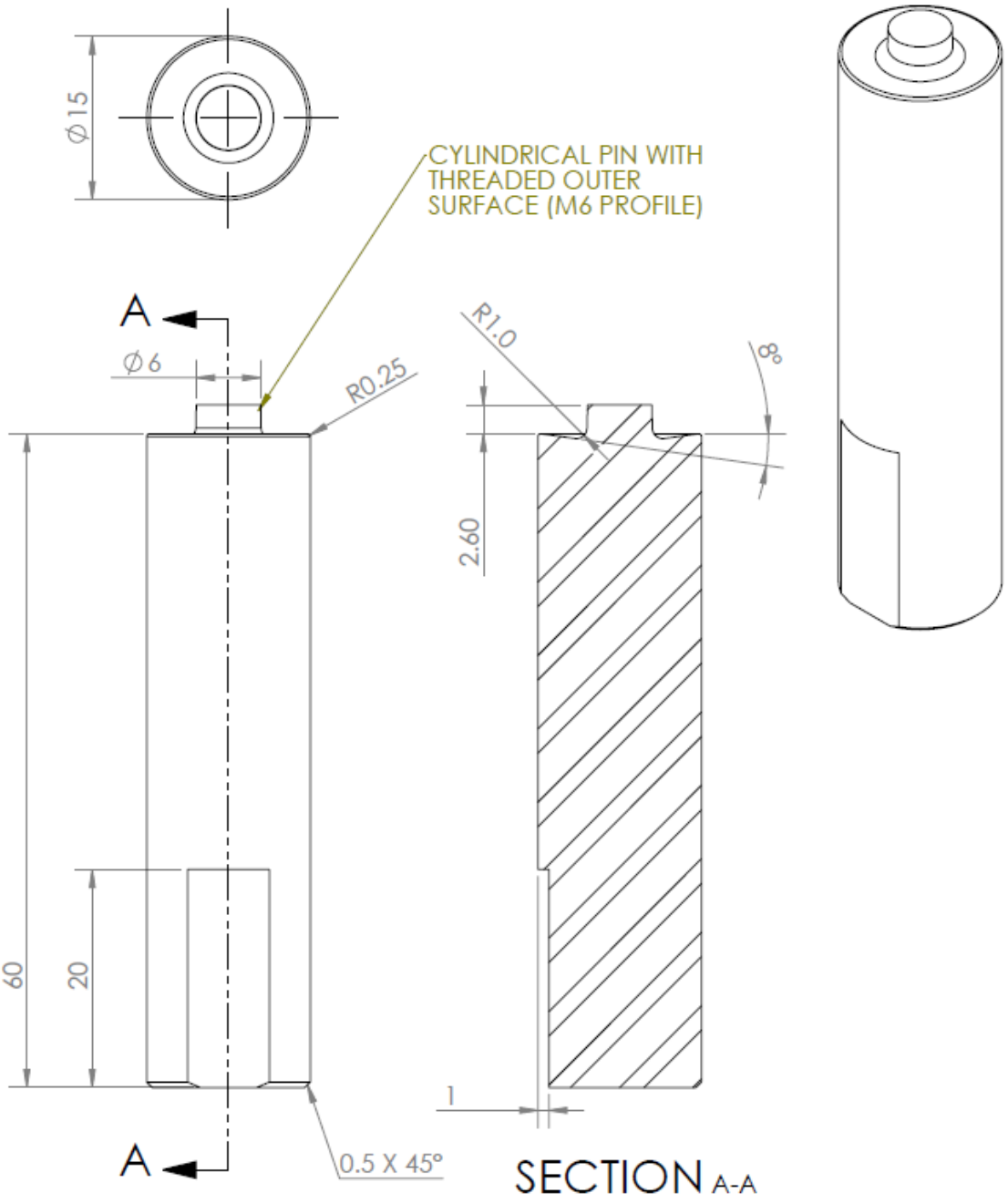

Figure 51: Drawing of Tool1

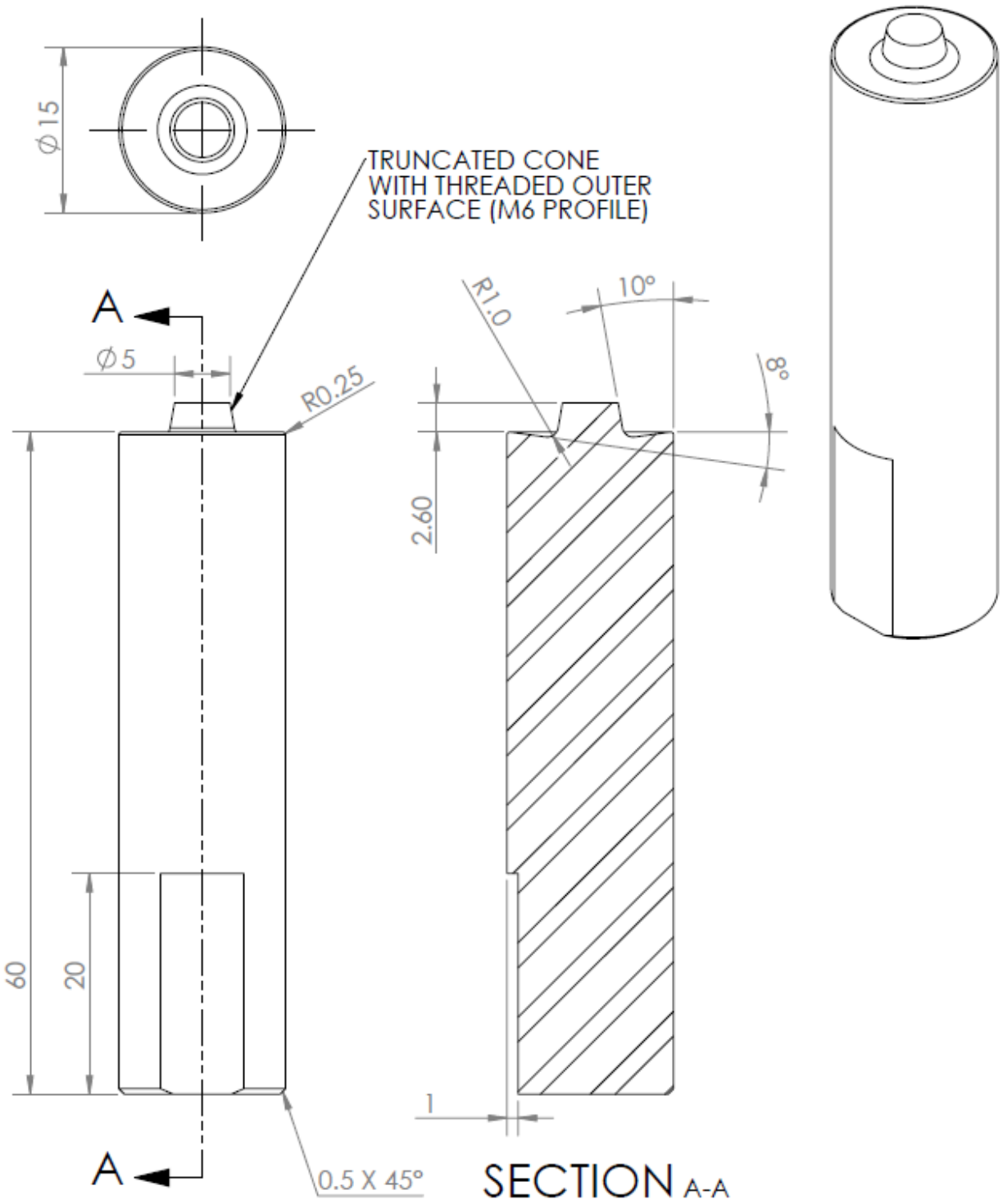

Figure 52: Drawing of Tool2

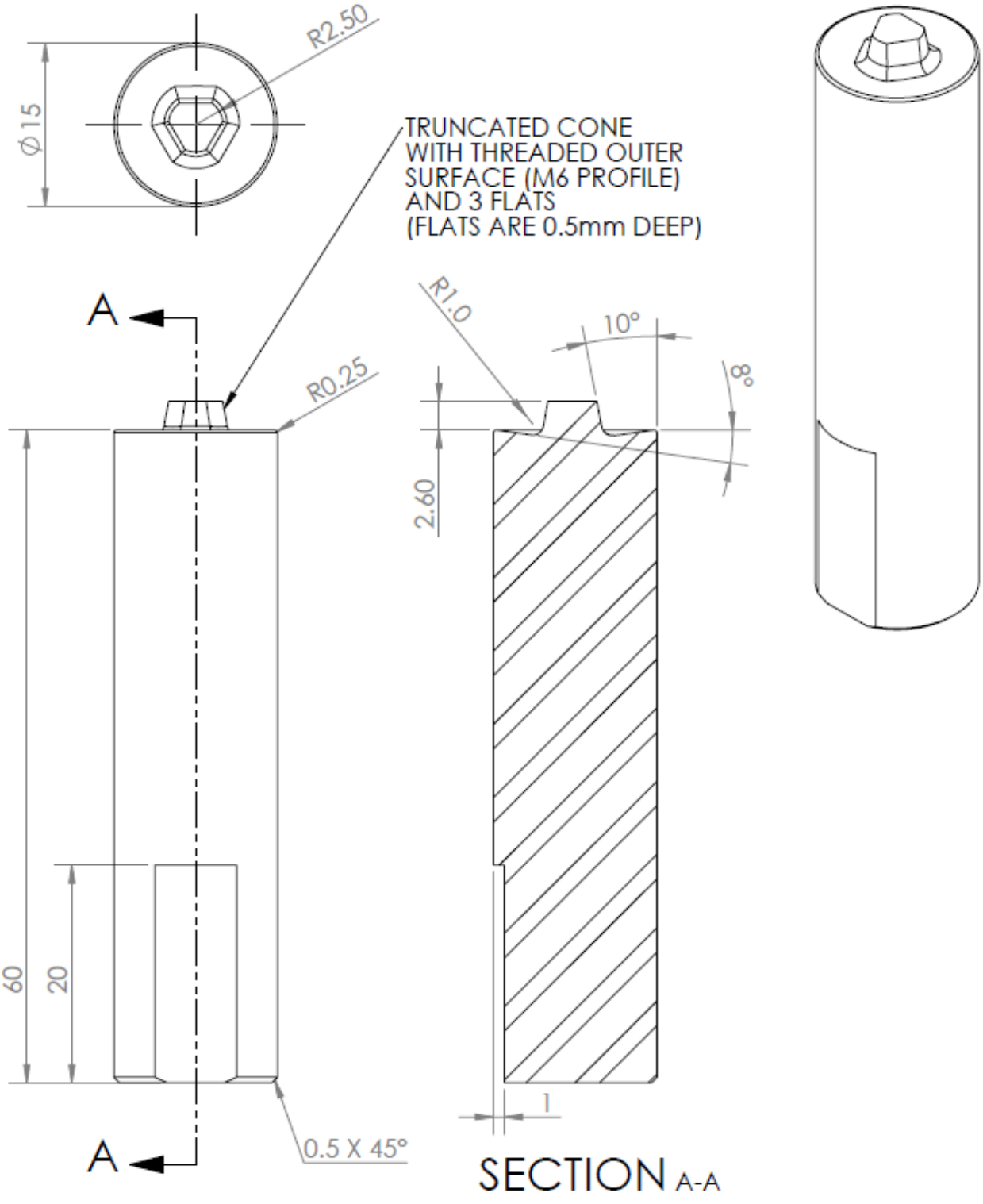

Figure 53: Drawing of Tool3

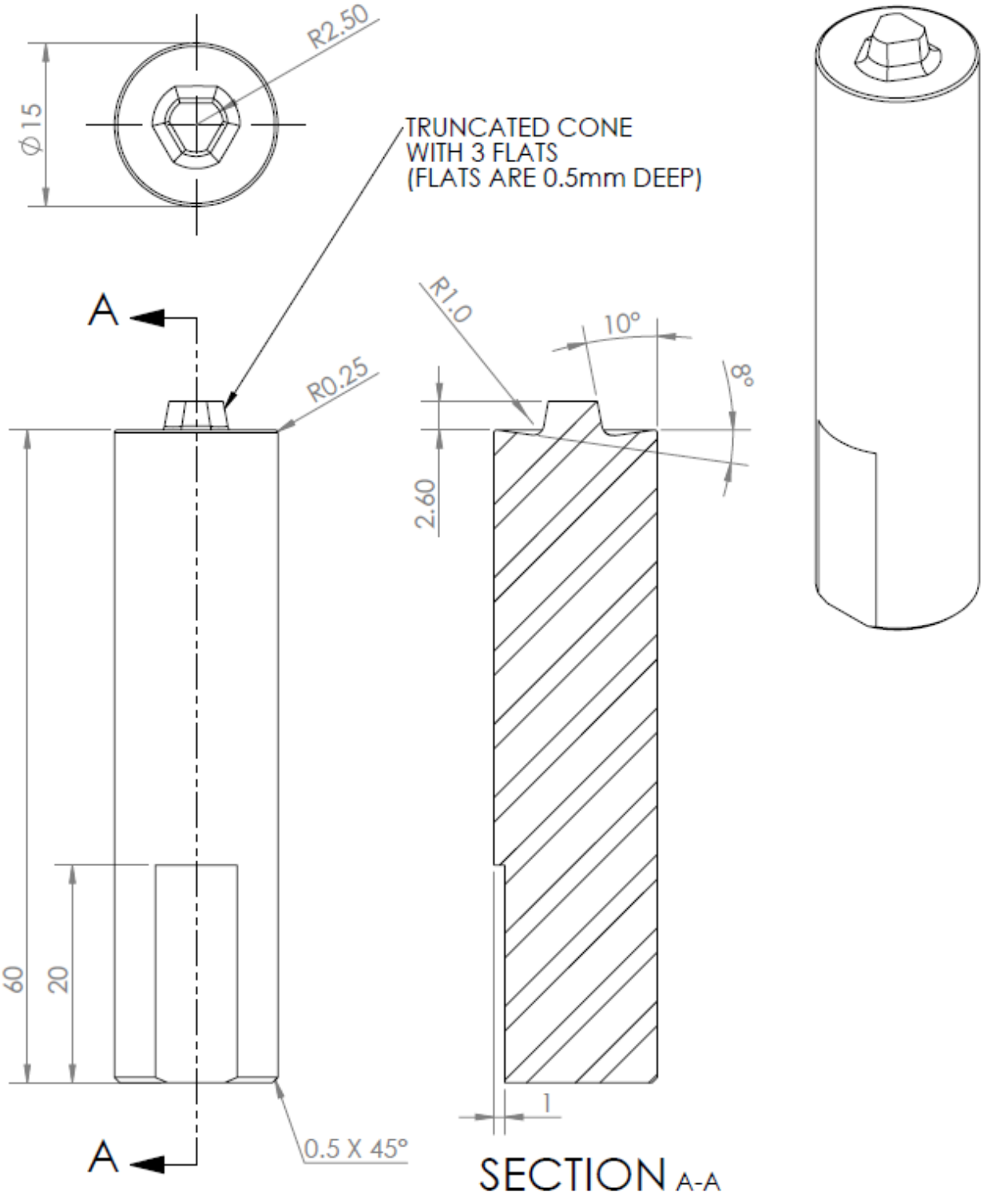

Figure 54: Drawing of Tool4

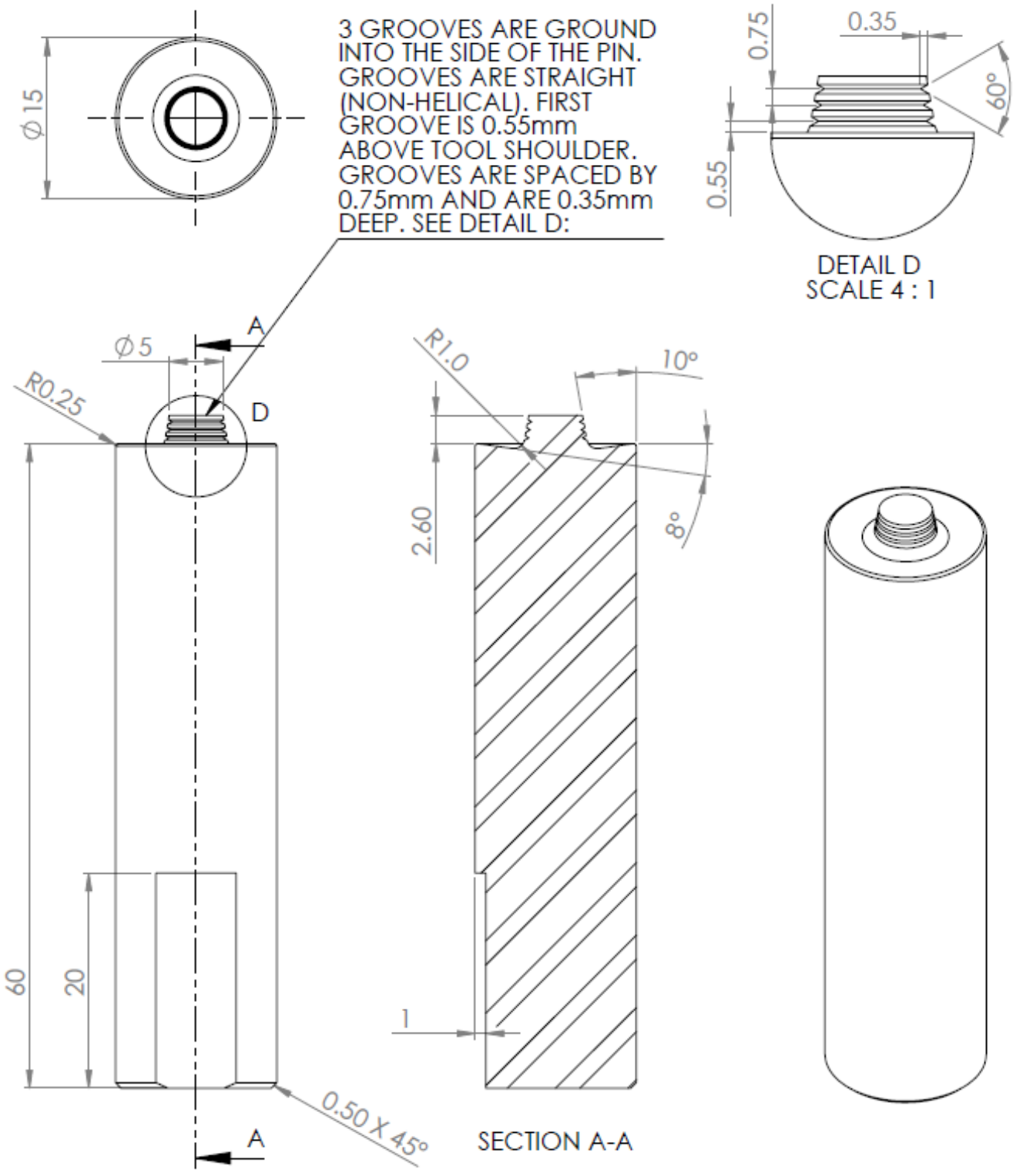

Figure 55: Drawing of Tool5